# MODELING WING TANK FLAMMABILITY

By

DHAVAL D. DADIA

A thesis submitted to the

Graduate School-New Brunswick

Rutgers, The State University of New Jersey

in partial fulfillment of the requirements

for the degree of

Master of Science

Graduate Program in Mechanical and Aerospace Engineering

written under the direction of

Professor Tobias Rossmann

and approved by

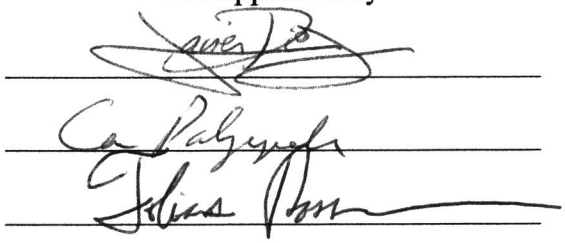

New Brunswick, New Jersey

October 2009

ABSTRACT OF THE THESIS

MODELING WING TANK FLAMMABILITY

By DHAVAL D. DADIA

Thesis Director:
Professor Tobias Rossmann

An investigation into the fire safety of a wing fuel tank has been performed to aid in the effort to eliminate or reduce the possibility of a wing fuel tank explosion in a commercial aircraft. A computational model is built to predict the generation of flammable mixtures in the ullage of wing fuel tanks. The model predicts the flammability evolution within the tank based on in-flight conditions of a wing fuel tank. The model is validated through supporting experiments performed in an altitude chamber, the wind tunnel facility as well as data obtained from flight tests. The results from the experiments are compared to the computational results. Computational results from the altitude chamber follow the general trend of the experimental results, but produce them at a different flash point. This is due to the replenishment of species with lower flash point at the surface of the fuel which emulates the flash point of the entire fuel to be lower. Experimental results for the aluminum wing tests from the wind tunnel experiments are in good agreement with the computational results as well.

A simpler model is developed from a program that calculates fuel air ratio within the ullage of fuel tanks in order to reduce the required number of inputs to the model. This model is applied to the data sets for the experiments performed in the altitude chamber and wind tunnel. For the tests conducted in the altitude chamber, the correlation

estimates the hydrocarbon concentrations extremely well during ascent and descent. During the on-ground condition the estimation is good, but not as accurate as the ascent or descent conditions. For the tests conducted in the wind tunnel, the computational values follow the general trend of the experimental values, but the computational values estimates the total hydrocarbon concentration approximately 10% lower than the experimental value consistently.

Flammability studies are also performed in order to track the effects of temperature, pressure, and oxygen concentration on the upper and lower flammability limits. For the temperature and pressure profiles considered in this work, it is found that the temperature and pressure effects on the flammability limits are minimal. In contrast, the oxygen concentration has a significant effect on the flammability limits of the vapor; the flammable region narrows with a decrease in oxygen concentration.

ACKNOWLEDGEMENTS

I would like to express sincere gratitude to Professor Tobias Rossman for his professional guidance and support. I also thank him for providing me an opportunity to grow as a student, and more importantly, as an engineer in the exceptional research environment that he creates. His uncompromising quest for excellence has shaped me significantly during my graduate research. I would like to thank Professor Constantine Polymeropoulos for his guidance and support throughout my study and Professor Javier Diez for his time in being a part of my committee.

I would also like to thank Mr. Gus Sarkos, Mr. Richard G. Hill, and Mr. Steven Summer at the Fire Safety Branch of the Federal Aviation Administration's William J. Hughes Technical Center for providing me with the support and facilities to conduct this research. These three professional individuals instilled in me extensive knowledge, wisdom, and insight about the field of aircraft fire safety that is represented in this thesis. Their guidance and encouragement during my research at the technical center was extremely valuable and truly appreciated.

I would also like to thank Mr. William Cavage, Mr. Robert Ochs, Mr. Harry Webster, Mr. Robert Morrison, Mr. Joseph DeFalco, and Mr. Rich Walters for their professional help in the development of the experimental apparatus and assistance in conducting numerous tests in the altitude chamber. Much thanks and appreciation goes out to the entire staff of the Fire Safety Branch of the Federal Aviation Administration's William J. Hughes Technical Center for aiding in the completion of this thesis.

I would like to thank my fellow scholars for their support throughout my collegiate experience. They are Christel Seitel, Megan Smith, James Fay, Mohamed

Sadik, Jonathan Doyle, Cassandra D'Esposito, Elan Borenstein, Tushar Saraf, and Vinesh Nishawala.

Finally, I would like to thank the Department of Mechanical and Aerospace Engineering at Rutgers University for providing me the opportunity to realize my true potential. I want to thank the entire department, faculty and staff for their support, kindness, and generosity.

# DEDICATION

I would like to dedicate this Masters Thesis to my grandfather, Khimchand M. Dadia, for inspiring me and my uncle, Praful H. Lathia, for being my biggest advocate. I would also like to dedicate it to all the members of my family. Their love, support and guidance has helped shape the person I am today. Their wisdom, encouragement and patience motivated me to achieve many goals in my life thus far. Their relentless faith and belief in me has taught me not to surrender thus helping me accomplish my biggest achievement. I will appreciate them forever and aim to make them proud as I endeavor to achieve my dreams and aspirations.

LIST OF TABLES

LIST OF FIGURES

# Chapter 1

# Introduction

## 1.1 Background and Motivation

Air travel has become a very common means of transporting people and cargo. There are incidents that occur that harm the safety of the payload of these aircrafts. One of the major safety issues being investigated by the Federal Aviation Administration (FAA) is the issue of fuel tank flammability. The accident rate for a heated center wing tank (CWT) airplane is 1 accident per 60 million hours of flight.[1] It is very tragic when an accident takes place, but on the other hand, one can learn from these events and try to understand the cause of the accident in order to prevent any other catastrophic event from occurring in the same manner. The Fire Safety Department at the Federal Aviation Administration's William J. Hughes Technical Center studies accidents that deal with fuel tank fires and tries to understand the underlying causes behind such incidents. The studies produced by them are then used to improve on existing regulations to reduce the likelihood of devastating accidents from occurring again.

The FAA has studied CWT flammability exhaustively, which resulted in the FAA releasing a final rule requiring the reduction of flammability in high risk fuel tanks. The study of fuel tank flammability was driven mostly after the catastrophic mid-air breakup of TWA flight 800. This incident occurred soon after the flight took off from J.F.K. airport in New York in July 1996. Accident investigators from the National Transportation Safety Board (NTSB) determined the cause of the crash occurred due to

the explosion of the nearly empty CWT. The explosion was ignited from an unconfirmed ignition source. The explosion occurred in part due to the fact that combustible vapor was being generated in the CWT due to heating of the bottom surface of the fuel tank by the heating ducts of the airplane.

The Aviation Rulemaking Advisory Committee (ARAC), which is mostly made up of people in the aviation industry, comment on regulations set by the FAA. The Fire Safety Division of the FAA provides the FAA with all the experimental studies and computational modeling work that support the rules and regulations set by the FAA. The flammability rule, released by the FAA in July of 2008, states "no fuel tank Fleet Average Flammability Exposure on an airplane may exceed three percent of the Flammability Exposure Evaluation Time (FEET) or that of a fuel tank within the wing of the airplane model being evaluated, whichever is greater. If the wing is not a conventional unheated aluminum wing, the analysis must be based on an assumed Equivalent Conventional Unheated Aluminum Wing Tank." [1] FEET is defined as "the time from the start of preparing the airplane for flight, through the flight and landing, until all payload is unloaded, and all passengers and crew have disembarked."[1]

Albeit the release of the rule to reduce flammability in a high risk fuel tank, the proposed rule does not differentiate between flammability in CWTs and WTs. The rule uses the flammability of a traditional unheated aluminum WT as the baseline for measuring the flammability in all tanks. When taking into consideration the flammability of fuel tanks, CWTs and WTs have different initial and boundary conditions. On May 5, 2006, a Boeing 727's wing tank exploded while the plane was still on the ground. The source of ignition was identified to be an electrical arc between a metallic surface and a

special Teflon sleeving.[1] There have been other cases similar to this one that has resulted in the explosion of wing tanks. Figure 1.1 shows the explosion of a wing tank of a China Airlines owned Boeing 737-800. This shows that flammable vapors can be generated in a wing tank as well, and this can pose as a viable threat to the aircraft industry. Thus studying the flammability in WTs can help justify amending the use of unheated aluminum WTs as the baseline for measuring the flammability in all fuel tanks and in doing so, it can help prevent accidents occurring in WTs.


**Figure 1.1 Explosion of a Wing Tank in a China Airlines Boeing 737-800**

## 1.2 Literature Review

### 1.2.1 Jet Fuel

Jet fuels have been modified considerably over the years. The first jet engine was designed to run on illumination kerosene since gasoline was in short supply during World War II. [2] The U.S. jet engines adopted kerosene to be used as the primary fuel as well and named it JP-1. JP-1 had a flashpoint of 109°F and a freeze point of -76°F. Due to its limited availability post World War II, JP-1 had to be modified with wide cut fuels. Wide-cut fuels are mixtures of various hydrocarbons that span the boiling range of gasoline and kerosene. Table 1.1 shows the various military fuels that have been used over the years. The table also shows the properties of Jet A, which is the most common fuel used in commercial aviation in the United States of America. Jet A is similar to the fuels used in the military. They only difference between the fuels is a few additives that change the properties of the fuel by a small amount.

| Fuel | Introduced | Type | Freeze Point °C | Flash Point °C |
|---|---|---|---|---|
| JP-1 | 1944 | kerosene | -60 | 43 |
| JP-2 | 1945 | wide-cut | -60 | |
| JP-3 | 1947 | wide-cut | -60 | |
| JP-4 | 1951 | wide-cut | -72 | |
| JP-5 | 1952 | kerosene | -46 | 60 |
| JP-6 | 1956 | kerosene | -54 | |
| JPTS | 1956 | kerosene | -53 | 43 |
| JP-7 | 1960 | kerosene | -43 | 60 |
| JP-8 | 1979 | kerosene | -47 | 38 |
| JP8+100 | 1998 | kerosene | -47 | 38 |
| Jet A | 1950 | kerosene | -40 | 38 |

**Table 1.1 Properties of military jet fuel**

### 1.2.2 Fuel Flash Point

The flash point of a flammable liquid is defined as the lowest temperature at which an ignitable mixture can be formed near the surface of the fuel. The flash point of a fuel is determined by the American Society for Testing Materials (ASTM) D56 standard, which is also referred to as the Tag closed cup test. A 50 ml specimen of the fuel is heated gradually in a container that can hold up to 130 ml. The vapor that is generated above the vessel due to the heating is exposed to a small flame for one second at regular temperature intervals. The temperature at which ignition first occurs is the called the flash point of the fuel. Flash point is a property of the fuel and it cannot give an accurate measurement of the flammability of the vapor generated due to a multi-component fuel. This is because the flash point is dependent on the vapor composition, which has been shown to vary for multi-component fuels as a function of temperature and mass loading. [3]

### 1.2.3 Fuel Vapor Pressure

Volatile liquids in enclosures will form vapor in the space above the liquid surface until there are as many molecules returning to the liquid phase as there are escaping. At this point the vapor is said to be saturated which can also be characterized to be at equilibrium. This state of equilibrium is considered to be dynamic in nature, because while the concentrations of the vapor and liquid are not changing, the molecules are still shifting phases from liquid to vapor and vice versa; but the rates are equal, hence producing a state of equilibrium. The vapor pressure of a liquid is the equilibrium pressure of a vapor above its liquid, which varies only with temperature.

In a fuel tank, which is a vented enclosure, at high altitudes there will be less air in the space above the liquid as a result of air being forced out of the tank to maintain the same pressure inside the tank as the ambient. If the liquid in the container remains at a constant temperature during the pressure drop, the liquid vapor pressure must remain constant as well. Since less air exists in the ullage at high altitudes, the overall concentration of the fuel in the vapor space increases. The empty space above the layer of fuel that contains air and fuel vapors is known as the ullage. This results in a higher concentration of fuel vapor at altitude at sea level for a liquid at constant temperature.

### 1.2.4 Mass Loading

Mass loading is a convenient way of describing the mass of fuel in a tank relative to the volume of the fuel tank it is contained in. It is defined as the mass of fuel per unit volume of the fuel tank. The density of jet fuel is estimated around 810 $kg/m^3$. Hence a tank that is 60% full would represent a mass loading of approximately 485 $kg/m^3$.

### 1.2.5 Center Wing Tank Flammability

Since the TWA flight 800 accident in July 1996, fuel tank safety has gained a lot of attention. Upon further investigation by the NTSB, it was determined that the probable cause of the explosion of the CWT was the result of an ignition of a flammable fuel/air mixture in the ullage of the tank. The NTSB also mentioned that one of the contributing factors were that the design and certification of the aircraft required only the preclusion of all potential ignition sources in order to prevent a fuel tank explosion.[18] Following the accident, the F.A.A. initiated rulemaking in order to re-evaluate the industry's approach

to fuel tank safety. They issued a number of Airworthiness Directives and issued a Special Federal Aviation Regulation (SFAR). SFAR 88 "would require design approval holders of certain turbine-powered transport category airplanes to submit substantiation to the FAA that the design of the fuel tank system of previously certified airplanes precludes the existence of ignition sources within the airplane fuel tanks." [4] The FAA has also conducted research into methods that could eliminate or significantly reduce the exposure of the airplanes to flammable vapors. While the SFAR 88 strived to eliminate ignition sources, the next step in reducing the likelihood of a fuel tank explosion for the FAA was to reduce the presence of flammable vapors in the fuel tanks. Thus, the FAA commissioned an Aviation Rulemaking Advisory Committee (ARAC) to provide specific recommendations and propose regulatory text for rulemaking to reduce the hazards associated with flammable vapors in fuel tanks. The ARAC recommended two feasible options; directed ventilation which would provide ventilation for the areas adjacent to the heated tanks, and ground-based inerting which would inert the tanks during ground operations. [5]

The ARAC evaluated three basic inerting design system concepts that would address the inerting of a heated fuel tank. The first concept was Ground-Based Inerting (GBI), the second concept being Onboard Ground Inerting (OBGI), and the third being Onboard Inert Gas Generating System (OBIGGS). GBI was a system that used ground-based nitrogen gas supply equipment to inert the heated fuel tanks. The OBGI was an onboard system that used nitrogen gas generating equipment to inert heated fuel tanks. OBIGGS was a system that used onboard nitrogen gas generating equipment to inert all the fuel tanks so that all the fuel tanks remain inert throughout the ground and typical

flight operations. It was decided that more research and development was required for rule making actions to be taken.[5]

The fuel tank flammability research group studies the effects on parameters such as temperature, pressure, oxygen concentration, and mass loading on the generation of flammable vapors in the ullage. This data is used to build computational models that will be able to predict fuel vapor concentrations in the ullage throughout a typical flight profile accurately. A vast amount of work has already been done by the fuel tank flammability research group.[4-10] Experiments were conducted within an altitude chamber simulating a CWT with a small amount of fuel heated from the bottom surface and then exposed to temperatures corresponding to high altitudes to determine the effects of low ambient temperature on the vapor concentrations in the ullage. It was determined that as the ambient temperature is decreased the ullage vapor concentration decreased as well.[6] Experiments were conducted to study the effects of mass loading on the fuel vapor concentration in the ullage of a CWT. It was established that a minimum mass loading of 0.08 to 0.15 $kg/m^3$ was necessary in order to have flammable vapors generated in the ullage. It was also noted that the distribution of the fuel had a significant effect on how long it takes to reach a peak flammable vapor concentration. The vapor will take a long time to reach it maximum vapor concentration when the liquid fuel is less dispersed.[7]

A study was done to study the Limiting Oxygen Concentration (LOC) required to inert jet fuel vapors at reduced fuel tank pressures. A fuel tank containing fuel with a mass loading of about 4.5 $kg/m^3$ was placed in a pressure chamber that would simulate altitudes from sea level up to 38,000 feet. The peak pressure was measured at various altitudes due to ignition occurring at oxygen levels approximately 1% to 1.5% above the

LOC. The LOC from sea level to 10,000 feet was determined to be 12% oxygen concentrations, and the oxygen concentration linearly increasing from 12% at 10,000 feet to 14.5% at 40,000 feet.[8] An OBIGGS system that uses aircraft bleed air to generate nitrogen-enriched air was developed by the FAA. This system was tested through a series ground and flight tests to evaluate the inerting system, as well as to measure the flammability of a CWT and a wing tank. The results showed that the system developed by the FAA operated as anticipated. The flammability measurements obtained showed trends similar to those obtained via computational models.[9]

## 1.3 Objectives of the Thesis

The objective of this research project is to develop a model that predicts the generation of flammable mixtures in the ullage of aircraft wing fuel tanks. The model will predict the flammability of the tank with conditions that will simulate an in-flight environment of a wing tank, where the wing tank will be radiatively heated from the top surface of the tank to simulate heating from the sun and the wing tank will at least be 60% full of fuel. This model will help in the development of fuel tank protection methods that will possibly eliminate or reduce the exposure of wing tanks to wing fuel tank fires and explosions. A model is a cheaper alternative to full scale experiments as it would use up a lot of time as well as financial resources. The model will be developed as a tool that could be used by companies to determine the flammability exposure time of a fuel tank. The flammability exposure time is used as a measurement to ensure the safety of fuel tanks. The model will be validated through supporting experiments run in the altitude chamber and the wind tunnel facility as well as data obtained from previous flight tests.

# Chapter 2

# Computational Model

The explosion hazard of flammable vapors in the ullage of wing tanks has been extensively studied and documented.[6-9] This occurrence has driven the development of an estimation method for the vapor generation in the wing fuel tank that experiences varying temperature and pressure as a result of flight conditions. This estimation is based on parameters that influence the generation of flammable vapors, such as the fuel flash point, vapor pressure, and mass loading among others.[10] The model also takes into consideration effects such as fuel vaporization from a liquid layer of fuel, condensation on the tank walls and ceiling, and different liquid Jet-A compositions. The model requires liquid fuel temperature, tank wall temperatures, ullage temperatures, ambient temperature, and pressure as inputs.

## 2.1 Model Description

A model has already been developed to predict flammability in CWT by computing the fuel to air ratio in the ullage of the tank. The model assumes the CWT to be a 2-D enclosure with a vent that is being heated from the bottom surface. Figure 2.1 shows the control volume of the CWT used by the computational model. The bottom surface being heated simulates air conditioning packs located underneath the center wing fuel tank. These air conditioning packs dissipate heat to its surroundings, thus creating a hot surface that heats up the bottom of the tank. The enclosure also contains a layer of fuel that accounts for the about 3% of the tank volume.

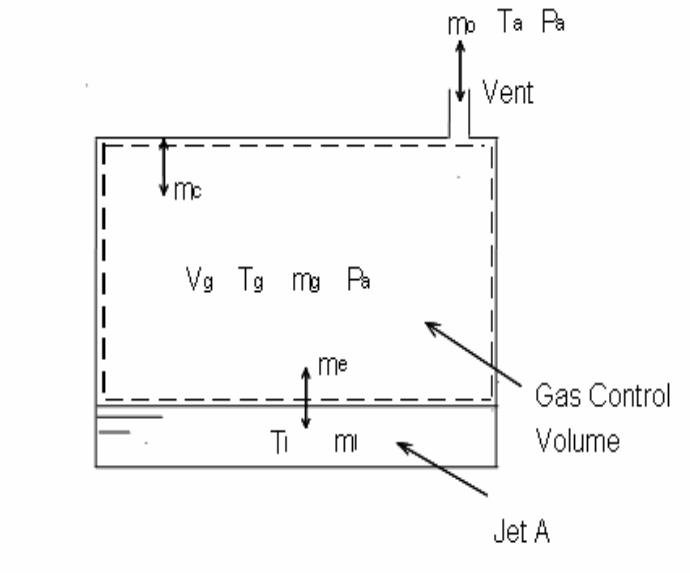


**Figure 2.1 Control Volume of a Center Wing Fuel Tank**

The problem attempted in this study is similar to the CWT, but there are variations in the parameters that require modification of the model. The wing fuel tank is assumed to be a vented 2-D enclosure that is radiatively heated from the top surface. This radiative heating simulates the tank being heated by the sun. The enclosure also contains fuel within the tank that accounts for more than 50% of the tank volume. Figure 2.2 shows the control volume of the wing fuel tank used by the computational model. The model requires the ullage temperature, average tank wall temperature, fuel surface temperature, ambient temperature, and pressure in order to set the initial conditions. At the beginning of the simulation, all the temperatures are set at approximately the same temperature in order to calculate the equilibrium mixture composition. The vapor pressure of each of the liquid species and the mass fraction of the vapor species are calculated at equilibrium. Other variables that need to be provided as inputs are:

- specific heat of the vapor at constant pressure
- gas density

- molecular weight of the air
- gas Prandtl number (Pr)
- number of components for fuel characterization
- molecular weight and boiling point of each of the components of the fuel
- volume fraction of each liquid component
- density of each pure liquid component
- number of carbon atoms of each liquid component
- dimensions of the fuel tank
- mass loading
- height of the ullage.

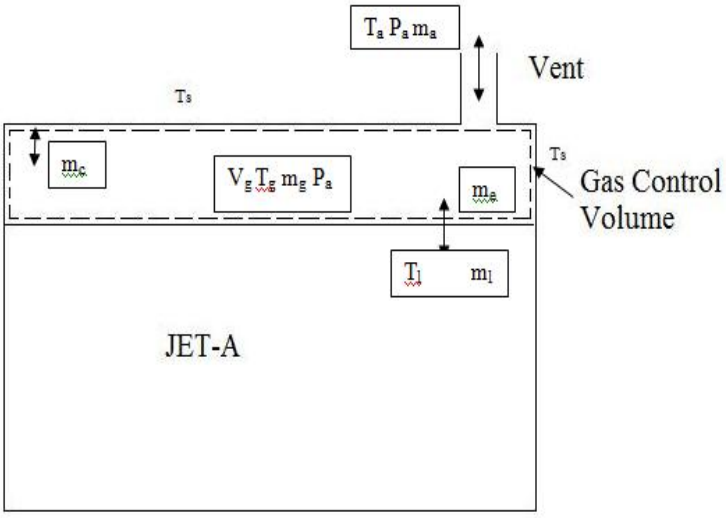


**Figure 2.2 Control Volume of a Wing Fuel Tank**

The initial stage of the flight profile comprises of the stage where the wing tank heats up from the radiation of the sun and the ascent stage where the wing tank pressure

decreases while it reaches cruising altitude. During this stage, the top surface temperature exceeds the fuel surface temperature and creates a stable temperature gradient. Although the stable temperature gradient suggests that there is no fluid motion within the ullage, it is assumed that the evaporation of fuel creates a well-mixed regime in the ullage. For the rest of the flight profile the fuel surface temperature exceeds the top surface temperature hence creating a well-mixed regime in the ullage due to unstable fluid circulation.

The assumptions made in the model are; the flow field in the tank is driven by forced convection between the liquid fuel, unheated sidewalls, and heated ceiling during the initial stages of the flight profile. For the rest of the profile, the flow field in the tank is driven by natural convection between all the surfaces in the ullage. For both of these flow fields, the gas within the ullage is considered to be well mixed. The heat and mass transport within the tank is expressed using empirical heat transfer correlations for estimating film heat and mass transfer coefficients. The well mixed assumption is justified in both flow fields because the natural and forced convection is considered to be in the turbulent regime. This is the case since the magnitude of the Rayleigh number, which is a parameter of free convection, based on the floor to ceiling temperature difference and tank height is typically of the seventh order of magnitude O ($10^7$).

The composition of the ullage gas was expressed in terms of N species consisting of N-1 fuel vapor components and atmospheric air. The vaporization rate of the fuel species is expressed in equation 2.1 where rate of evaporation of each component of the fuel is a function of the surface area of the liquid pool, convective heat transfer coefficient, density of the fuel, and the difference between the mass fractions of the component in the gaseous phase from its liquid phase.

$$\dot{m}_{ei} = A_i h_i \rho (y_{fi} - y_{gi}) \qquad i = 1 \ldots\ldots N-1 \tag{2.1}$$

Using the analogy between heat and mass transfer, the species Sherwood number (Sh) was expressed using the Nusselt number (Nu) as shown in equation 2.2. Nusselt number is the ratio of convective to conductive heat transfer across a boundary, and the Sherwood number is the mass transport between the convective and diffusive phases. Schmidt number (Sc) is the ratio of the momentum and mass diffusivities (D), and Prandtl number is the ratio of momentum and thermal diffusivities.[11]

$$Sh_i = \frac{h_i L}{D_i} = Nu \left(\frac{Sc_i}{Pr}\right)^{1/3} \tag{2.2}$$

For the forced convection flow field, the Nusselt number for the horizontal surfaces was estimated using equation 2.3.[11] Reynolds number (Re) is the ratio of inertial forces to viscous forces.[11] The free convection velocity that was calculated for the vertical surfaces was used to obtain the Reynolds number for the horizontal surfaces as well.

$$Nu = 0.664 Re^{1/2} Pr^{1/3} \tag{2.3}$$

For the natural convection flow field, the Nusselt number for the fuel surface was given by equation 2.4,[12] and the Nusselt number for the ceiling of the tank was given by equation 2.5.[11] Rayleigh number (Ra) is the product of Grashof (Gr) and Prandtl

numbers, where the Grashof number is the ratio between the buoyancy forces and viscous forces.[11]

$$Nu = 0.14(Ra)^{1/3} \tag{2.4}$$

$$Nu = 0.27(Ra)^{1/3} \tag{2.5}$$

The aforementioned correlations were applied for flight profiles with low cruising altitudes of 25,000 feet. For flight profiles with cruising altitudes of 34,000 feet, all correlations remained the same except for the free convection flow field correlation at the fuel surface, which is given by equation 2.6.[11]

$$Nu = 0.54(Ra)^{1/4} \tag{2.6}$$

This correlation is applicable for flow fields with Rayleigh numbers ranging between $10^4$ and $10^7$. Since all the flow fields in the ullage of the wing tank are estimated to be in the turbulent regime, vertical mixing is induced within the tank. Consequently, the Nusselt number on the vertical surfaces in the ullage is expressed using forced convection in equation 2.7.[11] The Reynolds number for this correlation is based on the free convection velocity and the height of the ullage.

$$Nu = 0.664Re^{1/2}Pr^{1/3} \tag{2.7}$$

The liquid surface species mole fraction is computed using Henry's Law as shown in equation 2.8.[10]

$$x_{fi} = \frac{x_{li} p_i}{p} \qquad i = 1 \ldots\ldots N-1 \tag{2.8}$$

The gas species mass fractions were related to the species mole fractions by the relationship in equation 2.9.[10]

$$y_i = \frac{x_i M_i}{\sum x_i M_i} \qquad i = 1 \ldots\ldots N-1 \tag{2.9}$$

The liquid density, $\rho_l$, is given by equation 2.10.[10]

$$\rho_l = \frac{\sum x_{li} M_i}{\sum \frac{x_{li} M_i}{\bar{\rho}_{li}}} \qquad i = 1 \ldots\ldots N-1 \tag{2.10}$$

In addition to the vaporization of the fuel in the tank, condensation of vapor species on the tank ceiling and the tank walls were accounted for when the wall temperature was equal or below the dew point temperature of the vapor mixture composition in the ullage. All of the aforementioned equations are used to estimate the condensation rate on the tank ceiling and sidewalls. An assumption is made that the condensation produces a thin static condensate film of spatially uniform but temporally

varying temperature and thickness, with the condensate layer temperature equal to the tank wall temperature.

The species mass balance for the control volume defined by the bulk gas within the tank ullage includes the rate of species vaporization, condensation, and outflow as shown in equation 2.11.[10]

$$\frac{dm_i}{dt} = (\dot{m}_{ci} - \dot{m}_{ei})(1 - \delta_{iN}) \pm \dot{m}_{oi} \qquad i = 1 \ldots \ldots N \tag{2.11}$$

Gases are assumed to follow ideal gas behavior so that $m_i$ is written as:

$$m_i = \frac{x_i M_i p V}{\bar{R} T_g} \qquad i = 1 \ldots \ldots N \tag{2.12}$$

Substituting equation 2.12[10] into 2.11[10] yields the following relationship for the variation of species mole fraction within the gas control volume:

$$\frac{dx_i}{dt} = \frac{\bar{R} T_g}{M_i V_p}\left[(\dot{m}_{ci} - \dot{m}_{ei})(1 - \delta_{iN}) \pm \dot{m}_{oi} - \frac{m_i}{p}\frac{dp}{dt} + \frac{m_i}{T_g}\frac{dT_g}{dt}\right] \qquad i = 1 \ldots \ldots N \tag{2.13}$$

Summation of the terms in equation 2.13[10] over all the species results in the relationship for the total rate of mass inflow (equation 2.14)[10] and mass outflow (equation 2.15)[10] respectively.

$$-\dot{m}_o \sum \frac{1}{M_i} = \sum \frac{1}{M_i}\left[(\dot{m}_{ci} - \dot{m}_{ei})(1-\delta_{iN}) - \sum \frac{m_i}{M_i p}\frac{dp}{dt} + \sum \frac{m_i}{M_i T_g}\frac{dT_g}{dt}\right] i = 1 \ldots N \quad (2.14)$$

$$\frac{\dot{m}_o}{M} = \sum \frac{1}{M_i}\left[(\dot{m}_{ci} - \dot{m}_{ei})(1-\delta_{iN}) - \sum \frac{m_i}{M_i p}\frac{dp}{dt} + \sum \frac{m_i}{M_i T_g}\frac{dT_g}{dt}\right] i = 1 \ldots N \quad (2.15)$$

The ullage control volume energy balance is then given by the following relationship which is used to compute the ullage temperature.

$$\frac{d}{dt}(m_g c_{pg} T_g) = \bar{h}_b A_b (T_b - T_g) - \bar{h}_t A_t (T_g - T_s) - \bar{h}_s A_s (T_g - T_s) + \dot{m}_c H_v + \dot{m}_e c_{pv} T_l - \dot{m}_c c_{pg} T_g + \dot{m}_o c_{pa} T_a \quad (2.16)$$

$$\frac{d}{dt}(m_g c_{pg} T_g) = \bar{h}_b A_b (T_b - T_g) - \bar{h}_t A_t (T_g - T_s) - \bar{h}_s A_s (T_g - T_s) + \dot{m}_c H_v + \dot{m}_e c_{pv} T_l - \dot{m}_c c_{pg} T_g - \dot{m}_o c_{pg} T_g \quad (2.17)$$

The left hand side of equations 2.16[10] and 2.17[10] represents the rate of energy storage; the first three terms on the right hand side of the equation represent rates of heat transfer from the floor, the ceiling and sidewalls respectively. The fourth term represents the latent heat release during condensation, and the last three terms represent the energy transfer associated with the evaporation, condensation, and the inflow (2.16) and outflow (2.17) of vent gas fluid streams respectively.

Species vapor pressures are commonly estimated using either Wagner's or Frost-Kalkwarf-Thodos' equations as indicated by Poling et al.[13] Wagner's equation is used during atmospheric conditions and the Frost-Kalkwarf-Thodos equation is used during sub-atmospheric conditions. The species diffusion coefficients are estimated using

Fuller's method. [13] For the low vapor concentrations considered, the gas viscosity and thermal conductivity used with the non-dimensional parameters in equations 2.2, 2.3, and 2.8 is taken from data in Incropera et al. [11] for pure air at the corresponding liquid-gas film temperature. The ullage gas specific heat, $c_{pg}$, is also that of pure air at the ullage gas temperature. The mean specific heat of the evolving vapors is computed at the liquid-ullage gas film temperature using the correlation in Lefebvre et al.[14] and the mean condensate latent heat of condensation is $3.6 \times 10^5$ J/kg, approximately equal to that of Jet-A at 30°C. [15]

### 2.1.1 Justification for Heat Transfer Correlations Used in the Model

The computational model for CWTs assumed the flow in the ullage to be driven by natural convection between the layer of heated fuel on the floor, and the unheated ceilings and sidewalls when the gas in the ullage is well mixed and the magnitude of the Rayleigh number is typically of the ninth order of magnitude O ($10^9$). When the Rayleigh number is smaller, the model switches to a mode of pure diffusion based on diffusion coefficients and the geometric dimensions of the ullage.

The heat transfer correlation used for the horizontal surfaces of the CWT is given by equation 2.18.[10]

$$Nu = 0.14(Ra)^{1/3} \tag{2.18}$$

The heat transfer correlations used for the vertical surfaces of the CWT was expressed using a correlation for laminar forced convection over a flat plate, as shown in equation 2.19, where the Reynolds number was calculated using the free convection velocity and the height of the ullage.

$$Nu = 0.664Re^{1/2}Pr^{1/3} \tag{2.19}$$

Using the CWT computational model on a WT yields results as shown in Figure 2.3. A time delay between the experimental and computational results can be noted when the pressure within the WT starts decreasing.

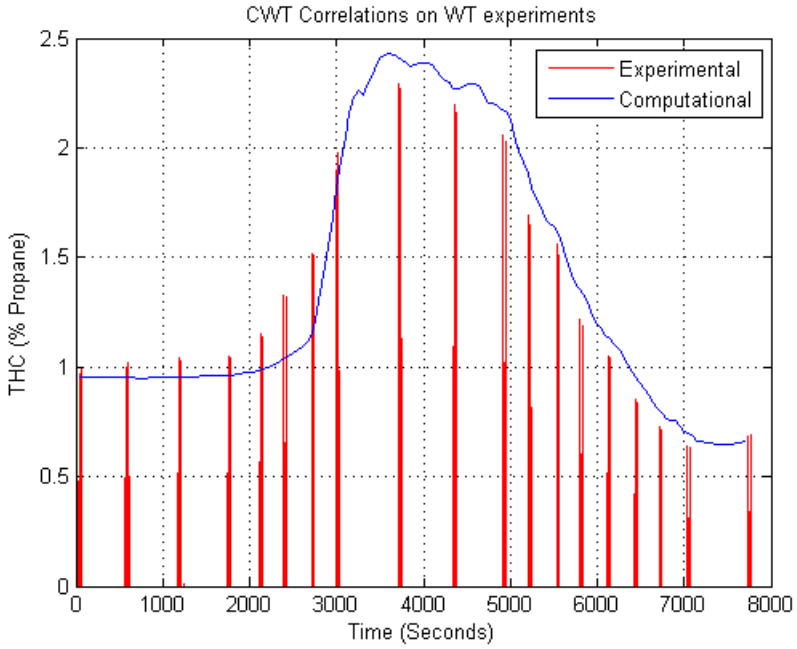


**Figure 2.3 Using CWT correlations on a WT setup**

In an attempt to unearth the source of the time delay, the effect of increasing Rayleigh number was studied as shown in Figure 2.4. The results shown in Figure 2.4 are from experiments run in the altitude chamber with an initial temperature of 80°F, a cruising altitude of 25,000 feet, and a mass loading of 60%. As can be seen, increasing the Rayleigh number had no effect on the time delay of the computational results. Changing the evaporation and condensation rates of the vapor in the ullage also had no significant effect on the time delay of the computational results.

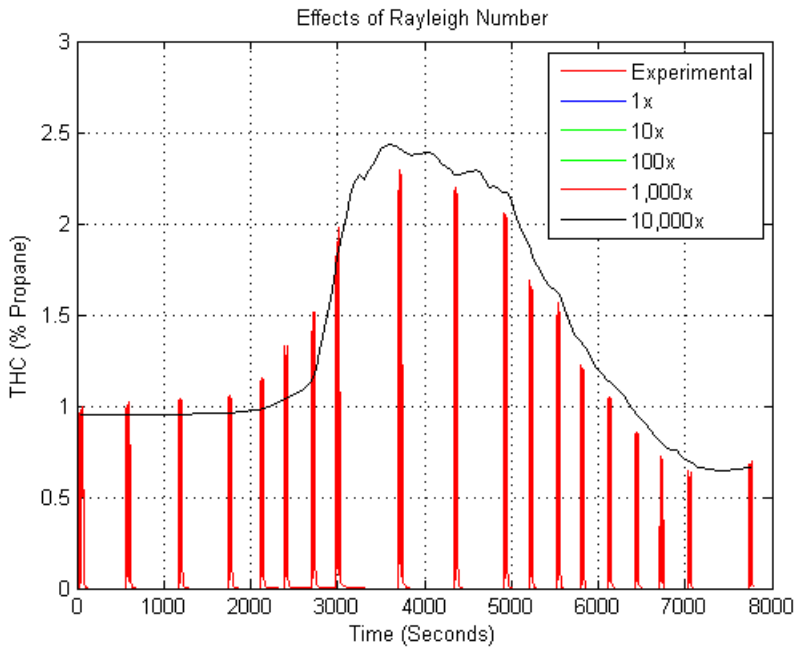


**Figure 2.4 Effects of increasing Rayleigh number**

From the temperature profiles of the experimental run as can be seen in A.1, it can be noted that the THC responds to the changes in the temperatures in the ullage. Hence, it can be said that the time delay is associated with the temperature profiles of the ullage. In order to obtain valid results from the computational model, different heat transfer correlations were used on the vertical and horizontal surfaces of the ullage to note their effect on the prediction of hydrocarbon generation in the ullage. It was noted that in order to predict the increase in THC during the ascent, the mode of heat transfer needed to be changed to a mode faster than diffusion. Figure 2.5 shows the estimated diffusive time scale for an experiment run in the altitude chamber with an initial fuel tank temperature of 80°F, 60% mass loading and the achieved cruising altitude being 25,000 feet. The time scale is calculated using equation 2.20[11], where x is the height of the ullage, D is the diffusion coefficient, and t is the time scale. The diffusion coefficient is estimated using

equation 2.21[11], where P is the pressure measured in Pascals and T is the temperature measure in degrees Kelvin. The analysis shows that the time scale of the diffusive process in the ullage of a wing tank is in the range of 0.1 to 0.3 seconds. The time step for the computational model to reach a quasi steady state of equilibrium is in minutes. This shows that the diffusive process is fast enough to cause rapid thermal changes within the ullage. Hence, changing the heat transfer correlations to forced convection over a flat plate on all surfaces in the ullage during the ground and ascent stages of the flight ensured the computational model would follow the trend of the experimental results as seen in Chapter 4 of this thesis.

$$x \approx 2\sqrt{Dt} \tag{2.20}$$

$$D \approx P^{-1}T^{3/2} \tag{2.21}$$

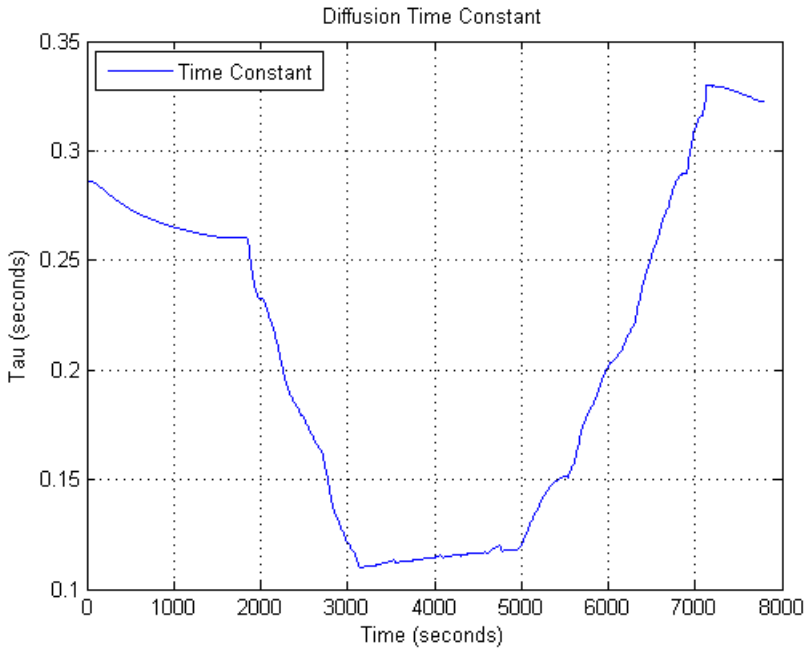


**Figure 2.5 Estimated diffusive time constant calculated from an experiment run in the altitude chamber with an initial fuel tank temperature was 80°F, cruising altitude achieved was 25,000 feet, 60% mass loading**

The faster mode of heat transfer during the ground and ascent stages of the flight profile suggests that the change in temperature in the ullage has an immediate effect on THC. It can be said that this computational model does not apply theoretically to the prediction of vapor generation in the ullage of a wing tank with the heat transfer correlations used, but by altering the heat transfer correlations to speed up the time response of the activity in the ullage, the model can be made to predict the generation of flammable vapors in the ullage of a WT.

## 2.2 Fuel Characterization

The fuel used in the tests, commonly known as Jet-A or JP-8, is a multi-component fuel that consists of a very large number of species. The components are predominantly paraffins, but can include cycloparaffin, aromatic, olefin, and other hydrocarbons. Each of these components has unique chemical properties such as molecular weight, boiling point, and vapor pressure. The overall liquid fuel takes on unique properties that depend entirely on the quantity and properties of the individual components. Hence, fuel specifications usually are expressed in terms of allowable ranges of properties that reflect physical, chemical, and combustion behavior of the fuel rather than a specific chemical composition.[15] Equilibrium vapor pressure calculations can be made for a fuel with a known composition that account for the vapor pressures of the individual components.

Jet fuels can be characterized by speciation using a gas chromatograph combined with a flame ionization detector. This method characterizes the fuel at its flash point. Over 300 hydrocarbons could be used to fully characterize a single batch of Jet-A and JP-

8. Albeit speciation characterizes the fuel comprehensively, it is not the most efficient or effective method to characterize the fuel in order to model it.

Woodrow et al.[16] has shown that for the prediction of the overall vapor pressure of JP-8 samples at temperatures common to those of a fuel tank, it is sufficient to characterize the fuel using a number of *n*-alkane reference hydrocarbons as determined by gas chromatography. This technique effectively reduces the number of components to model from over 300 to just sixteen alkanes that range from C5 to C20. This work portrays the liquid composition of the JP-8 samples with different flash points, in terms of the mole fractions of the C5 to C20 alkanes. The flash point does not determine the composition of a complex liquid fuel such as Jet-A. However, data obtained from Shepherd et al.[17] with Jet-A samples of different flash points illustrates that vapor pressures at their equilibrium at different temperatures decreased with increasing flash point. Hence, the data from Woodrow et al. [16] and Shepherd et al. [17] suggests that fuel flash points, combined with characterization in terms of the normal alkanes can be used to choose the fuel composition suitable for estimating liquid vapor equilibrium and multi-component fuel vaporization from a fuel tank. The range of fuel flash points for the fuels used in Shepherd et al. [17] was between 120°F and 125°F (~322 K and ~325 K), while the flash point range in Ochs et al.[18] was between 115°F and 120°F (~319 K and ~322 K). Table 2.1 shows the species mole fractions and flash point of three different Jet-A liquid fuel compositions.

| No. of Carbon Atoms | Fuel 1 FP = 322.3 K | Fuel 2 FP = 325.2 K | Fuel 3 FP = 319.7 K |
|---|---|---|---|
| 5 | 0.005 | 0.032 | 0.05 |
| 6 | 0.03 | 0.22 | 0.16 |
| 7 | 0.96 | 1.08 | 1.10 |
| 8 | 5.01 | 2.85 | 4.02 |
| 9 | 11.50 | 7.77 | 12.80 |
| 10 | 21.70 | 15.60 | 26.21 |
| 11 | 23.80 | 20.00 | 24.40 |
| 12 | 17.30 | 18.10 | 16.90 |
| 13 | 9.84 | 15.20 | 9.08 |
| 14 | 5.37 | 10.50 | 3.90 |
| 15 | 2.95 | 5.49 | 1.15 |
| 16 | 1.11 | 2.10 | 0.20 |
| 17 | 0.42 | 0.82 | 0.02 |
| 18 | 0.012 | 0.13 | 0.01 |
| 19 | 0.00 | 0.112 | 0.00 |
| 20 | 0.00 | 0.00 | 0.00 |

**Table 2.1 Percentage mole composition and flash point of three Jet-A liquid composition.[16]**

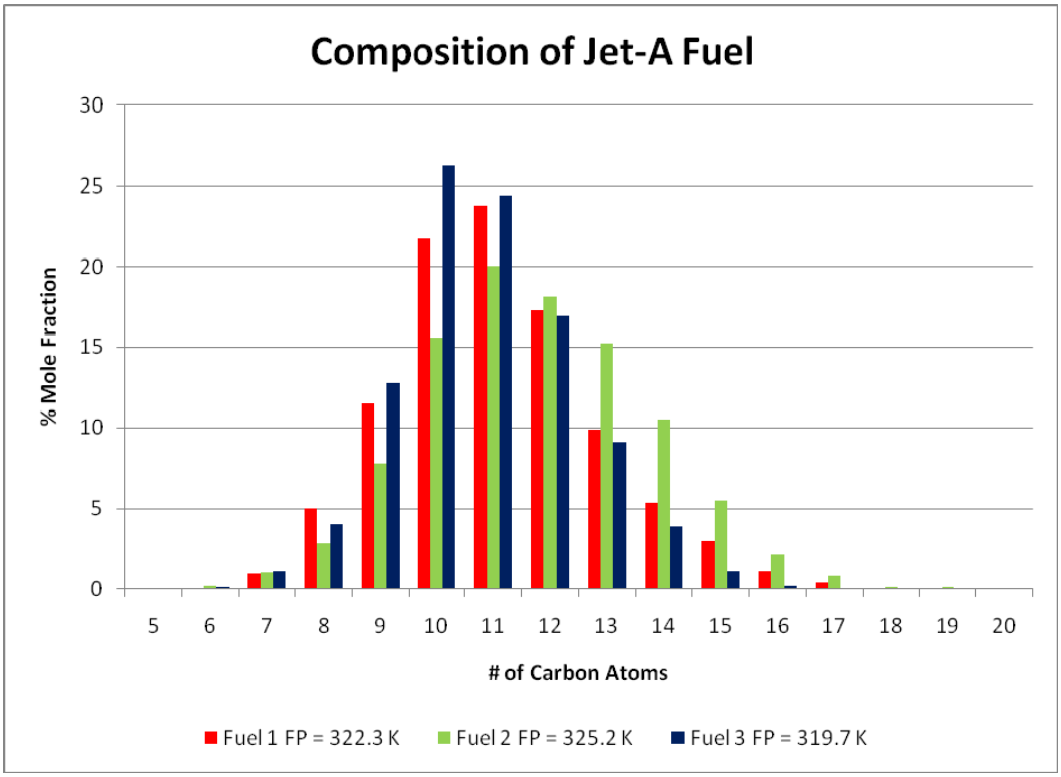


**Figure 2.6 Composition of Jet-A Fuel**

# Chapter 3

# Validation Experiments

## 3.1 Experimental Setup

All experiments were performed at the William J. Hughes Technical Center facility in Atlantic City, New Jersey with the support and supervision of the Fire Safety Team of the Federal Aviation Administration's Airport and Aircraft Research and Development Division. The setup was designed to study the effect of the varying temperature and pressure conditions on hydrocarbon concentrations in the ullage. The tank used for the experiment was subjected to varying fuel, surface, and ambient temperatures and sub-atmospheric pressures while containing high mass loadings of jet fuel. All data was collected on a computer with a data acquisition system. The software was designed and setup by the engineers working at the center.

### 3.1.1 The Altitude Chamber

The experiments were performed in FAA's environmental chamber, as shown in Figure 3.1. Inner dimensions of the chamber were 1.83m x 1.83m x 2.448m. The chamber was capable of controlling the temperature to as low as -100°F, via a cascade-type air conditioning unit. Pressure was reduced to simulate flight conditions using a vacuum pump attached to the chamber. The pressure in the chamber was controlled manually with a release valve that varied the rate at which a vacuum was created in the chamber. Temperature and pressure within the chamber were monitored with integrated

thermocouples and a pressure gauge.

**Figure 3.1 Fuel tank placed in the altitude chamber**

### 3.1.2 The Fuel Tank

The fuel tank, as shown in Figure 3.2, was constructed using 0.635cm thick aluminum sheets cut to size and welded to form a cube with outer dimensions of 0.914m x 0.914m x 0.610m. Two access panels measuring 0.305m x 0.457m were located on the top surface. The first access panel consisted of an aluminum plate with openings for thermocouple pass-thru, ullage sampling, and ullage venting. The second access panel was fitted with an aluminum frame which encompassed the borders of the opening, while an aluminum foil was used to cover the opening. This served as a pressure relief mechanism in the event of any reaction and/or explosion within the tank. In addition, it

helped in the fueling and emptying of the tank while also providing access to the inside of the tank enabling proper placement of all instrumentation. The tank was placed on a 0.610 m high stand in order to move the tank in and out of the chamber with ease. It was also helpful in draining the tank through a 0.635cm valve in the bottom of the tank.

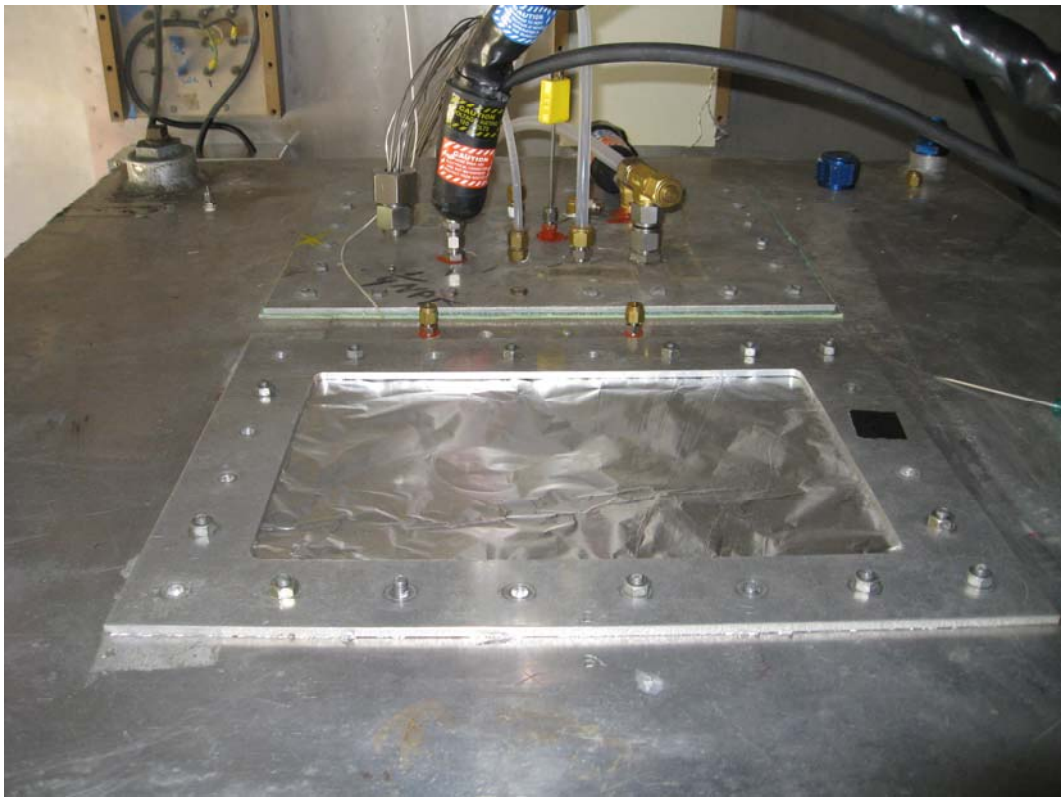

**Figure 3.2 Fuel tank instrumented with thermocouples and hydrocarbon analyzer sample lines.**

### 3.1.2.1 Temperature Measurement

The fuel tank was equipped with eleven K-type thermocouples placed at different points throughout the tank. Seven thermocouples were 1/16” flexible thermocouples, and four were 1/16” surface mount thermocouples. Three thermocouples were placed in the ullage, two were placed in the fuel, two on the sides of the tank, one at the surface of the

fuel, one on the bottom surface, one on the top surface, and one was placed outside the tank to measure the ambient air temperature.

#### 3.1.2.2 Hydrocarbon Analyzer

A flame ionization detector (FID) type hydrocarbon analyzer, as shown in Figure 3.3, was used to measure the THC in the ullage of the fuel tank in terms of volumetric concentration relative to the calibration gas. The calibration gas used throughout the testing was propane. The analyzer used in the experiments uses a fuel that is a 40%/60% mixture of hydrogen and helium. The flame burns at a temperature at which most organic compounds are pyrolyzed, producing positively charged ions and electrons. A potential difference is applied between two electrodes near the burner. The electrons are drawn towards the high voltage electrode and the ions are attracted towards the collector electrode. The ions at the collector plate induce a current upon touching the plate. This current is directly proportional to the amount of hydrocarbons in the sample and provides an accurate THC measurement in terms of volumetric concentration relative to the calibration gas. The calibration gas used in this experiment was propane.


**Figure 3.3 Flame ionization detector hydrocarbon analyzer**

To prevent condensation within the vapor sample, all sample lines leading to the analyzer were heated and maintained at 93°C using temperature controllers and insulated rope heaters. The pump built into the analyzer was not able to maintain the sample pressure at low ambient pressures. Therefore, the sample lines were attached to a pump with heated heads which drew the sample from the tank at sub-atmospheric pressures during the testing. The pump heads were also maintained at 93°C by utilizing temperature controllers.

In order to verify that the ullage was well mixed, samples were taken at two separate locations using two heated lines. One sample line was drawing a sample half an inch away from the ceiling of the tank, whereas the other line was drawing a sample six inches from the ceiling of the tank.

## 3.2 Experimental Procedure

The general purpose of the experiments was to generate a data set that can be used to validate the computational model built to calculate the hydrocarbon concentrations in the ullage of a wing tank during typical ground and flight conditions. The starting conditions played an important role in the calculations; hence it was necessary for the system to reach equilibrium before the experiment was started. To achieve this, the fuel was allowed to sit in the tank overnight to reach equilibrium. The tank was in the altitude chamber which was closed to maintain a constant temperature.

### 3.2.1 Jet Fuel

The jet fuel used in the testing was obtained from the Atlantic City International Airport which was delivered to a fuel storage facility near the test site. The fuel needed for each test was then pumped into two fuel drums and loaded onto a pickup truck. The truck was then driven over to the altitude chamber to deliver the fuel into the experimental fuel tank. Once the fuel was loaded into the fuel tank, the empty fuel drums were stored outside the laboratory due to Technical Center safety regulations. After the experiments were run the following day, the used fuel was then collected in the fuel drums and dumped into a large underground fuel tank just outside the laboratory. This used fuel in the underground fuel tank was used by two jet engines that power an Air Induction Wind Tunnel Facility in the same location. It is possible for the fuel to be reused by the jet engines because the fuel is only heated during the experiments. Since a large amount of fuel was used during the testing, three different batches of fuel were used

during experimentation. A sample from each batch of fuel was sent to a Fuels Research Facility at the Technical Center to measure its flash point.

### 3.2.2 Hydrocarbon Analyzer

The hydrocarbon analyzer required a warm-up procedure in order to obtain accurate readings. The analyzer took approximately 4-5 hours to warm-up; hence the analyzer was turned on a day before the beginning of testing and was run until the end of the week. The procedure began with turning on the burner oven heater and the heated sample lines. The oven temperature stabilized at 93°C, and then the sample pump was switched on and allowed to run for approximately 30 minutes. Then the flame in the FID was lit by purging the fuel and sample lines for 1 minute and then pressing the igniter button. Once the flame was lit the analyzer was subjected to natural air, for 30 minutes, to obtain a zero hydrocarbon concentration. Then 2% propane was passed through the analyzer to calibrate it to 20,000 ppm. Then 4% propane was passed through the analyzer to verify if the analyzer read 40,000 ppm. This linearity check allowed for a hydrocarbon concentration range from 0 to 40,000 ppm, which was adequate for all the tests performed. A sample from the ullage of the tank was taken every 10 minutes from each heated line, except when the chamber was experiencing ascent and descent. During ascent or descent a sample was drawn from each heated line every 5 minutes. The reason for sampling the ullage at certain time steps instead of sampling it continuously was that at higher altitudes the FID would draw more than the necessary amount required. This extra air would then be wasted by dumping it out into the laboratory. Also, once the FID drew the sample, hydrocarbon free air from the chamber would flow into the tank, which

would dilute the sample and cause the FID readings to be false. Taking into consideration the high response time of 0.2 seconds of the FID, flow rate of the sample pump, and the length of the sample lines a sample time of 30 seconds was agreed upon to avoid excess air from getting into the tank. Due to the multiple sample lines, the sample was first drawn from the port half an inch away, after which it would draw a sample from ambient air, and then it would draw a sample from the port four inches away.

### 3.2.3 Flight Profile

The flight profile is the temporal variation of the pressure and temperature for the duration of the flight. A sample flight scenario that mimicked a routine flight was constructed for the testing. It consisted of average ascent and descent rates that have been used in similar experimental setups. Figure 3.4 shows the flight profile that was used for the tests. The flight scenario created consisted of a period of 30 minutes at sea level which mimics the period of time during which the plane sits on the ground for boarding, refueling etc. It is during this time that the wing tanks warm up through radiation from the sun. The scenario then changes to the plane ascending to an altitude of 34,000 feet at the rate of 1133.33 feet per minute. The plane then cruises at this altitude for 30 minutes, after which it begins its descent at the rate of 680 feet per minute. The plane then rests on the ground for 10 minutes which concludes the round of testing.

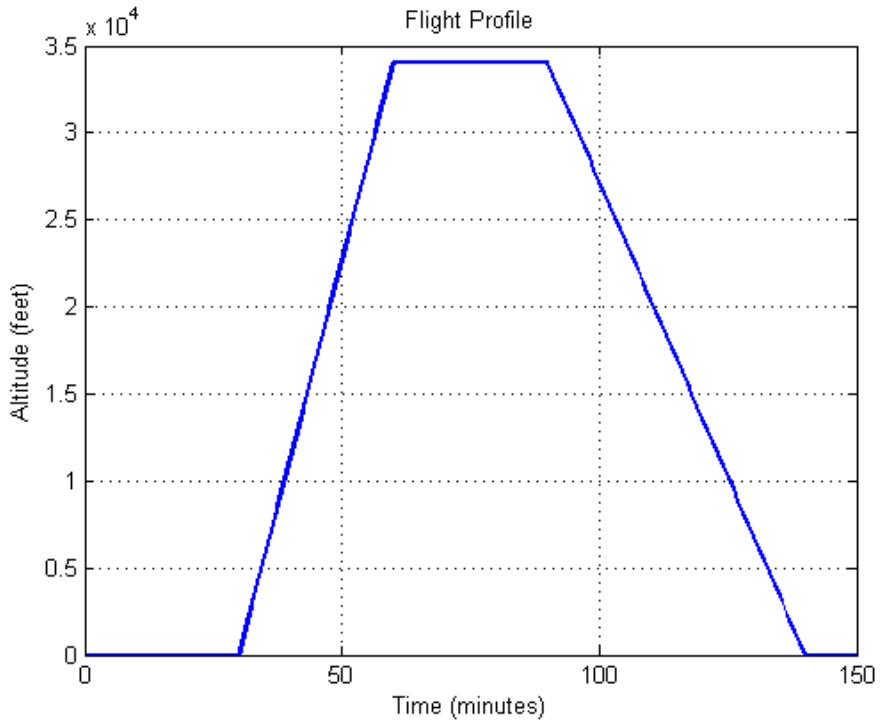


**Figure 3.4 Flight profile with a cruising altitude of 34,000 feet.**

The equation shown below converts a known altitude into pressure, and it was used because the instrumentation controlled the altitude chamber with a pressure gauge. This formulates a pressure profile as shown in Figure 3.5.

$$P = \left( \frac{Alt}{145450} + 1 \right)^{5.2561} \bullet 14.7 \tag{3.1}$$

where:
P: pressure in psi.
Alt: altitude in feet.

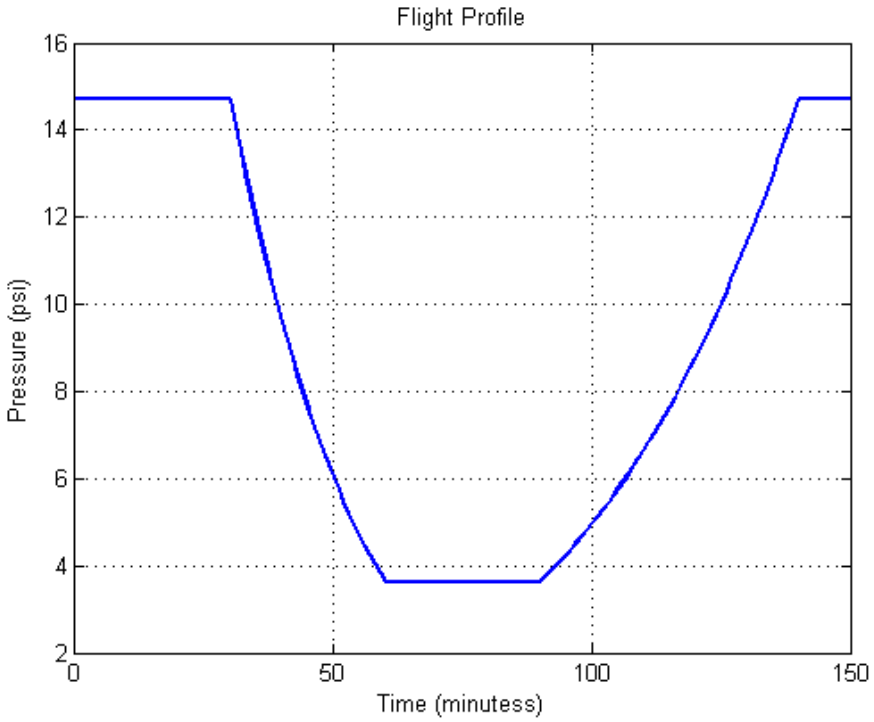


**Figure 3.5 Pressure profile with a cruising altitude of 34,000 feet.**

The output obtained from the pressure transducer during the experiments fluctuated substantially due to the sensitivity of the pressure transducer. The model calculations were sensitive to the pressure, since these pressure changes were used to calculate the inflow and outflow of ambient air in and out of the tank respectively. The inflow of air into the tank can reduce the ullage vapor concentration whereas the outflow of air can increase the ullage vapor concentration. Hence the pressure profiles used in the computations were averaged to refine the data.

### 3.2.4 Heating System

A Workforce overhead radiant space heater shown below in Figure 3.6 was used during the experiments. It was a 1500 watt quartz heater with a pull chain switch capable

of producing 5200 Btu per hour. The heater was attached to the ceiling of the altitude chamber directly above the center of the tank to ensure the top surface of the tank was being heated evenly. Once the tank had reached a state of quasi equilibrium, the heater was turned on to its lowest setting for the first 30 minute period of the testing. The top surface temperature increased at an average rate of 1°F/minute over the initial 30 minute time period that the heater was turned on.

**Figure 3.6 Workforce overhead radiant space heater.**

## 3.3 Test Matrix

Several tests were performed to generate data that can be used as inputs for the computational model and also to compare computational and experimental results. Tests were performed at two mass loadings, two cruising altitudes, and three starting temperatures. Table 3.1 shows in detail the tests that were performed. Three different sets

of fuels were used for the experiments And each were tested to determine their flash point values. The flash points were measured to be between 125°F and 130°F.

| | 60% Mass Loading | | 80% Mass Loading | |
|---|---|---|---|---|
| | Cruising Altitude | | Cruising Altitude | |
| Temperature | 25000 feet | 34000 feet | 25000 feet | 34000 feet |
| 80°F | X | X | X | X |
| 90°F | X | X | X | X |
| 100°F | X | X | | |

**Table 3.1: Test matrix.**

## 3.4 Model Calculations

The data obtained from these tests performed in the altitude chamber were converted into text files to be used by the code as input data. The input files were comprised of fuel surface temperature, average ullage temperature, top wall temperature, modified ambient pressure, and the ambient temperature. The fuel properties obtained from Woodrow et al.[16], such as mole fractions of C5 to C20 alkanes, their corresponding boiling points and densities, and coefficients from Wagner's equations were also placed into the code, as text files, to be used as inputs.

# Chapter 4

# Results from the Altitude Chamber

## 4.1 Post-Processing

The output obtained from the computation was in the form of text files. These files were read by MATLAB in order to generate graphs that compared the experimental results to the computational results. A short code was written in order to read the output files, perform simple mathematics, and some data reduction algorithms.

## 4.2 Computational Results

Figures 4.1 through 4.10 show the results from the experiments performed in the altitude chamber. The titles in each of the figures describe the conditions under which the experiments were run. For example, “100 F, 34000 feet, 60% loading” would indicate that at the beginning of the test, all the temperatures stabilized at 100°F. The cruising altitude for the test was 34,000 feet, and that the fuel tank had a mass loading of 60%. Each graph also has 4 different lines representing the computational results for different flash point values. The data points denoted by “x” notations indicate the experimental values observed during the experimental testing.

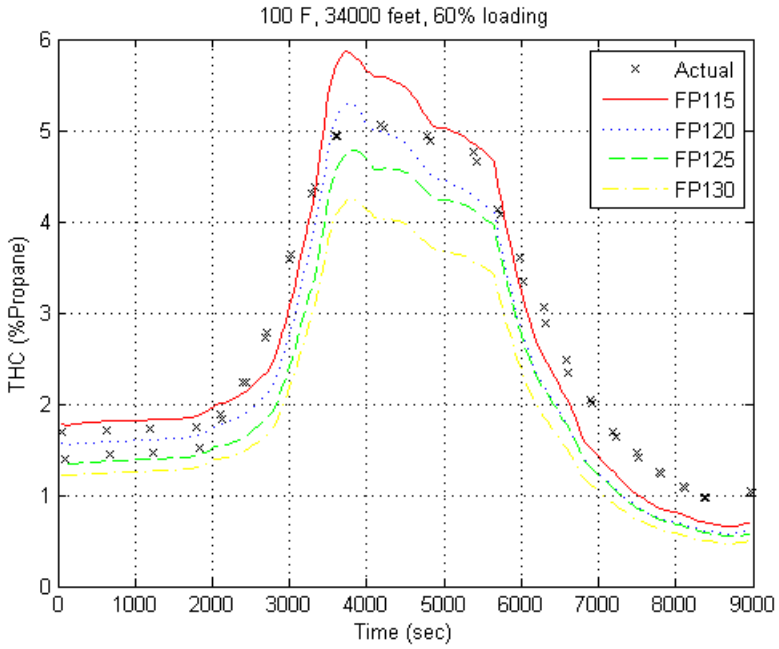


**Figure 4.1: Comparison of computational values calculated using the wing tank flammability model with measured experimental results obtained from tests run in an altitude chamber. Initial fuel tank temperature was 100°F, cruising altitude achieved was 34,000 feet, 60% mass loading**

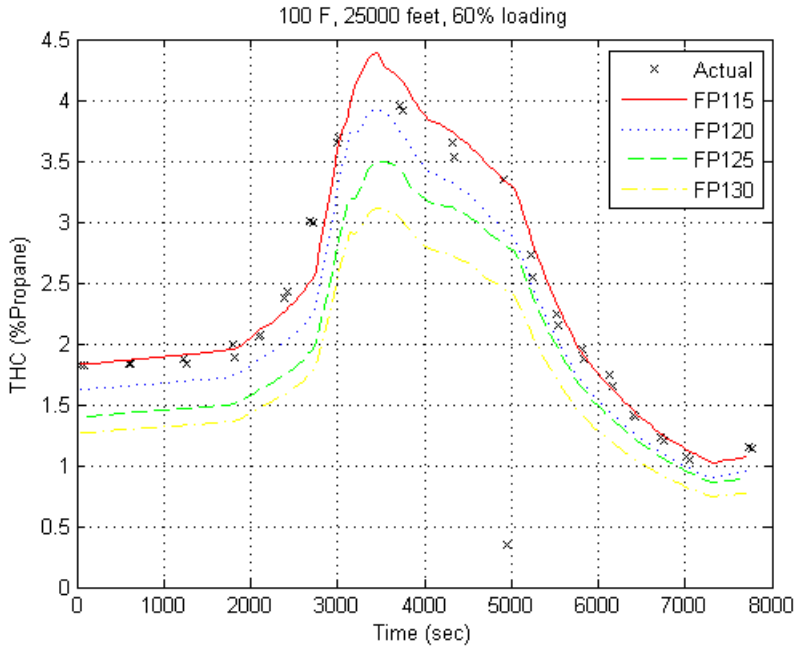


**Figure 4.2: Comparison of computational values calculated using the wing tank flammability model with measured experimental results obtained from tests run in an altitude chamber. Initial fuel tank temperature was 100°F, cruising altitude achieved was 25,000 feet, 60% mass loading**

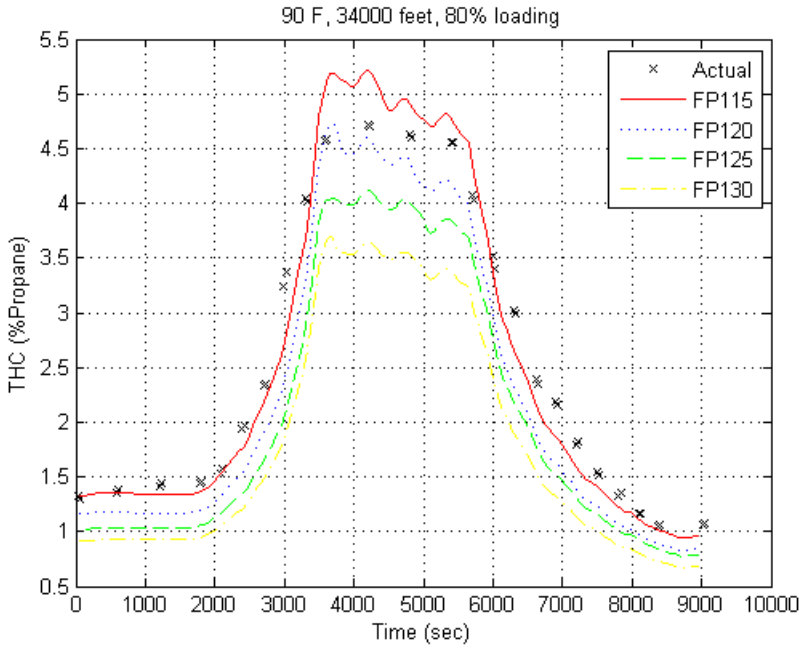


**Figure 4.3: Comparison of computational values calculated using the wing tank flammability model with measured experimental results obtained from tests run in an altitude chamber. Initial fuel tank temperature was 90°F, cruising altitude achieved was 34,000 feet, 80% mass loading**

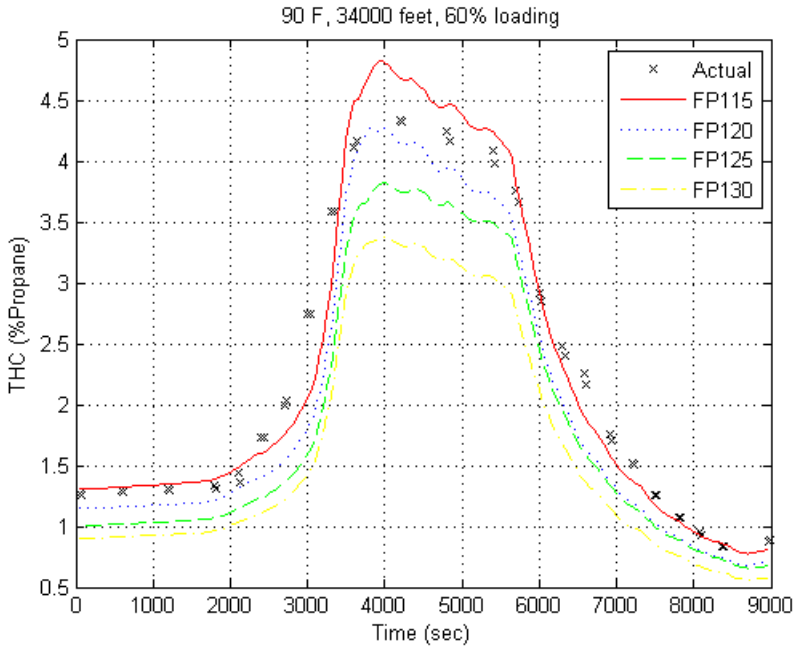


**Figure 4.4: Comparison of computational values calculated using the wing tank flammability model with measured experimental results obtained from tests run in an altitude chamber. Initial fuel tank temperature was 90°F, cruising altitude achieved was 34,000 feet, 60% mass loading**

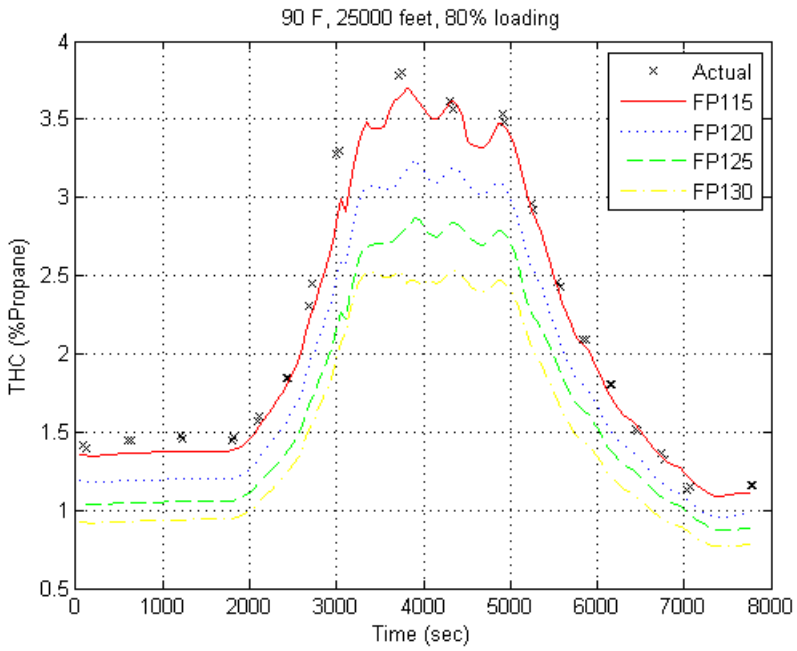


**Figure 4.5: Comparison of computational values calculated using the wing tank flammability model with measured experimental results obtained from tests run in an altitude chamber. Initial fuel tank temperature was 90°F, cruising altitude achieved was 25,000 feet, 80% mass loading**

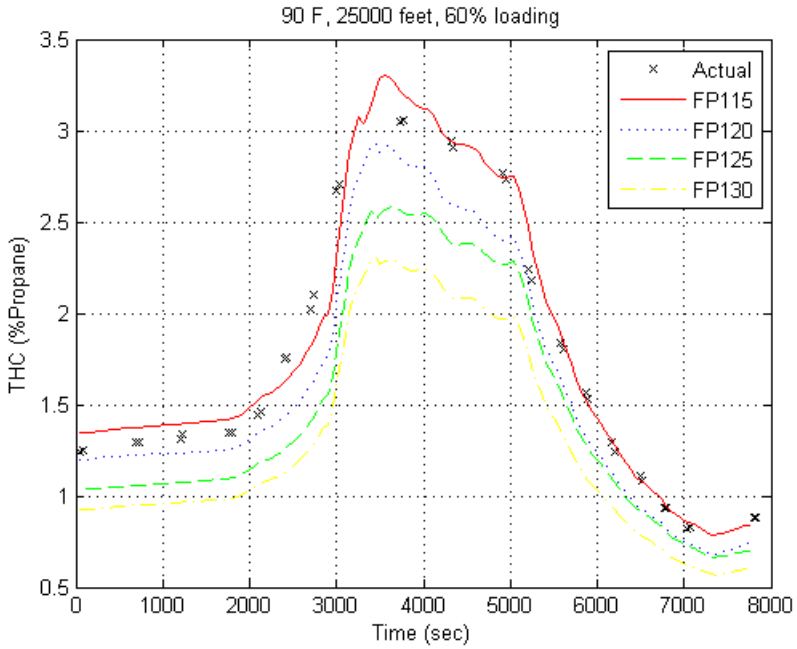


**Figure 4.6: Comparison of computational values calculated using the wing tank flammability model with measured experimental results obtained from tests run in an altitude chamber. Initial fuel tank temperature was 90°F, cruising altitude achieved was 25,000 feet, 60% mass loading**

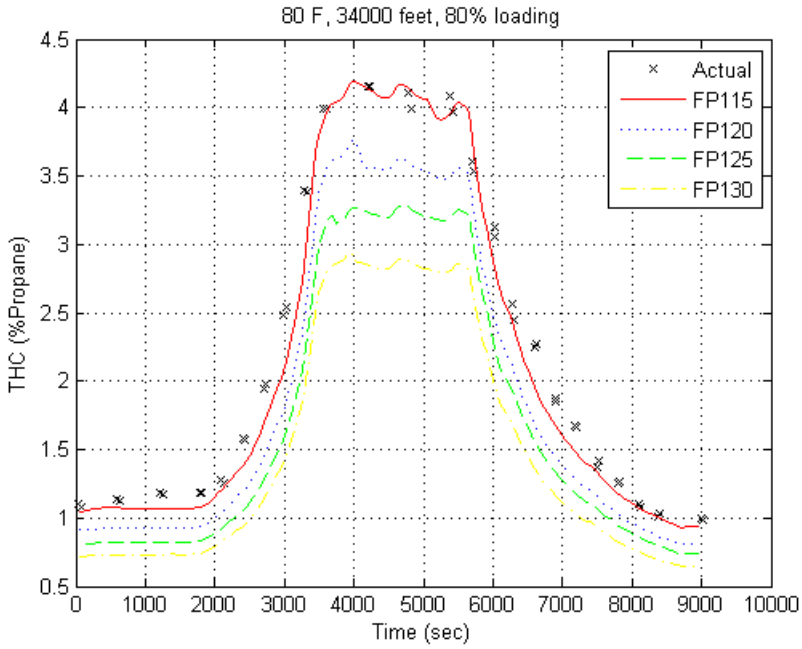


**Figure 4.7: Comparison of computational values calculated using the wing tank flammability model with measured experimental results obtained from tests run in an altitude chamber. Initial fuel tank temperature was 80°F, cruising altitude achieved was 34,000 feet, 80% mass loading**

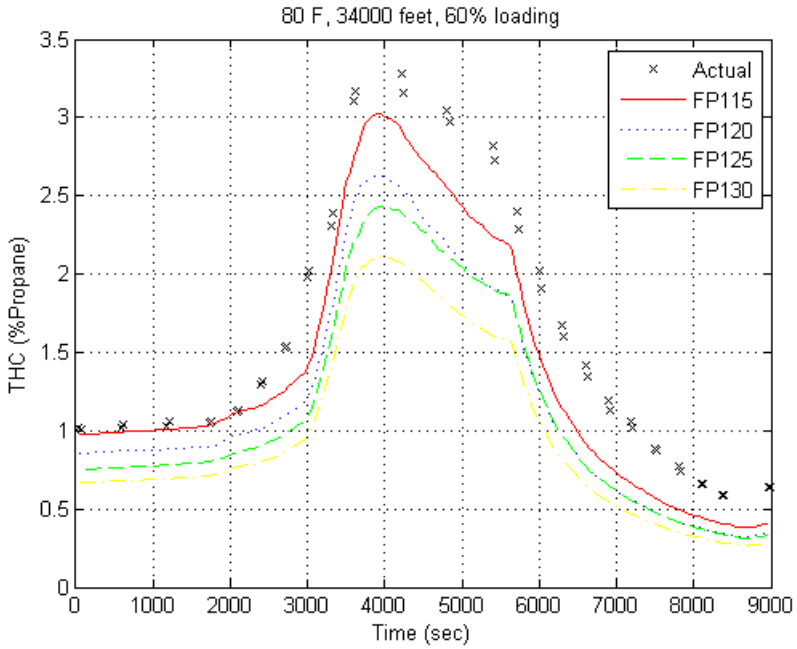


**Figure 4.8: Comparison of computational values calculated using the wing tank flammability model with measured experimental results obtained from tests run in an altitude chamber. Initial fuel tank temperature was 80°F, cruising altitude achieved was 34,000 feet, 60% mass loading**

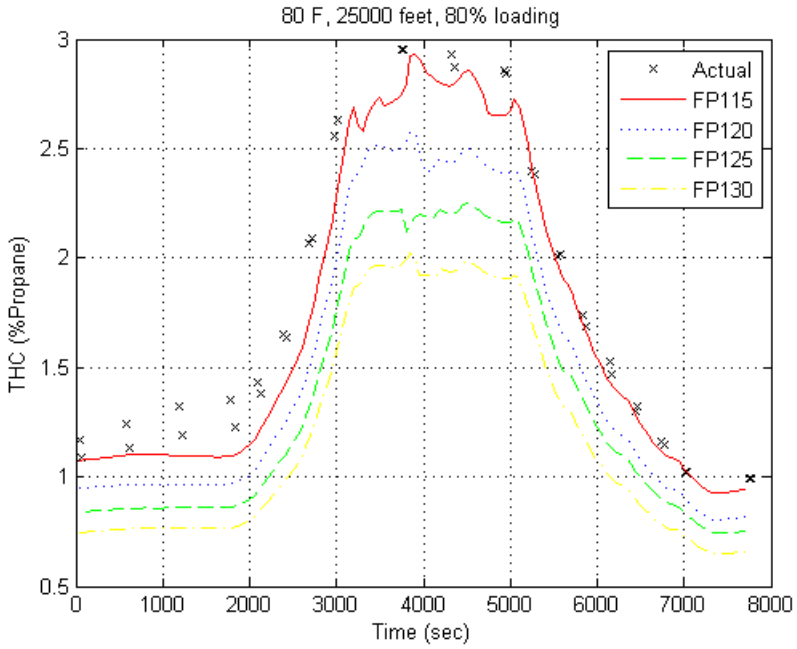


**Figure 4.9: Comparison of computational values calculated using the wing tank flammability model with measured experimental results obtained from tests run in an altitude chamber. Initial fuel tank temperature was 80°F, cruising altitude achieved was 25,000 feet, 80% mass loading**

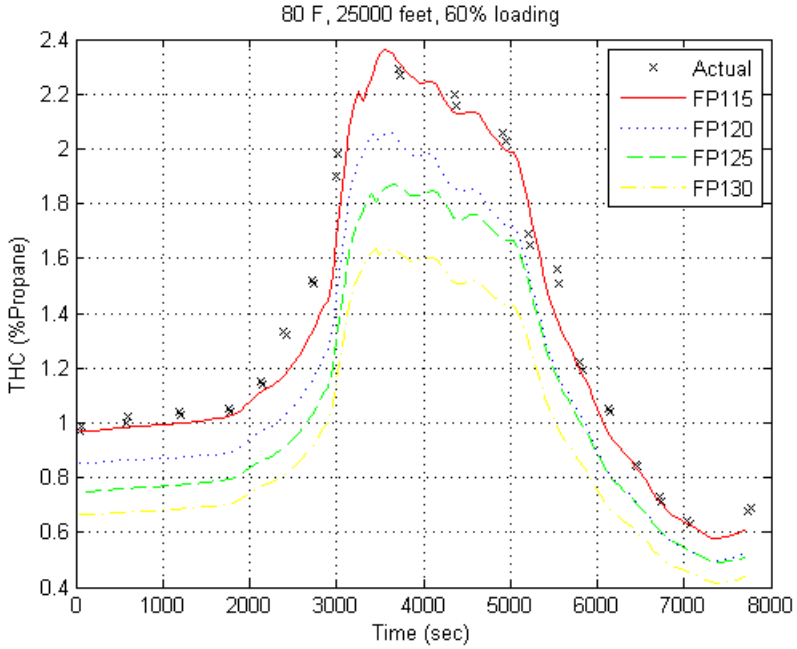


**Figure 4.10: Comparison of computational values calculated using the wing tank flammability model with measured experimental results obtained from tests run in an altitude chamber. Initial fuel tank temperature was 80°F, cruising altitude achieved was 25,000 feet, 60% mass loading**

The results from the experiments conducted in the altitude chamber are in good agreement with the computational data. Most of the experimental data lies near the flash point values of 115°F although all the fuel used in the experiments had a flash point between 125°F and 130°F. This phenomenon can possibly be explained by the replenishment of lower flash point species at the surface of the fuel. The bulk of the fuel is in a stable configuration and due to the temperature difference throughout the fuel and the amount of fuel present in the tank; the species with low flash points diffuse to the surface of the fuel which then evaporates into the ullage. The model takes into account the evaporation of these species into the ullage, which would emulate a fuel with lower flash point. In the case of the CWT, due to the presence of a small amount of fuel in the tank, the species with low flash points are depleted from the fuel. Hence, it can be said that for the case of a WT the flash point of the fuel at the fuel surface is not well represented by the flash point of the fuel at the beginning of the test. From the results seen above one can conclude that the computations follow the trend of the experimental results.

Another reason for this phenomenon to occur can be explained by the work done by Woodrow et al.[16] The liquid and vapor composition of the CWT, which has a low mass loading, will be substantially different from the WT, which has a high mass loading. This is due to the depletion of the more volatile components, lower carbon number alkanes, from the liquid fuel and their under-saturation in the vapor leading to measurably lower total vapor pressures for fuels with a low mass loading. Hence a different approach is needed to estimate vapor compositions of fuels with higher mass loadings.

## 4.3 Discussion of Results

After observing the results from the experiments run in the altitude chamber, one can propose a hypothesis on the relation between THC and initial temperature and THC and pressure. These effects are observed and described in this section.

### 4.3.1 Effects of Temperature

The relation between THC and initial temperature was studied. Figure 4.11 illustrates the observed experimental values of THC under three different initial temperature conditions. All three cases have the same flight profile with a cruising altitude of 25,000 feet, and the same mass loading of 60%. The lowest line depicts an initial temperature of 80°F, above which is the line depicting an initial temperature of 90°F. The top most line depicts an initial temperature condition of 100°F. From the graph it can be deduced that under the same loading conditions and pressure profile, the THC increases with an increase in the initial temperature.

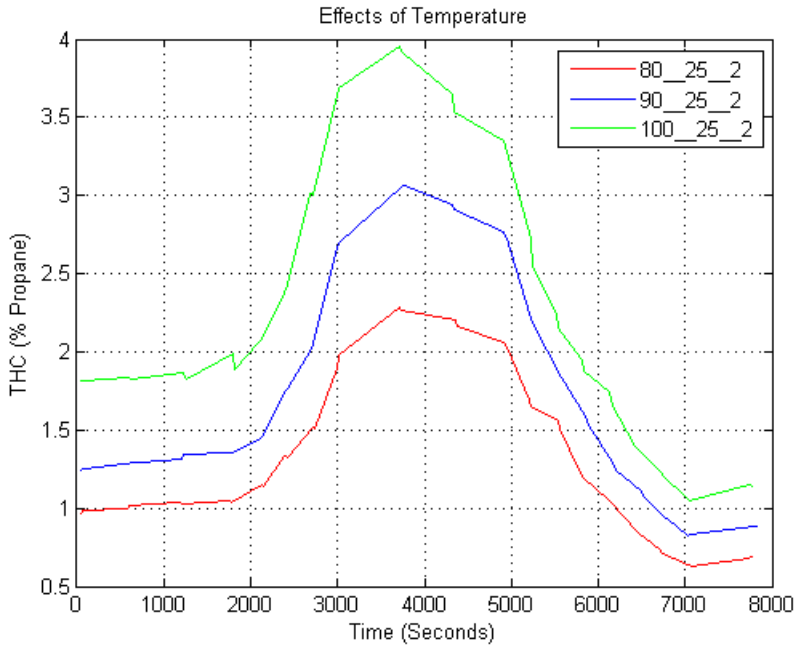


**Figure 4.11 Effects of temperature on the generation of flammable vapors in the ullage of wing tanks**

### 4.3.2 Effects of Pressure

The relation between THC and pressure at the cruising altitude was studied. Figure 4.12 illustrates the observed experimental values of THC under two different initial temperature conditions. All the cases are at a mass loading of 60%, and at each initial temperature condition two different flight profile cases are shown. The cases with a flight profile consisting of a cruising altitude of 25,000 feet are depicted with a solid line, and the cases with a flight profile consisting of a cruising altitude of 34,000 feet are depicted with a dashed line. From the graph it can be deduced that at the same initial temperature conditions and mass loading, the THC increases as the altitude increases. This phenomenon occurs because at high altitudes the air in the ullage is vented out of the tank to ensure the pressure in the tank is the same as the ambient pressure. During an

ambient pressure drop, if the liquid stays at a constant temperature, the liquid vapor pressure is constant as well. At high altitudes, there is less air present in the ullage, hence the overall volumetric concentration of fuel in the ullage increases.[18]

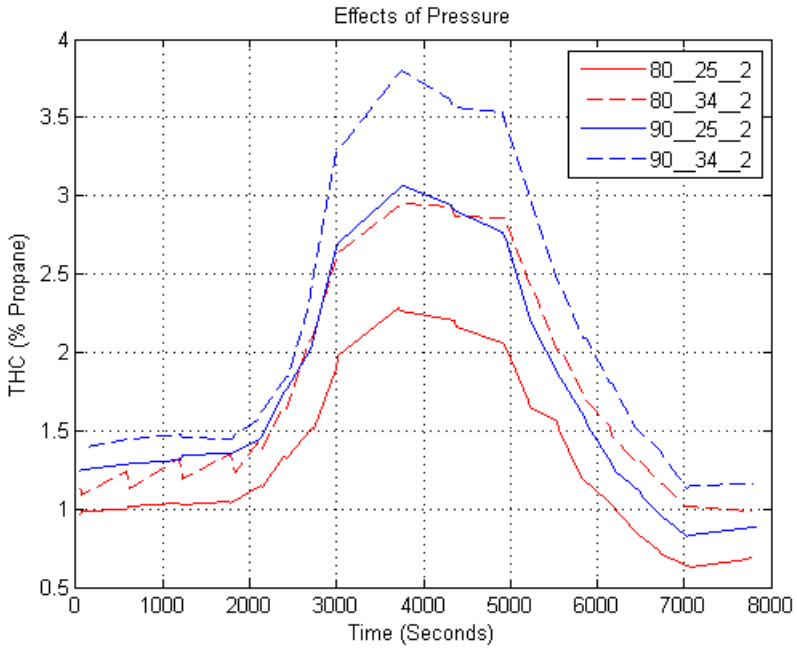


**Figure 4.12 Effects of pressure on the generation of flammable vapors in the ullage of wing tanks**

### 4.3.3 Effects of Mass Loading

The effect of mass loading on THC was studied. Figure 4.13 illustrates the observed experimental values of THC under the same initial temperature condition and flight profile. The only difference between the two tests is the mass loading of 60% and 80%. The case with a mass loading of 60% is depicted with a solid line and the case with a mass loading of 80% is depicted with a dashed line. It can be inferred that at high altitudes, THC increases at a higher mass loading. This trend is expected since there is more fuel available in the tank that can evaporate to form flammable mixtures.[7] Another

valid explanation for this trend can be the fact that at the higher mass loading the ullage is 50% smaller than at the lower mass loading. Hence, the surface area of the sidewall is reduced, which reduces the surface on which the vapor can condense while the evaporation rate stays the same. Hence, this increase in THC value due to the effect of mass loading is justified by more evaporation and less condensation within the ullage of the WT.

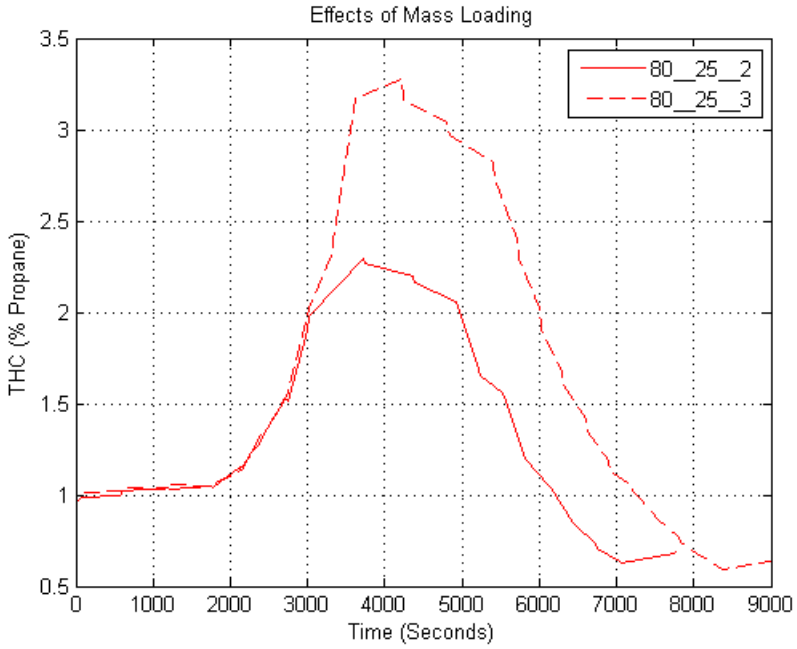


**Figure 4.13 Effects of mass loading on the generation of flammable vapors in the ullage of wing tanks**

# Chapter 5

# Results from Experiments Run by the FAA

## 5.1 Air Induction Facility Tests

The FAA has accumulated experimental data to understand wing tank flammability in commercial aircraft.[9] Tests have been run in the environmental chamber as well as the air induction facility to examine variables that affect the flammability of the ullage space in a commercial aircraft. The intent of this research is to compare the data obtained from these tests to data obtained from flight tests in an effort to gauge the fleet average flammability exposure time.

### 5.1.1 Air Induction Facility

The airflow induction facility, as shown in Figure 5.1, is a wind tunnel facility that has two test sections. One is a high speed test section with a 1.68 m diameter, which can generate commercial transport airplane flight speeds at a reduced static pressure. The second is a low speed test section with a 2.74 m octagon cross section that can generate wind speeds of 120 miles per hour. The wind tunnel is a unique induction type which is non-return. It is operated by exhausting the flow from two Pratt & Whitney J-57 jet engines into the diffuser section of the wind tunnel. This primary flow generates a secondary flow into the wind tunnel nozzle and through the test section. It can be used to study a variety of parameters associated with the flight of an aircraft. [19]

**Figure 5.1 Air Induction Facility**

### 5.1.2 Experimental Setup

The fuel tank, as shown in Figure 5.2, was used for the experiments conducted in the air induction wind tunnel. It had inner dimensions of 0.914m x 0.914m x 0.305m, thickness of 0.635 cm, and was instrumented with 12 thermocouples and a sample port for measuring the THC in the ullage. Six thermocouples were placed on each surface of the tank, two in the ullage, and the other four were placed at 2, 4, 6, and 8 inches from the bottom surface of the tank. The tank had replaceable top and bottom panels that could be used for aluminum wing simulations as well as composite wing simulations. The other surfaces of the tank were insulated in order to minimize any thermal effects from the surroundings. An aerodynamic nose and tail piece were attached to the tank in order to properly simulate a wing tank and avoid any recirculation of air at the back of the tank. Figure 5.3 shows the test article placed in the high speed section of the wind tunnel.[20]

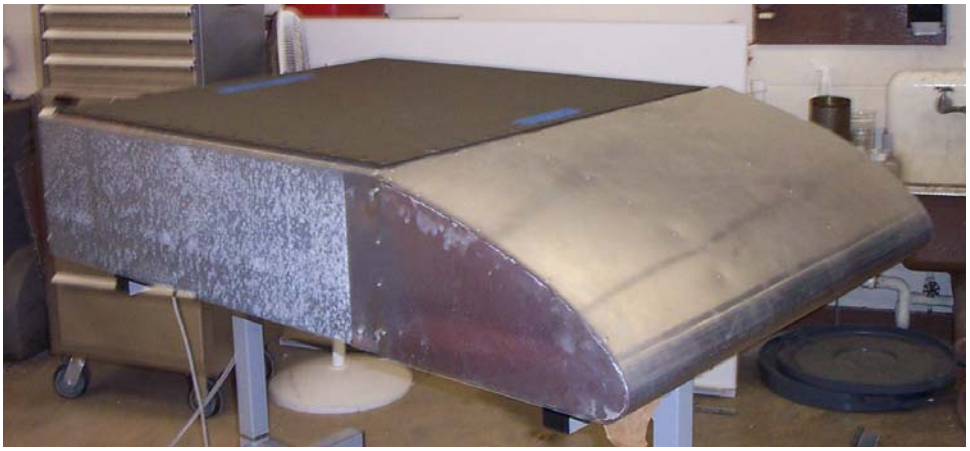

**Figure 5.2 Wing tank experimental setup in the air induction facility**

**Figure 5.3 Wing tank in the high speed test section of the wind tunnel**

### 5.1.3 Experimental Procedure

The test article that was placed in the high speed section of the wind tunnel and the top surface was heated with radiant heaters for an hour. After the hour passed, fuel that was preconditioned in a sealed fuel drum to 90°F was pumped into the tank. Then the tank was heated for another hour after which, the heaters were removed and the wind

tunnel was turned on to warm up for about 5–10 minutes. The wind tunnel was then turned to 90% of its capacity for half an hour. A pressure drop is created in the test section when the wind tunnel is turned on to 90% of its capacity. Figure 5.4 shows a sample flight profile during one of the tests. The test section with the test article in the wind tunnel observes wind speeds of up to 0.5 mach.

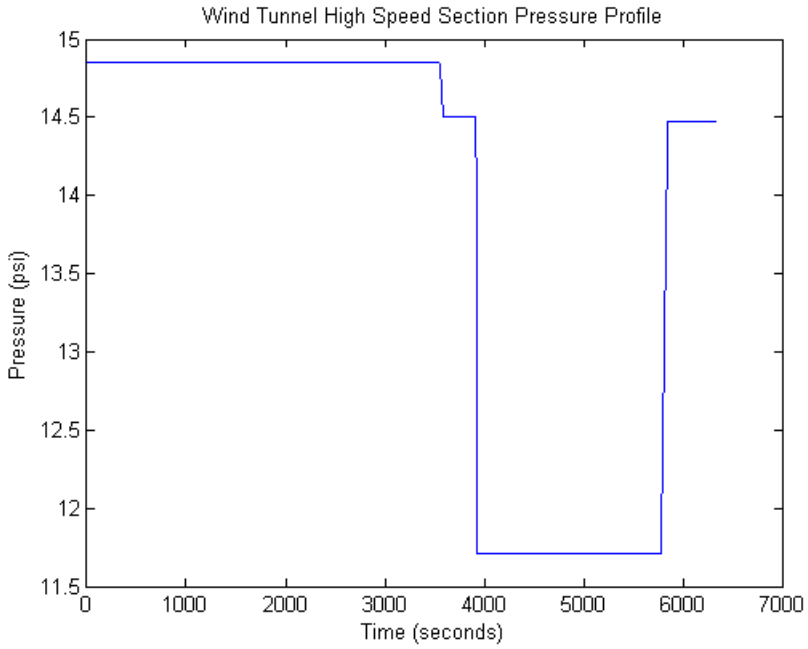


**Figure 5.4 Wind Tunnel High Speed Section Flight Profile**

### 5.1.4 Experimental Results

The data obtained from the experiments conducted in the air induction facility was used as input into the computational model.[20] The results obtained from the code were then compared against the experimental results as shown in figures 5.5 through 5.13. The title in each figure explains the type of top and bottom surface panels, the mass loading, and the heat setting that was used. For example, “Aluminum wing, 80% loading,

Heat 1" would indicate that the top and bottom surfaces of the fuel tank were made out of aluminum. The tank was filled with a mass loading of 80%, and that the heaters were set on the low heat setting. Heat 2 would mean that the heaters were set on the high setting.

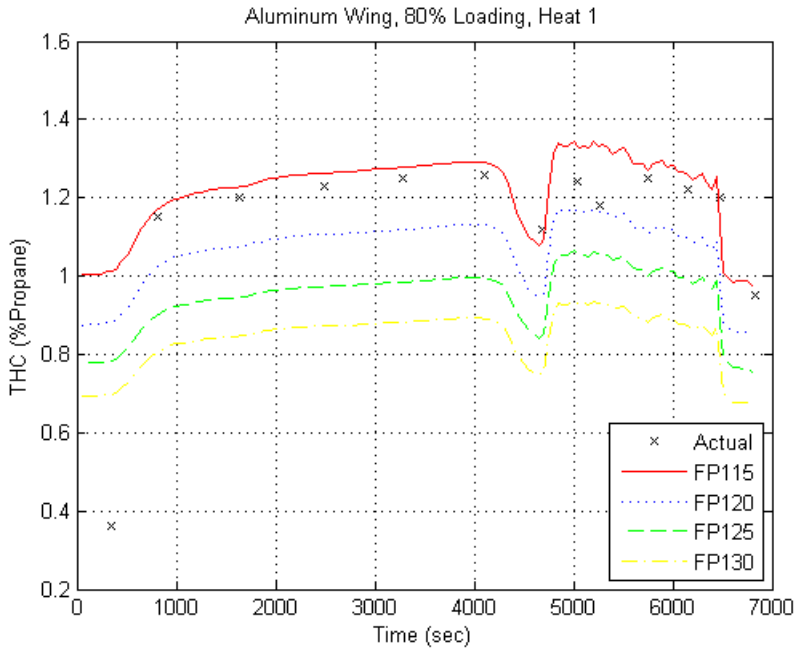


**Figure 5.5 Comparison of computational values calculated using the wing tank flammability model with measured experimental results obtained from tests run in a wind tunnel in a fuel tank with top and bottom surfaces made out of aluminum. The tank was heated on a low setting with 80% mass loading**

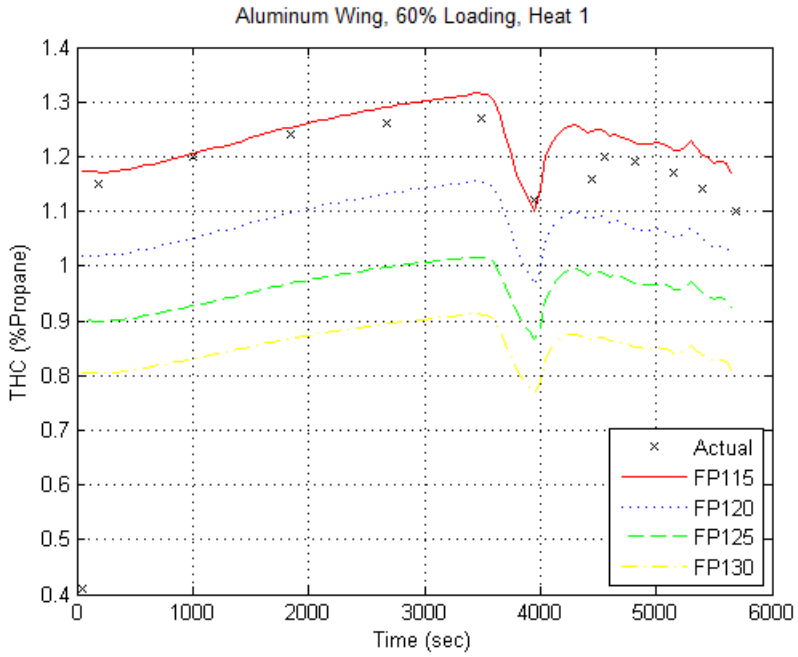


**Figure 5.6 Comparison of computational values calculated using the wing tank flammability model with measured experimental results obtained from tests run in a wind tunnel in a fuel tank with top and bottom surfaces made out of aluminum. The tank was heated on a low setting with 60% mass loading**

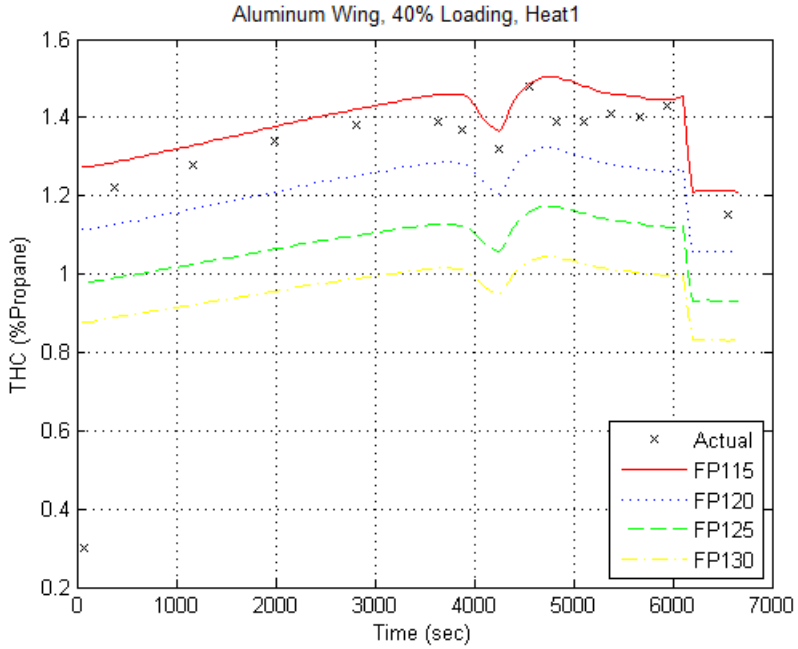


**Figure 5.7 Comparison of computational values calculated using the wing tank flammability model with measured experimental results obtained from tests run in a wind tunnel in a fuel tank with top and bottom surfaces made out of aluminum. The tank was heated on a low setting with 40% mass loading**

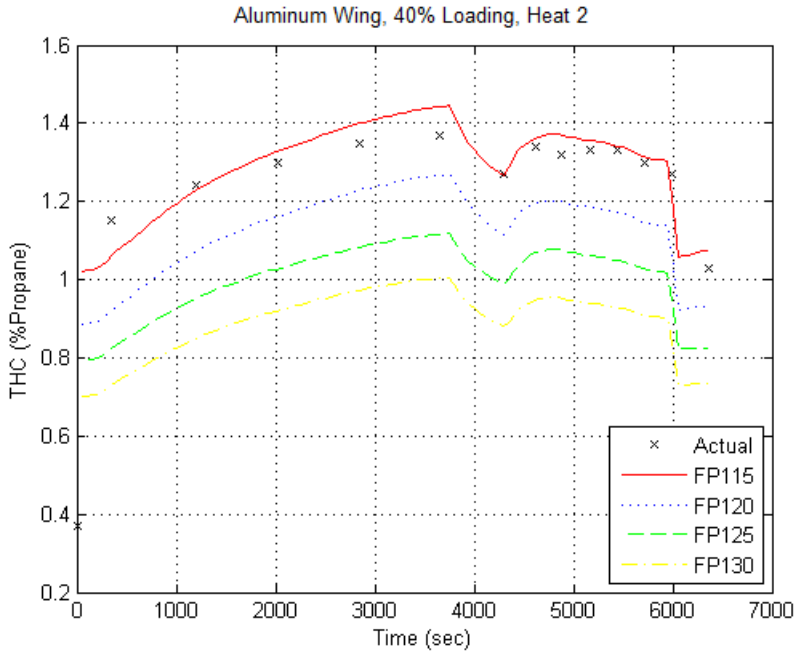


**Figure 5.8 Comparison of computational values calculated using the wing tank flammability model with measured experimental results obtained from tests run in a wind tunnel in a fuel tank with top and bottom surfaces made out of aluminum. The tank was heated on a high setting with 40% mass loading**

The results shown in figures 5.5 - 5.8 are from the aluminum wing tank. The computational values decline when the tunnel is turned on to 90% of its capacity. This decline in THC values is associated to the pressure drop created by turning the wind tunnel on close to its maximum capacity. As can be seen from the results, the computational results follow the same general trend as the experimental results. Similar to the environmental chamber tests, the experimental values lie near the computational values computed at a flash point of 115°F instead of predicting values between flash point values of 125°F and 130°F. This is due to the reason mentioned in section 4.2.

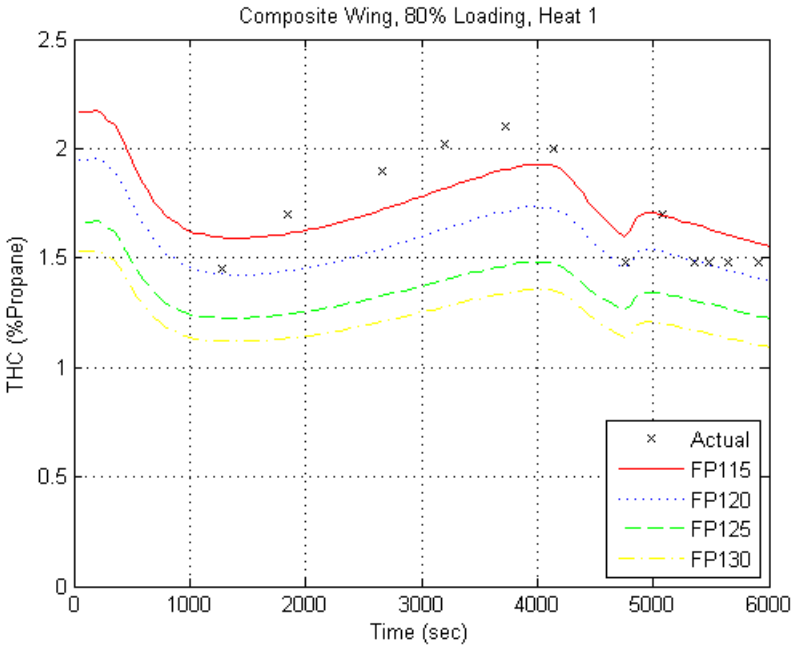


**Figure 5.9 Comparison of computational values calculated using the wing tank flammability model with measured experimental results obtained from tests run in a wind tunnel in a fuel tank with top and bottom surfaces made out of composite material. The tank was heated on a low setting with 80% mass loading**

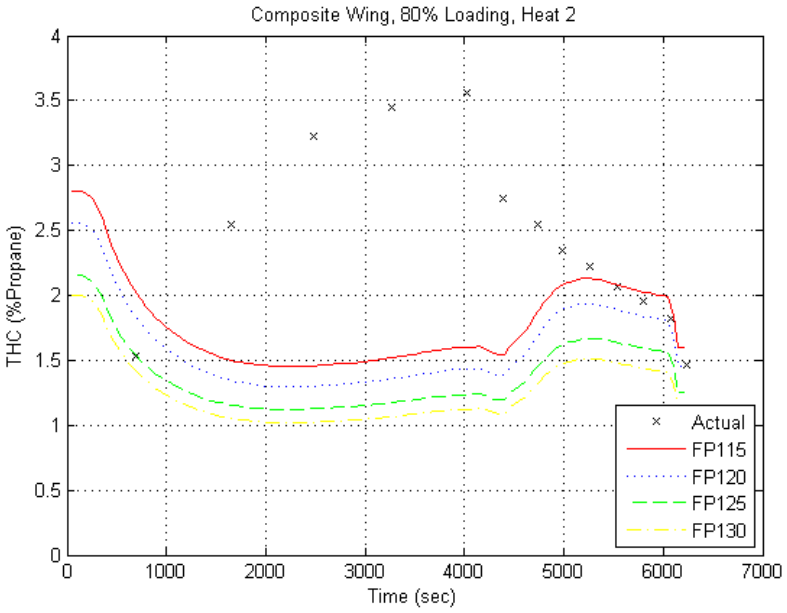


**Figure 5.10 Comparison of computational values calculated using the wing tank flammability model with measured experimental results obtained from tests run in a wind tunnel in a fuel tank with top and bottom surfaces made out of composite material. The tank was heated on a high setting with 80% mass loading**

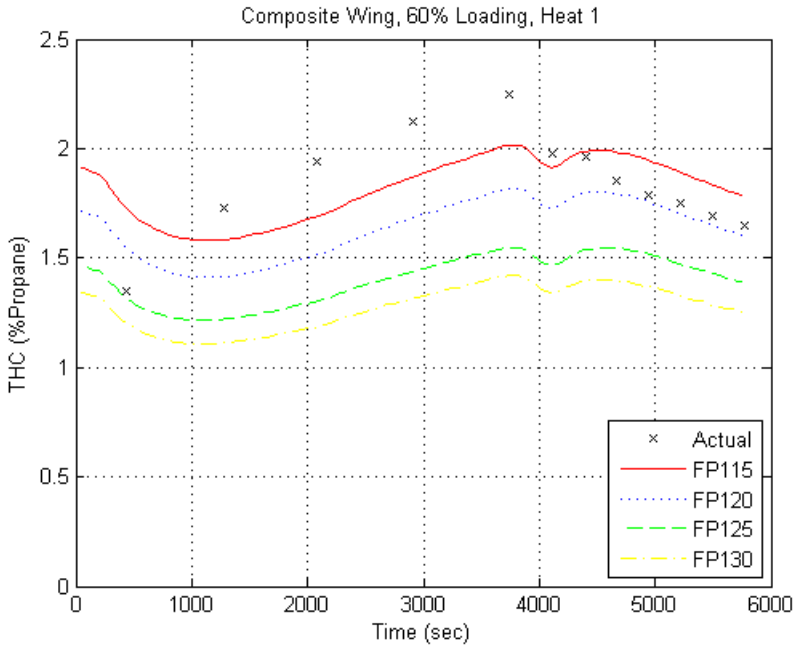


**Figure 5.11 Comparison of computational values calculated using the wing tank flammability model with measured experimental results obtained from tests run in a wind tunnel in a fuel tank with top and bottom surfaces made out of composite material. The tank was heated on a low setting with 60% mass loading**

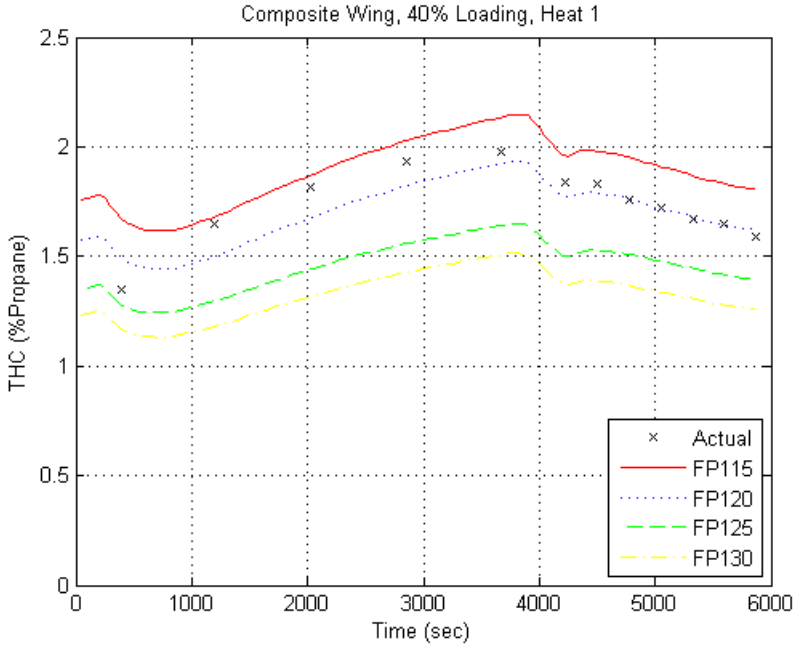


**Figure 5.12 Comparison of computational values calculated using the wing tank flammability model with measured experimental results obtained from tests run in a wind tunnel in a fuel tank with top and bottom surfaces made out of composite material. The tank was heated on a low setting with 40% mass loading**

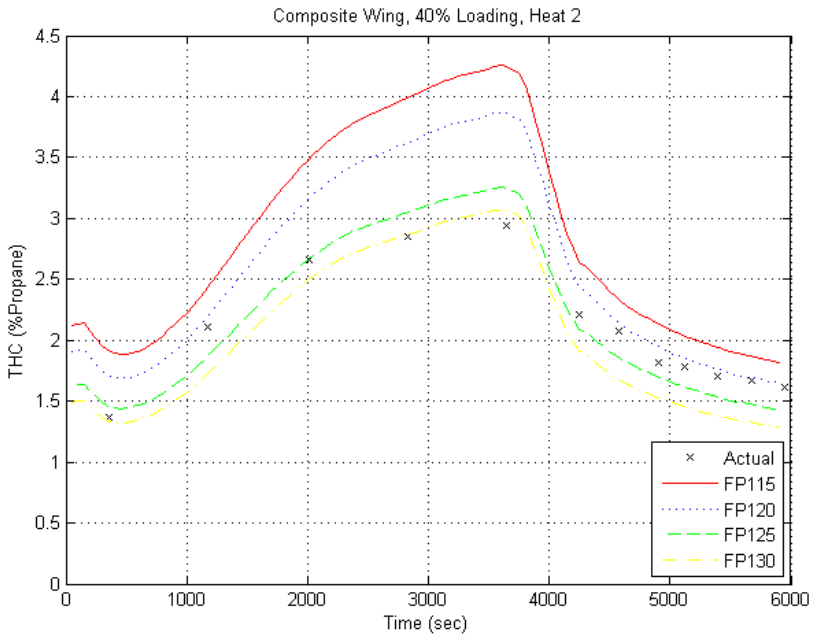


**Figure 5.13 Comparison of computational values calculated using the wing tank flammability model with measured experimental results obtained from tests run in a wind tunnel in a fuel tank with top and bottom surfaces made out of composite material. The tank was heated on a high setting with 40% mass loading**

The results shown in figures 5.9 – 5.13 are from the composite wing tank. The results obtained from the computational model do not match the experimental results during the heating of the wing tank due to the nature of the composite material to retain the heat in a particular area instead of equally distributing it throughout the entire surface. Composite materials have a higher heat capacity and lower thermal conductivity than aluminum. In Figure 5.10, the experimental THC values are much larger than the computational values, whereas in Figure 5.9 the experimental THC values are reasonably higher than the computational values. This can be explained by the temperature difference between the top surface of the tank and the liquid fuel temperature. For the case with the lower heat setting the temperature difference was on average about 50°F, but for the case with the higher heat setting the temperature difference was on average

about 100°F. The same does not apply for the case with a 40% mass loading and the higher heat setting since the temperature difference between the top surface temperature and the liquid fuel temperature was on average about 50°F.

Although the computational model is not built to tell the difference between the material of the wing tank, the heat transfer induced by the aluminum wing tank and the composite wing tank seem to be the cause of the disagreement between the experimental and computational values. The computations match the experimental results when the wind tunnel is turned on, which means that the composite wing tank dissipates heat similarly to the aluminum wing tank. It also means that when the wind tunnel is turned on the heat transfer inside the composite wing tank resembles the heat transfer inside of an aluminum wing tank.

## 5.2 Flight Test

A flight test was run by the FAA in order to study the dynamics of center wing tank and wing tank flammability. The tests were performed on one of NASA's 747shuttle carrier aircraft (SCA) as shown in Figure 5.14. The tanks were instrumented with thermocouples on various surfaces to measure temperature and a NDIR (Non-Dispersive Infra-Red) hydrocarbon analyzer to measure the THC in the fuel tanks. The NDIR is able to take THC measurements continuously by measuring the THC in the sample and pumping it back into its source. [9]


**Figure 5.14 NASA 747 SCA used for gathering flight test data.** [9]

### 5.2.1 Experimental Setup

The wing tank in the NASA 747 SCA was instrumented with eight T-type thermocouples positioned as described in Table 5.1. Five of these thermocouples were mounted on metallic surfaces with an epoxy-retaining patch that would ensure that the thermocouple is measuring only the surface temperature and not that of the surroundings. The other three thermocouples were suspended in air to measure the temperature at a particular location. Figure 5.15 shows the approximate location at which the thermocouple were located.

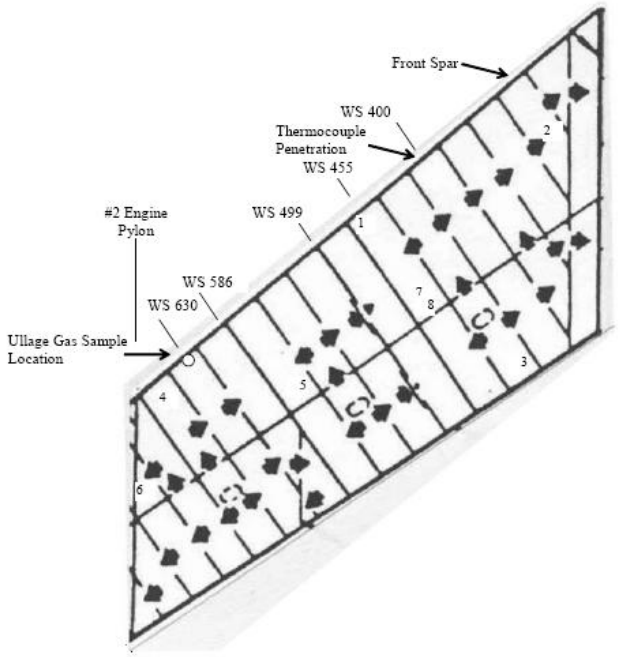


**Figure 5.15 Top view of the NASA 747 wing tank with thermocouple locations.** [9]

| Thermocouple # | Description | Location |
|---|---|---|
| 1 | Wing tank forward spar surface temperature | Front spar surface, WS 455, 25″ from tank bottom |
| 2 | Wing tank inboard fuel temperature | 4’ from front spar, WS 310, 6″ from tank bottom |
| 3 | Wing tank rear spar surface Temperature | Rear spar surface, WS 435, 25″ from tank bottom |
| 4 | Wing tank ullage temperature | 2″ from front spar, WS 650, 4″ from tank top |
| 5 | Wing tank mid-fuel/ullage temperature | 25″ from front spar, WS 586, 13" from tank bottom |
| 6 | Wing tank outboard wall surface temperature | 6′ from front spar, WS 715, 12″ from tank bottom |
| 7 | Wing tank bottom surface temperature | 8′ from front spar, WS 455, tank bottom surface |
| 8 | Wing tank top surface temperature | 8′ from front spar, WS 455, tank top surface |

**Table 5.1 NASA 747 wing tank thermocouple locations.** [9]

### 5.2.2 Results from the Flight Test Data

The results from the NASA 747 flight test were converted into text files to be used as inputs in the computational model. The computational model assumed a rectangular geometry for the WT with a 60% mass loading. The results obtained from the computational model are shown in figures 5.16 – 5.18. The computational results were computed only for the 130°F flash point since all the data seemed to lie below this flash point curve.

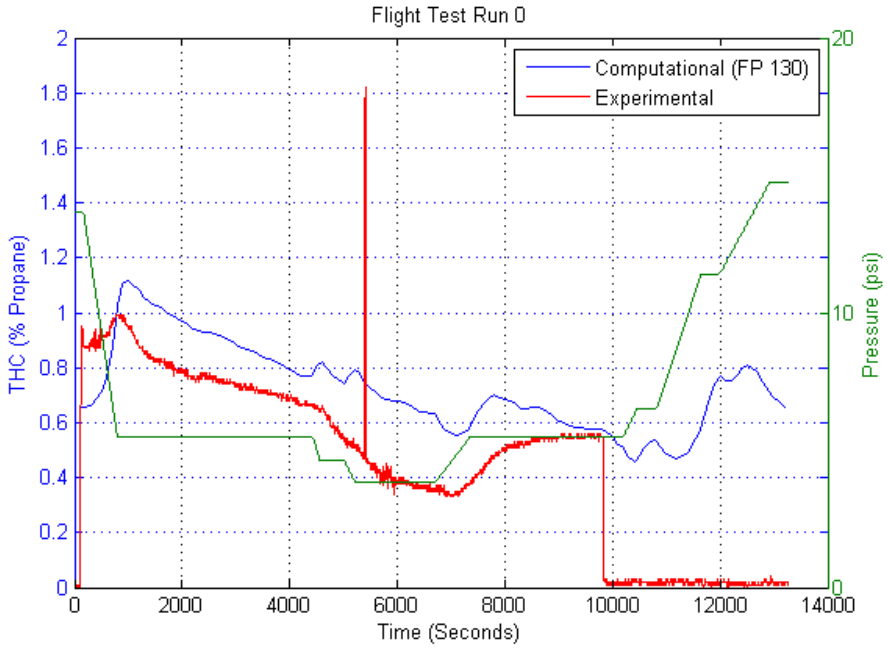


**Figure 5.16 Comparison of computational values calculated using the wing tank flammability model with measured experimental results obtained from tests run in a NASA SCA 747 aircraft. Flight Test Run 0**

Figure 5.16 shows that the computational results agree fairly well with the experimental results and follow the general trend of them. However the computations are not accurate with respect to the flash point of the fuel. An unknown failure in the NDIR occurs after approximately 2 ¾ hours, which accounts for the zero reading shown by the experimental value. This test was run with the OBIGGS apparatus turned off.

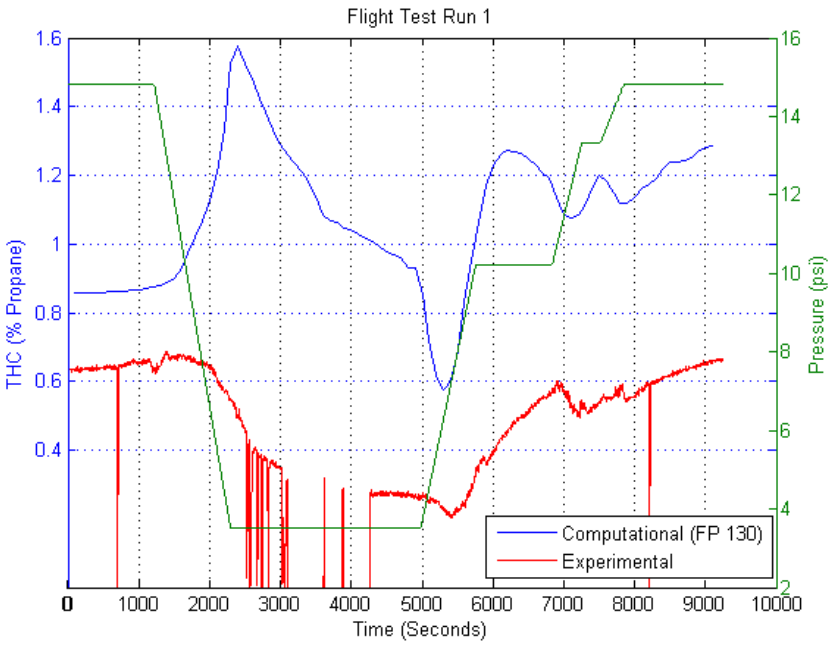


**Figure 5.17 Comparison of computational values calculated using the wing tank flammability model with measured experimental results obtained from tests run in a NASA SCA 747 aircraft. Flight Test Run 1**

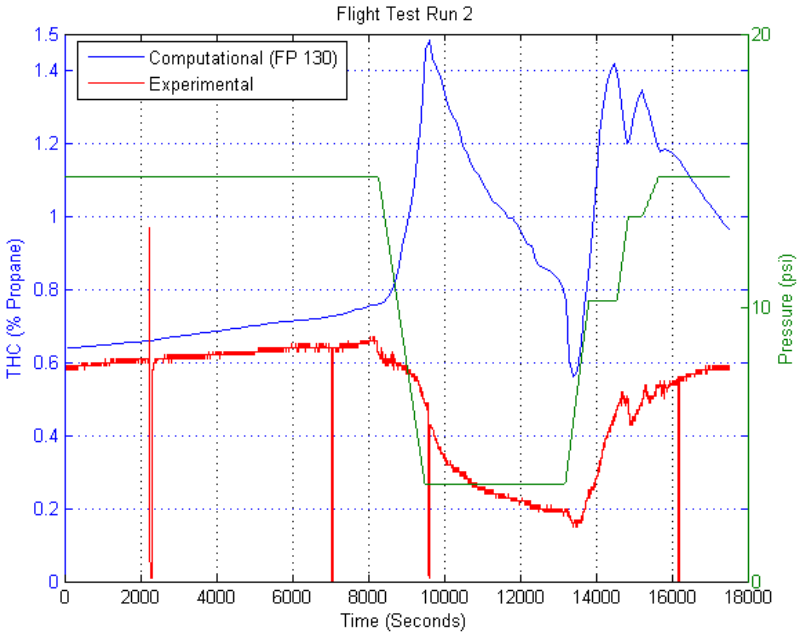


**Figure 5.18 Comparison of computational values calculated using the wing tank flammability model with measured experimental results obtained from tests run in a NASA SCA 747 aircraft. Flight Test Run 2**

For the tests shown in Figure 5.17 and Figure 5.18, the THC values calculated by the computational model do not agree with the experimental values. The computational values seem to follow the general trend during the ground stage and descent. The disagreement in values occurs during the aircraft's ascent and cruising stage. It was proposed that these inconsistencies were caused due to the thermal layering of the fuel. The wing tank is compartmentalized, which causes the fuel to layer thermally. One of the model's basic assumptions is that the temperature of all the liquid fuel is the same, and all of the ullage remains at the same temperature as well. This can be assumed when the Rayleigh numbers of the gases in the ullage are in the turbulent regime. Another reason for this inconsistency might be that there may be cold spots in the tank that allow for excessive condensation that is not accounted for in the computational model. Another justification for these inconsistencies could be that flight test 1 and flight test 2 were run with the OBIGGS apparatus turned on which could interfere with the natural flow of air within all the tanks.

In an attempt to modify the computational values to follow the trend of the experimental values, the bottom surface temperature was used as the input for the computations instead of the liquid fuel temperature. Figure 5.19 shows the difference between the bottom surface temperature and the liquid fuel temperature. The results obtained are shown in Figure 5.20 and Figure 5.21. For these cases the computational values follow the general trend seen with the experimental values, however the computational values are approximately 15-20% higher than the experimental values.

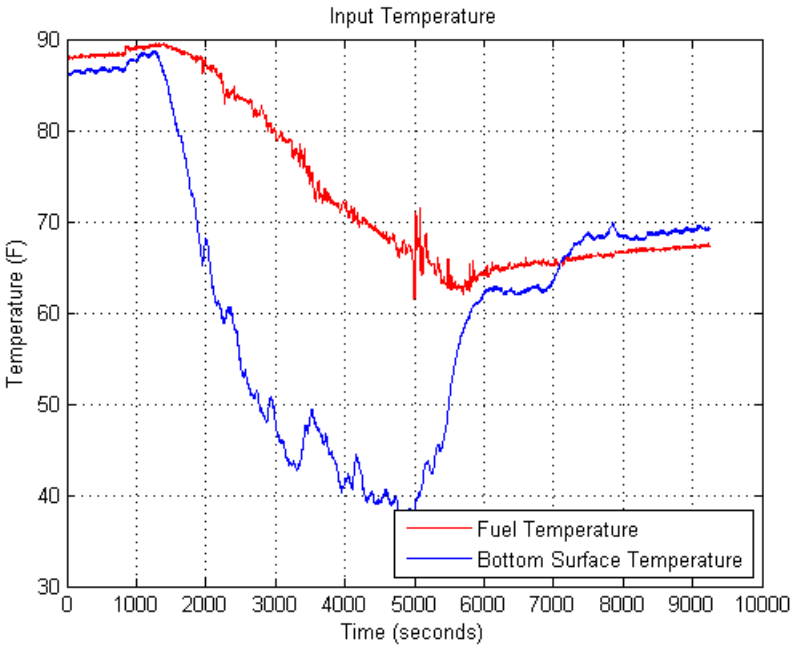


**Figure 5.19 Input Temperature**

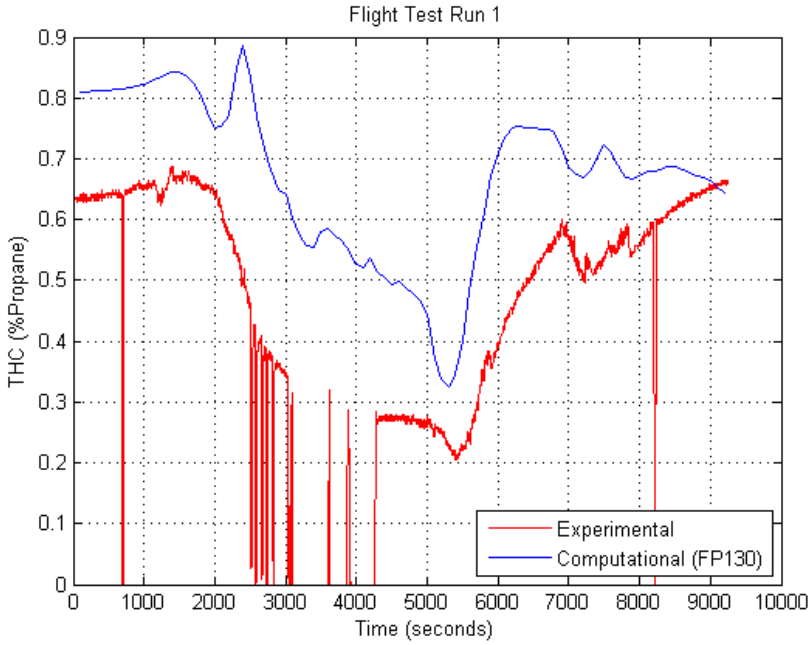


**Figure 5.20 Comparison of computational values calculated using the wing tank flammability model with measured experimental results obtained from tests run in a NASA SCA 747 aircraft with modified inputs from flight test run 1**

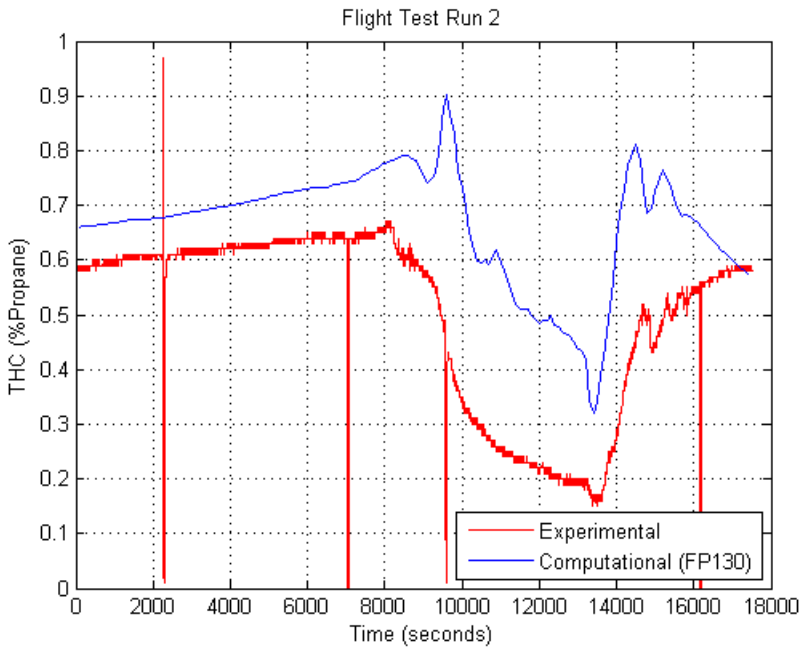


**Figure 5.21 Comparison of computational values calculated using the wing tank flammability model with measured experimental results obtained from tests run in a NASA SCA 747 aircraft with modified inputs from flight test run 2**

The FAA had conducted some studies to observe THC values determined by an NDIR and a FID at the same time. It was noted that the NDIR produced values that were about 15% to 20% lower than the ones observed by the FID. This study could explain why the computational values, albeit following the trend of the experimental values, are approximately 15% to 20% away from the experimental values.[21]

# Chapter 6

# Dual Thermocouple Method

Computational models that require many input values are not practical in real-life situations such as in this case. The previous computational model requires many temperature inputs and makes many assumptions. Invasion of the tank to acquire such data can be hazardous to the structure and integrity of the fuel tank. It also exposes the tank to additional potential ignition sources. Computational models help in determining factors that influence the physics behind the problem, but it usually comes at a cost. In order to simplify things a model was designed that would require only the ullage temperature and liquid fuel temperature as inputs and would be simple to use.

## 6.1 Background

The dual thermocouple method is based on a fuel air ratio (FAR) calculator that was created by Ivor Thomas of the FAA.[22] The FAR calculator is a model that predicts fuel vapor pressure and hence the fuel air ratio for multiple fuel types over a range of altitudes, temperatures, and mass loadings. This model is based on two laws, Raoult's Law and the Ideal Gas Law. The Ideal gas law can be seen in equation 6.1.

$$PV = nRT \tag{6.1}$$

Raoult's Law states that the vapor pressure of an ideal solution is dependent on the vapor pressure of each chemical component and the mole fraction of the component

present in the solution. The vapor pressure of a compound can be expressed as show in equation 6.2, where A, B, and C are constants also known as Antoine coefficients. These coefficients are already tabulated in reference books such as Poling et al. [13]

$$log_{10}P_{vp} = A - \frac{B}{T + C - 273.15} \tag{6.2}$$

By assuming the ullage to be comprised of mostly air and the molecular weight of fuel, a fuel air ratio of the ullage can be obtained. This fuel air ratio can then be converted into a THC using equation 6.3, where the average molecular weight of the fuel used was 132.4 and the $C_{ratio}$ was the carbon ratio, 9.58/3.

$$\left[\frac{Mass_{fuel}}{Mass_{air}}\right] = \frac{(ppm\ C_3H_8 \times 10^{-6})(C_{ratio})(MW_{Fuel})}{MW_{air}} \tag{6.3}$$

This model characterizes the fuel by simplifying the complex multi-component fuel into a number of compounds that are separated by their alkane boiling points. All the compounds with the same carbon number were assigned together. By this process, the model only had to deal with 19 compounds for its calculations. The properties of each compound alkane were determined using an ASTM D2887 distillation curve. This model is able to calculate a THC value as a propane equivalent over different temperature and pressure conditions.

## 6.2 Description of the Model

The FAR calculator is used to calculate THC over a range of temperatures and pressures. The results obtained from the FAR calculator are plotted as shown in Figure 6.1. It is observed that at constant temperature the THC increases with decrease in pressure.

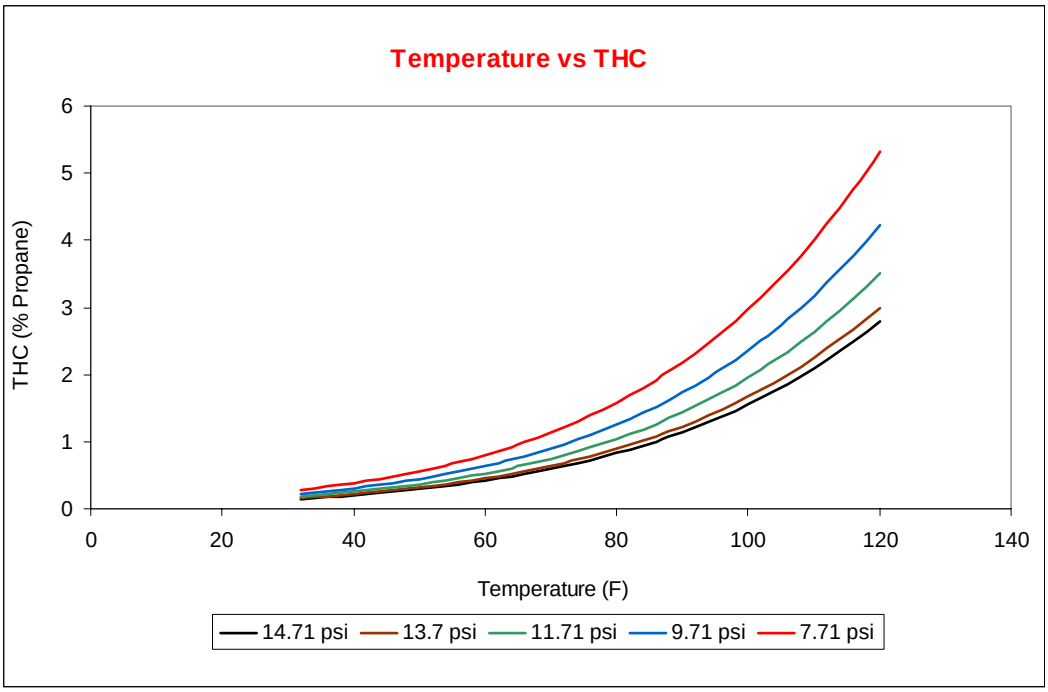


**Figure 6.1 THC values obtained using the FAR calculator**

A simple correlation was sought in order to calculate a THC value based on a known temperature and pressure. A correlation between the pressure and the calculated THC value was observed in the graph obtained from the FAR calculator. By multiplying the THC value with the pressure that it was calculated at, a scaled THC value was obtained. When the scaled THC value was plotted against temperature, as shown in

Figure 6.2, a correlation defined by a $12^{th}$ order polynomial was observed. The temperature that is related to the scaled THC values is referred to as the film temperature.

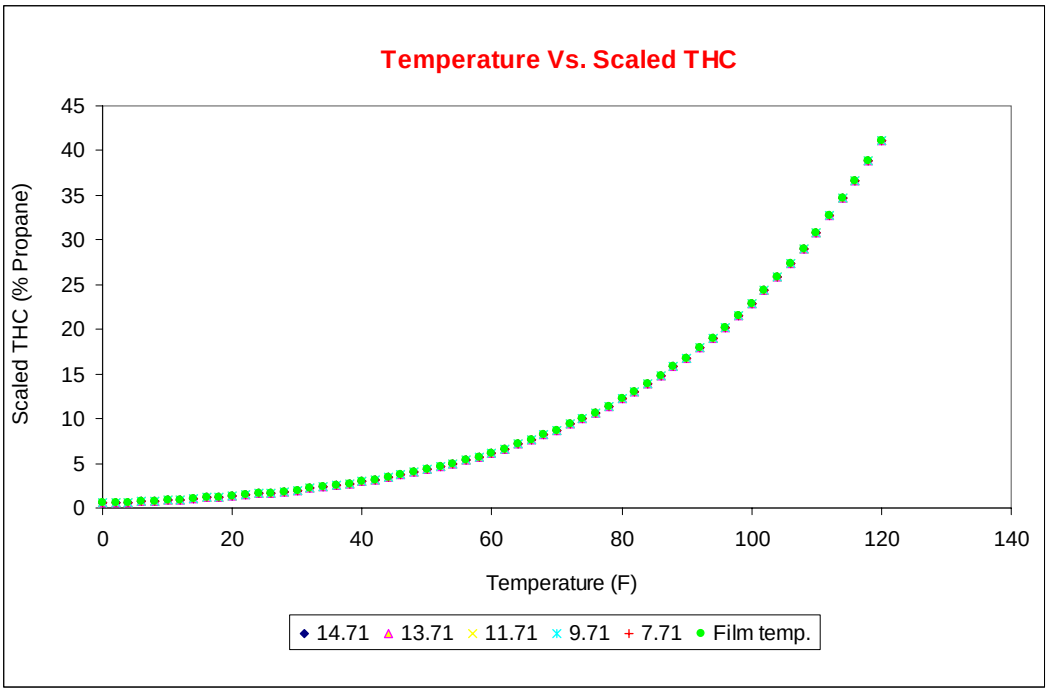


**Figure 6.2 Scaled THC plotted against temperature**

Using the obtained correlation, given a film temperature, a scaled THC value can be calculated. Then, by dividing out the pressure at which the scaled THC is calculated at, an actual THC value is obtained.

In order to see how well the dual thermocouple method works, the experimental THC values and pressure data from the NASA 747 flight test was used to compute a film temperature and see how well it correlated with the ullage temperature.

## 6.3 Results

In order to obtain a film temperature from the flight test data, the THC values of each flight test was multiplied by the measured pressure. These values were then plugged

into a code written in FORTRAN. The code used the Newton-Raphson method to find the roots of the polynomial correlation. The root of the polynomial correlation at a given scaled THC value is the sought film temperature. This correlation was applied to four sets of flight test data. The results were then combined and divided in a way such that it would show easily where the correlation agrees and disagrees with the computational model.

The results were divided based on an ascending or descending flight profile. They were also based on whether the ullage temperature was greater than the liquid fuel temperature and vice versa. When the ullage temperature is greater than the liquid fuel temperature, the situation is referred to as a stable configuration. This creates layers of air in the ullage which are at different temperatures as shown in Figure 6.3. This occurs because an enclosure heated from above the ullage space usually forms thermal layers and there is no mixing in the ullage. On the other hand, when the liquid fuel temperature is greater than the ullage temperature, the situation is referred to as an unstable configuration. This is due to the fact that when an enclosure is heated from below, natural convection induces mixing in the ullage as can be seen in Figure 6.4.

**Figure 6.3 Stable Mixing Configuration**

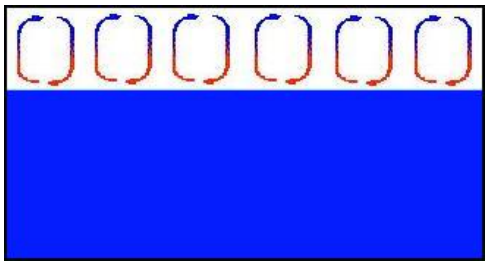

**Figure 6.4 Unstable Mixing Configuration**

The correlations from all four sets of flight test data are shown in figures 6.5 – 6.8. Figure 6.5 shows the correlations from a stable mixing configuration during an ascending profile with a correlation coefficient of 0.89. Figure 6.6 shows the correlations from an unstable mixing configuration during an ascending profile with a correlation coefficient of 0.98. Figure 6.7 shows the correlations from a stable mixing configuration during a descending profile with a correlation coefficient of 0.41. Figure 6.8 shows the correlations from an unstable mixing configuration during a descending profile with a correlation coefficient of 0.93. All the correlations except the one for a stable mixing configuration during a descending profile show good correlation with the model. The correlation coefficient for each condition is displayed at the top of each figure.

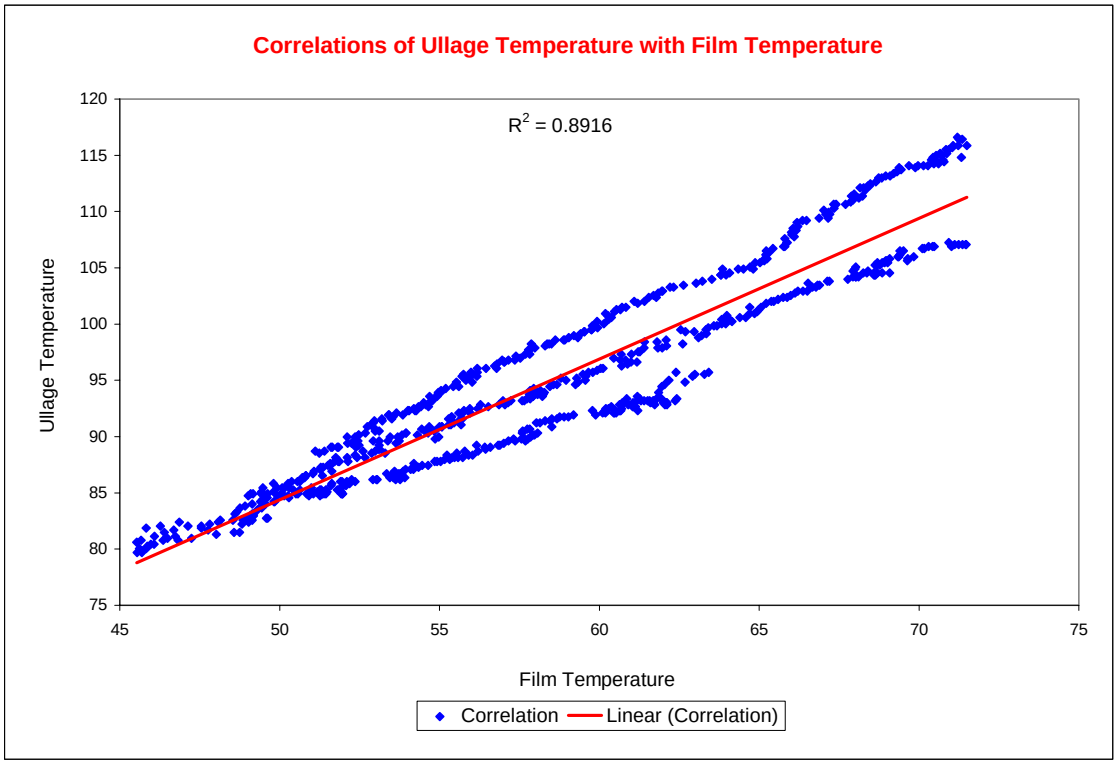


**Figure 6.5 Stable Mixing Configuration, Ascending Profile**

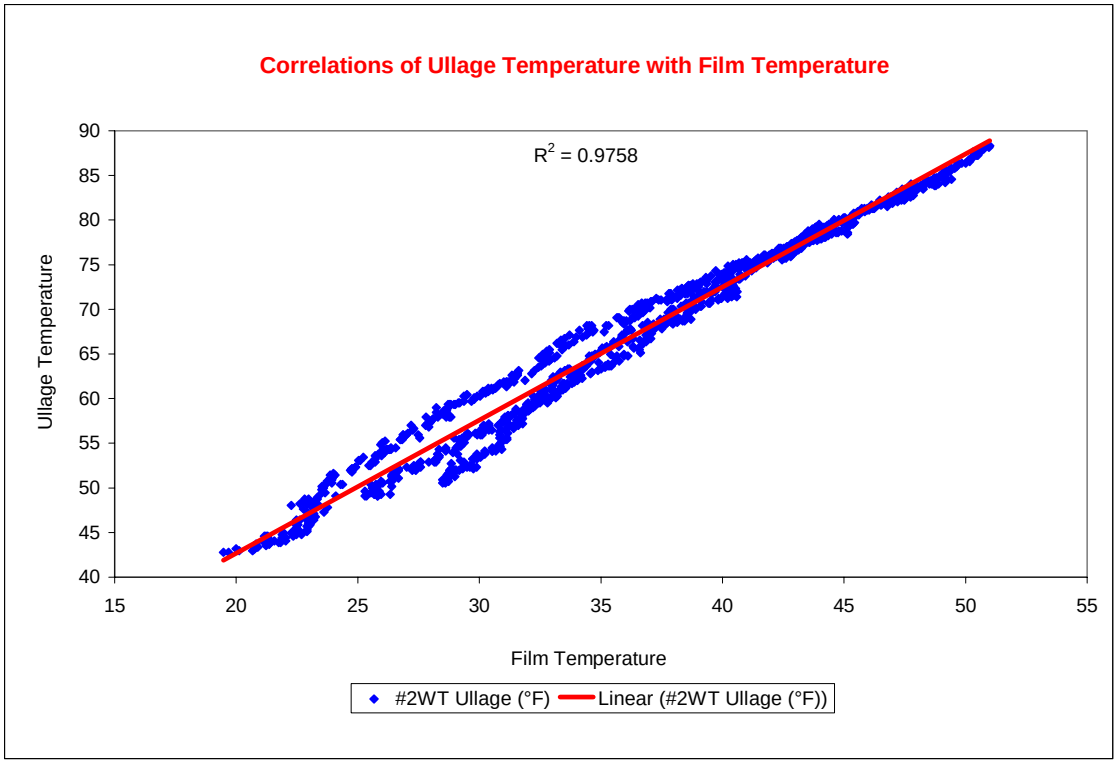


**Figure 6.6 Unstable Mixing Configuration, Ascending Profile**

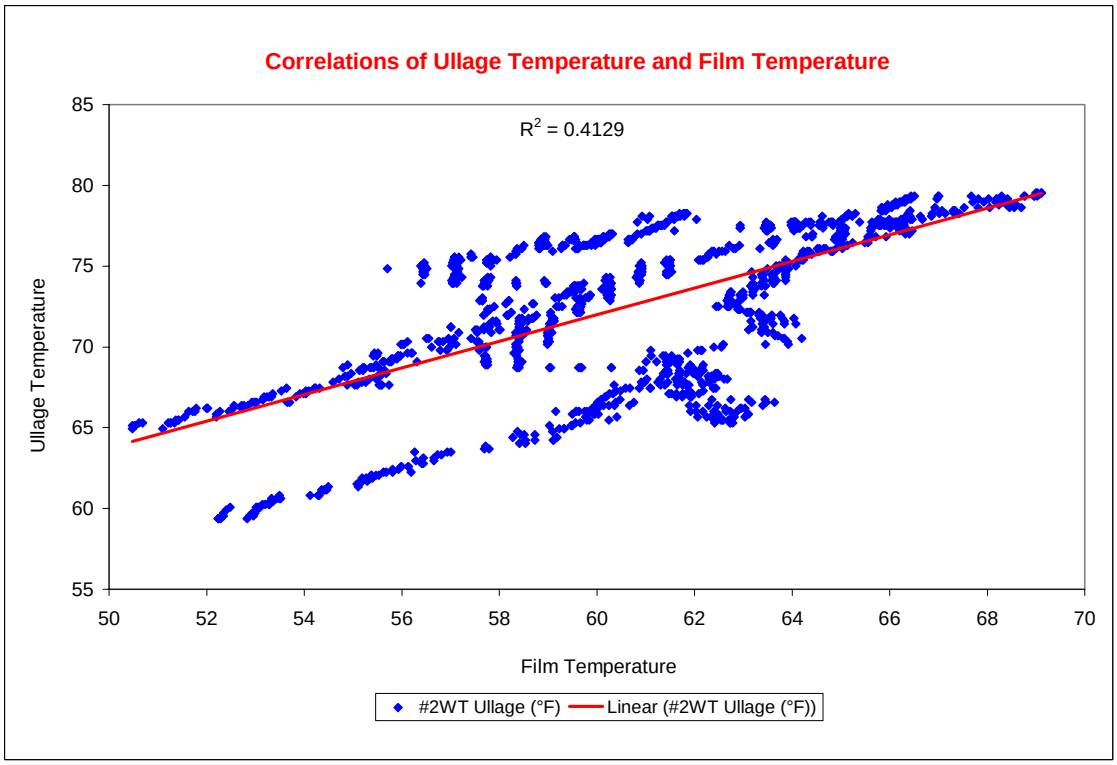


**Figure 6.7 Stable Mixing Configuration, Descending Profile**

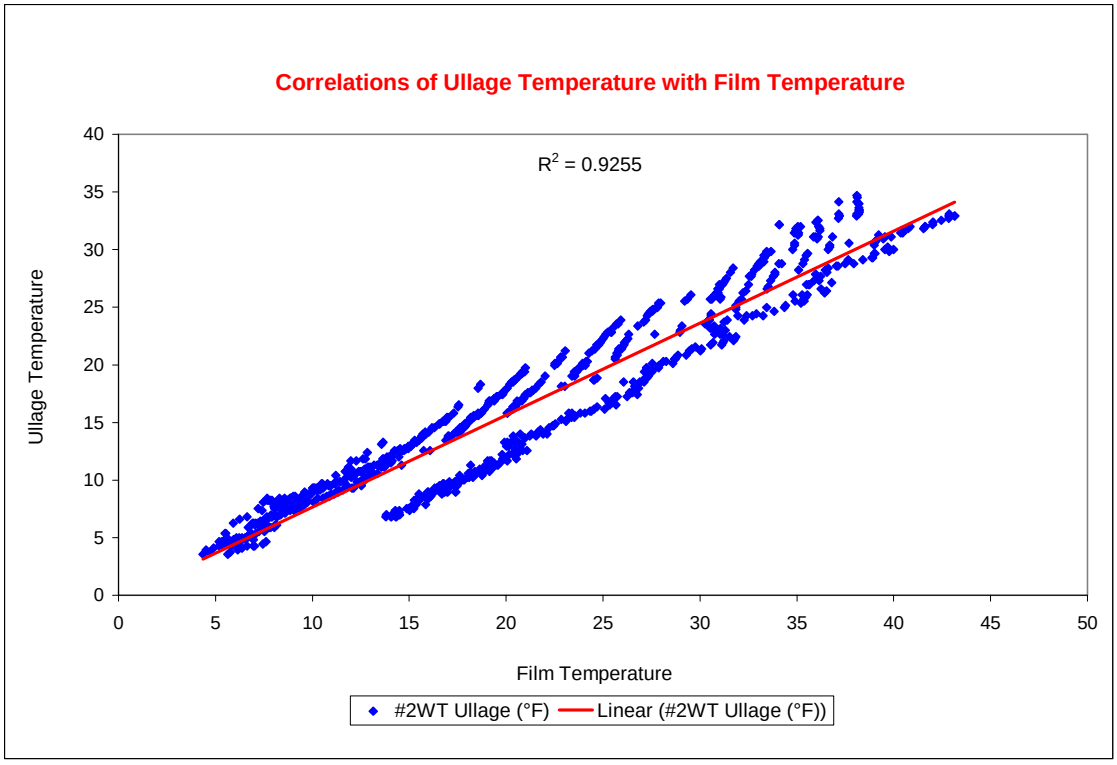


**Figure 6.8 Unstable Mixing Configuration, Descending Profile**

The results show that the unstable mixing configuration has a better correlation than the stable mixing correlation. Bairi et al.[23] has experimentally and numerically studied natural convection in an air filled 2D enclosure at various geometrical and thermal configurations. This study has shown that an enclosure when heated from below and kept cold at the top, with active sidewalls, has the highest Nusselt number values. The Nusselt number is a measure of heat transferred through convective heat transfer. Whereas, when the top wall is heated and the bottom wall is cold the Nusselt number reaches a minimum which means that the fluid is stratified and the main mode of heat transfer is conduction rather than convection. The cases with the unstable mixing configuration show better correlations than the cases with stable mixing configurations.

This validates the statement that the unstable mixing configuration has higher rates of heat transfer than the stable mixing configuration.

In order to see how efficiently the dual thermocouple method estimates THC in experimental situations, inputs from the experimental data was entered into developed correlations as further mentioned. For the experimental results from the altitude chamber and wind tunnel, the measured fuel surface temperature was input into equation 6.4 to yield a scaled THC value. A THC value was then obtained by substituting the value from equation 6.4 into equation 6.5. These THC values obtained using the 12$^{th}$ order polynomial and the fuel surface temperature was compared to the THC values measured experimentally in the WT.

$$\begin{aligned} Scaled\ THC = \quad & 1.05 \times 10^{-24} T^{12} \mid 8.64 \times 10^{-22} T^{11} \quad 3.10 \times 10^{-19} T^{10} \mid 6.37 \\ & \times 10^{-17} T^{9} - 8.23 \times 10^{-15} T^{8} + 7.22 \times 10^{-13} T^{7} - 4.14 \times 10^{-11} T^{6} \\ & + 1.91 \times 10^{-9} T^{5} + 7.10 \times 10^{-9} T^{4} + 6.93 \times 10^{-6} T^{3} + 5.13 \times 10^{-4} T^{2} \\ & + 0.025T + 0.56 \end{aligned} \tag{6.4}$$

$$THC = \frac{Scaled\ THC}{Pressure\ (psi)} \tag{6.5}$$

Figure 6.9 and 6.10 are representative of the best case scenario for each type of experimental run and computational values obtained by using the Dual Thermocouple Method. Figure 6.9 shows the experimental values and the computational values obtained for the experiment run in the altitude chamber with an initial temperature of 90°F, a cruising altitude of 34,000 feet, and a mass loading of 80%. The computational values follow the general trend of the experimental values pretty accurately except for when the chamber simulates an on-ground condition. The most reasonable explanation for this phenomenon is that the chamber is at constant temperature and pressure while on the

ground. Whereas, the model relies on temperature and pressure changes to calculate the THC, which is best shown by the correlations.

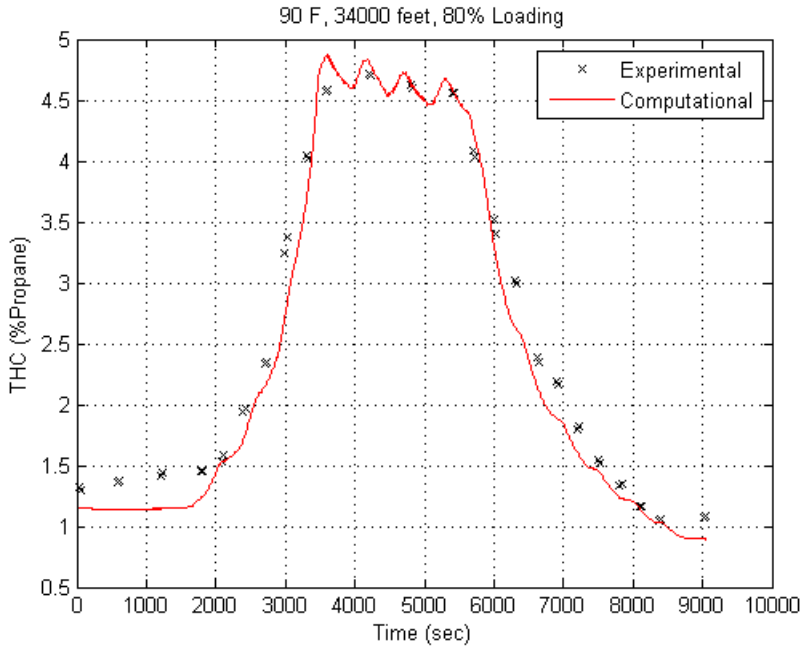


**Figure 6.9 Comparison of computational values calculated using the dual thermocouple method with measured experimental results obtained from tests run in an altitude chamber. Initial fuel tank temperature was 90°F, cruising altitude achieved was 34,000 feet, 80% mass loading**

Figure 6.10 shows the experimental and computational values obtained for the experiment run in the wind tunnel with an aluminum wing tank at a mass loading of 80% and a high heat setting. The computational values follow the general trend of the experimental values, but the computational values estimates the THC approximately 10% lower than the experimental value consistently. The most reasonable explanation for this phenomenon might be that the tank in the wind tunnel mostly undergoes temperature changes and as established before, the model relies on changes in temperature and pressure to calculate THC.

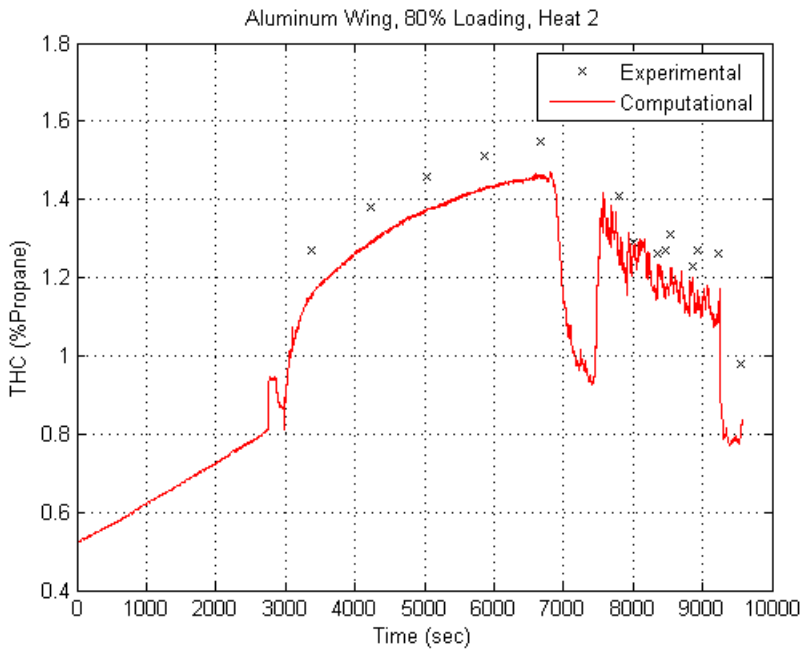


**Figure 6.10 Comparison of computational values calculated using the dual thermocouple method with measured experimental results obtained from tests run in a wind tunnel in a fuel tank with top and bottom surfaces made out of aluminum. The tank was heated on a high setting with 80% mass**

The Dual Thermocouple Method works well in the case of a WT because the generation of vapors in the ullage of a WT is mostly governed by the temperature of the ullage. Due to the presence of a large quantity of fuel in the tank when compared to the situation of a CWT, the fuel acts like a thermal mass that responds quickly to changes at its surface.

These results show that the Dual Thermocouple Method can be used effectively to estimate the general trend of the total hydrocarbon concentration with just a fuel surface temperature and the ambient pressure within the fuel tank.

# Chapter 7

# Modeling Flammability

## 7.1 Objective

The Fuel Tank Flammability Reduction Rule[1] published by the FAA requires that the fleet average flammability exposure of each fuel tank may not exceed 3 percent of the flammability exposure evaluation time. The model that is used to calculate the FEET of the tank defines the flammability limits to be a function of the flash point of the fuel. It also defines the flammability limits to change linearly with change in altitude. The relations for the lower flammability limit and the upper flammability limit can be seen in equation 7.1 [24] and equation 7.2 [24] respectively, where the flash point is measured in degrees Fahrenheit and the altitude is measured in feet.

$$LFL = (flash\ point - 10) - \frac{Altitude}{808} \tag{7.1}$$

$$UFL = (flash\ point + 63.5) - \frac{Altitude}{512} \tag{7.2}$$

The model also takes into consideration the limiting oxygen concentration (LOC) in the tank. LOC can be defined as the concentration of oxygen below which combustion is not possible regardless of the concentration of fuel. After conducting tests in a pressure vessel at the FAA simulating altitudes from 0 to 38,000 feet, it was determined that the LOC from sea level through 10,000 feet was 12% oxygen concentration. The LOC

beyond 10,000 feet varied linearly from 12% at 10,000 feet to approximately 14.5% at 40,000 feet. [8]

Important variables that influence flammability such as temperature, pressure and oxygen concentration need to be taken into consideration in order to represent flammability in a wing tank accurately. Hence, a need to develop a model that takes the influence of the variables on flammability limits into consideration was observed.

## 7.2 Theory

A base model was sought that could predict the flammability limits of the fuel based on the temporal changes of the temperature, pressure, and oxygen concentration. As established before, the fuel used in this study is a multi-component fuel characterized as alkanes from C5 to C20. In order to model flammability limits for the fuel, the flammability limits of each alkane with their particular dependence on temperature, pressure, and oxygen concentration had to be determined. Using the Le Chatelier's Mixing Rule a final flammability limit is established which takes into consideration the dependence of flammability limit on temperature, pressure, and oxygen concentration. Le Chatelier proposed an empirical mixing rule, as shown in equation 7.3, that predicts the flammable limit of lean fuel air mixtures,

$$LFL_{mix} = \frac{1}{\sum_{i=1}^{N} \frac{y_i}{LFL_i}} \tag{7.3}$$

where $y_i$ is the mole fraction of the $i^{th}$ component considering only the combustible species and $LFL_i$ is the lower flammability limit of the $i^{th}$ component in volume percent. This mixing rule can also be applied to calculate the upper flammability limit of the mixture using the same equation and replacing the lower flammability limit with the upper flammability limit as shown in equation 7.4.

$$UFL_{mix} = \frac{1}{\sum_{i=1}^{N} \frac{y_i}{UFL_i}} \tag{7.3}$$

In order to model flammability, the flammability limits had to be estimated using numerical methods since the experimental values of the upper and lower flammability limits were available only for alkanes below decane. Flammability limits can be estimated using various techniques, a couple of which are mentioned below. One of the methods estimates the flammability limits as a function of the stoichiometric concentrations of fuel. Equations 7.4 [25] and 7.5 [25] describe how to calculate the lower and upper flammability limits respectively, and equation 7.6 [25] explains the origins of the variables used. For the calculations relevant to the current work, y in equation 7.6 was assumed to be zero.

$$LFL = \frac{0.55(100)}{4.76m + 1.19x - 2.38y + 1} \tag{7.4}$$

$$UFL = \frac{3.50(100)}{4.76m + 1.19x - 2.38y + 1} \tag{7.5}$$

$$C_mH_xO_y + zO_2 \rightarrow mCO_2 + \frac{x}{2}H_2O \quad (7.6)$$

The other method estimates flammability limits by correlating them with a function of the heat of combustion of the fuel, as shown in equations 7.7 and 7.8 where $\Delta H_c$ is the heat of combustion of the fuel (in $10^3$ kJ/mol). [25]

$$LFL = \frac{-3.42}{\Delta H_c} + 0.569\Delta H_c + 0.0538\Delta H_c^{\,2} + 1.80 \quad (7.7)$$

$$UFL = 6.30\Delta H_c + 0.567\Delta H_c^{\,2} + 23.5 \quad (7.8)$$

Of the two methods shown above to estimate the flammability limits, the first method was used in the flammability model since it provided more accurate results when compared to results obtained experimentally.[26]

As discussed earlier, flammability limits vary with change in temperature, pressure, and oxygen concentration. Derived empirical equations, as shown in equations 7.9 and 7.10, are available in Crowl et al. [25] for flammability limit dependence on temperature. In the equations displayed below, $\Delta H_c$ is the net heat of combustion in kcal/mole and T is the temperature in °C. These equations were used in the flammability model as the temperature dependence of flammability limits.

$$LFL_T = LFL_{25} - \frac{0.75}{\Delta H_c}(T - 25) \quad (7.9)$$

$$UFL_T = UFL_{25} + \frac{0.75}{\Delta H_c}(T - 25) \quad (7.10)$$

Arnaldos et al [27] has established a method to predict the variation of flammability limits at reduced pressure conditions for $C_mH_nO_x$ type fuels. This work utilizes a complex method of calculating data necessary to obtain a curve representative of the entire flammable envelope with respect to pressure. Using the available data already calculated and tabulated by Arnaldos et al [27] for heptane, only the upper flammability limit portion of the entire envelope was generated, as shown in Figure 7.1, since pressure has little influence on the LFL except at pressures lower than 50 mm of Hg, where flames do not propagate.[25] This curve was used in the flammability model to obtain the pressure dependence of flammability limits. The model assumes the heptane pressure dependence curve as the upper flammability pressure dependence for all the alkanes.

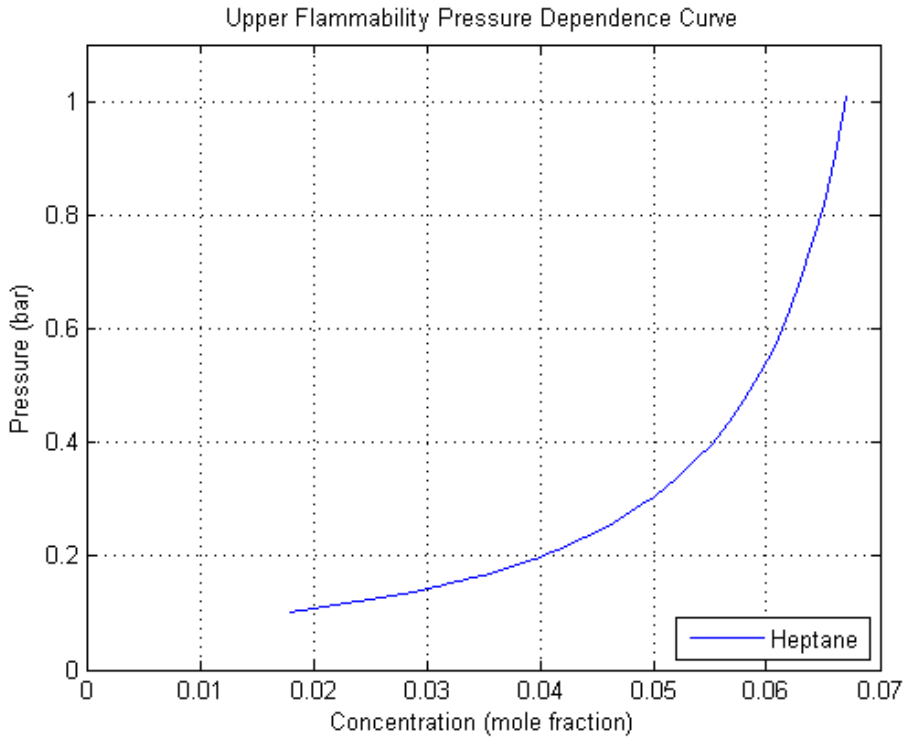


**Figure 7.1 Upper Flammability Pressure Dependence Curve**

The inflammability point for various fuels lies between 11% and 13% oxygen concentration by volume percent. By making an assumption that the inflammability points for the C5 to C20 alkanes is 12.5% oxygen concentration and that the lower flammability limit does not change with oxygen concentration, a simple flammability limit calculator that is based on oxygen concentration can be generated. By connecting straight lines between the lower and upper flammability limit to the inflammability point, as shown in Figure 7.2, we can calculate the upper flammability limit at any oxygen concentration between 21% and 12.5% oxygen concentration.

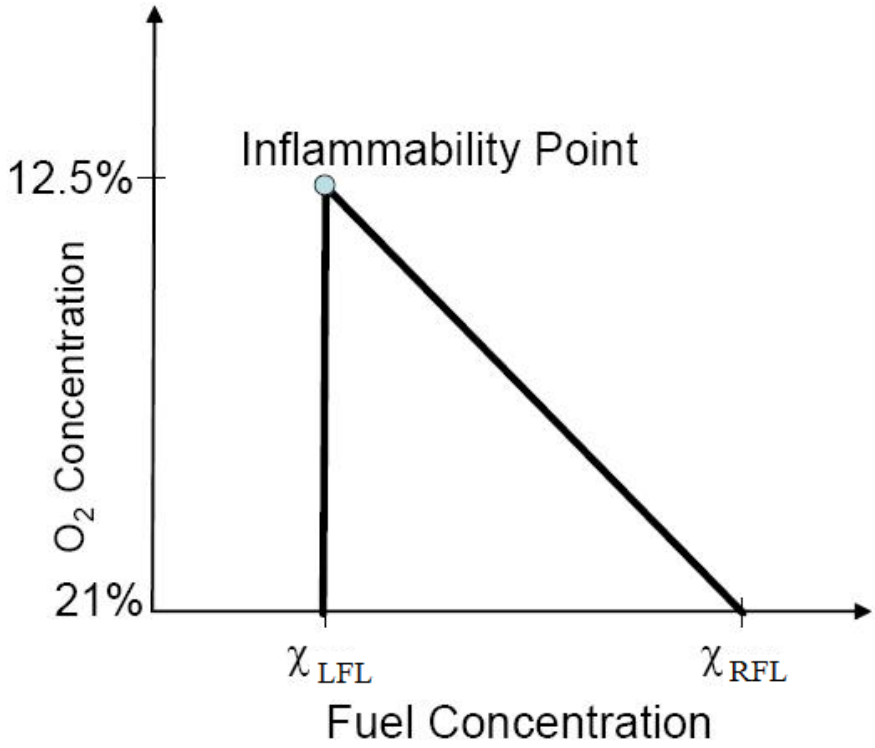


**Figure 7.2 Model of the Inflammability Map**

## 7.3 Results

A program was written in MATLAB to obtain an inflammability map based on the temperature and pressure dependence correlations as shown in Figure 7.3. The program then calculated the lower and upper flammability limits based on the specified oxygen concentration by calculating the slope of the line from the upper flammability limit to the inflammability point and then determining what is the flammability at the specified oxygen concentration.

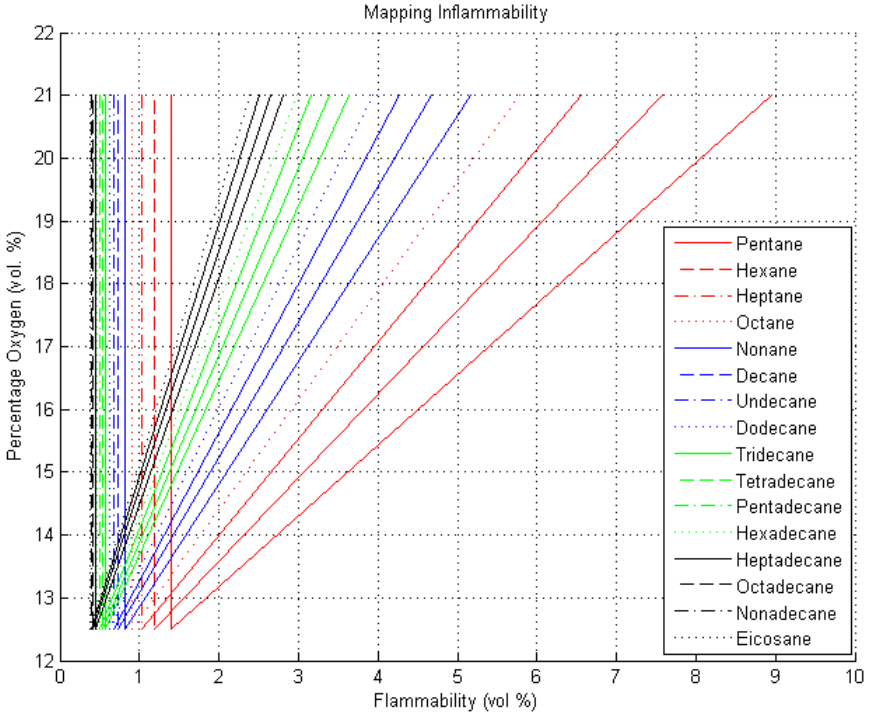


**Figure 7.3 Mapping Inflammability for all Alkanes**

Figure 7.4 and Figure 7.5 show the lower and upper flammability limits for the entire experimental run in the altitude chamber with the initial temperature at 80°F, flight profile with a cruising altitude of 25,000 feet, and a 60% mass loading respectively. These figures show the flammability limits calculated based on just the temperature

dependence correlation. Overall, the lower flammability limit changes by only 0.012 volume percent and the upper flammability limit changes by only 0.028 volume percent. It can be interpreted from the results that both the upper and lower flammability limits are not influenced significantly by the temperature dependence correlation.

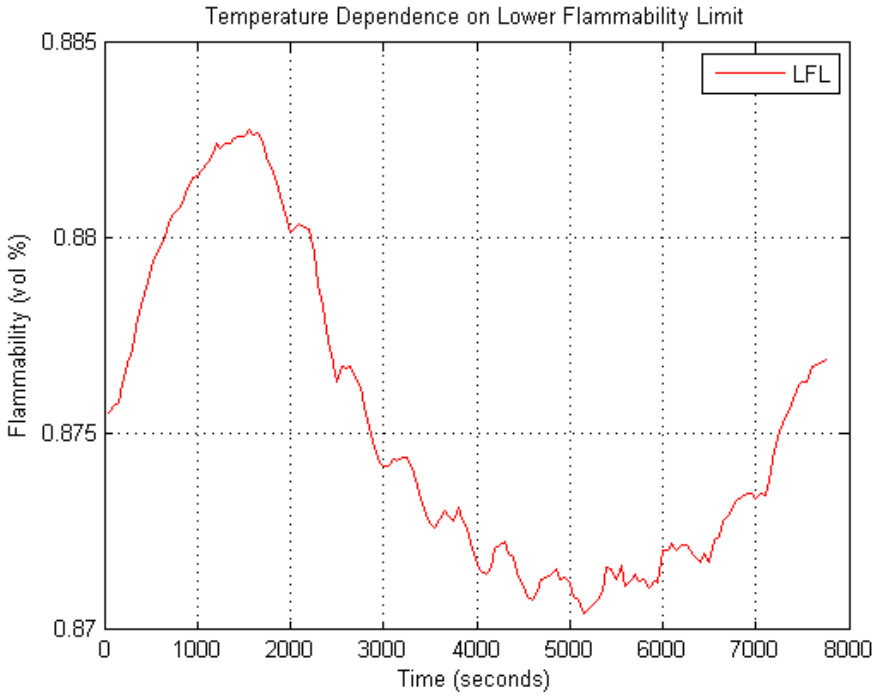


**Figure 7.4 LFL of JP-8 with a temperature dependence correlation for experiment run in the altitude chamber with initial fuel tank temperature of 80°F, cruising altitude achieved of 25,000 feet, and 60% mass loading**

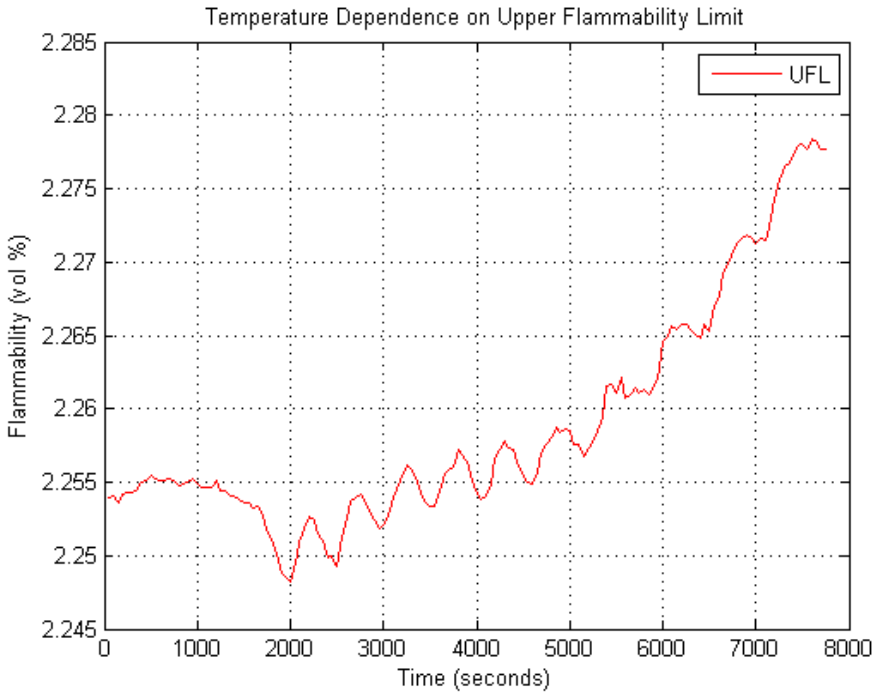


**Figure 7.5 UFL of JP-8 with a temperature dependence correlation for experiment run in the altitude chamber with initial fuel tank temperature of 80°F, cruising altitude achieved of 25,000 feet, and 60% mass loading**

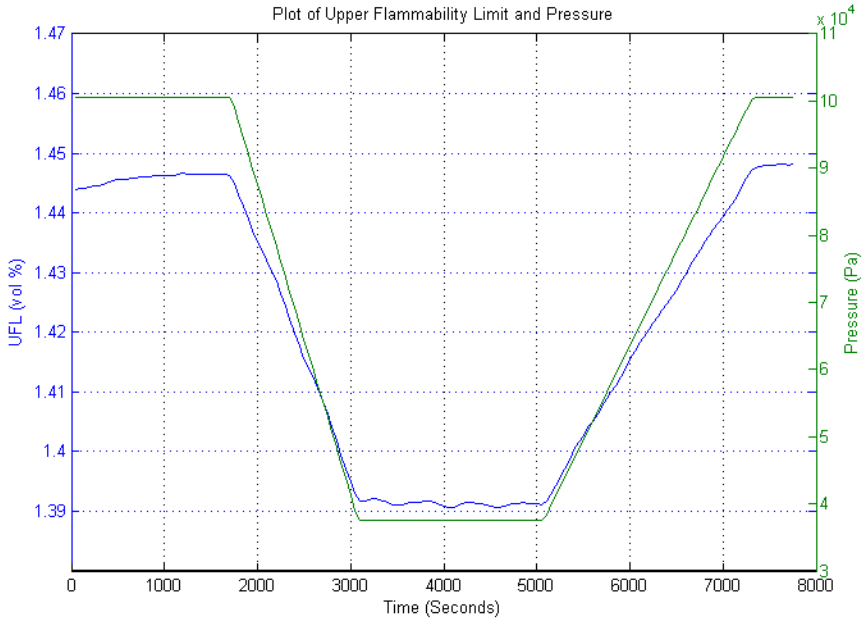


**Figure 7.6 Plot of Upper Flammability Limit and Pressure for experiment run in the altitude chamber with initial fuel tank temperature of 80°F, cruising altitude achieved of 25,000 feet, and 60% mass loading**

Figure 7.6 takes a closer look at the effect of pressure on the upper flammability limit. The trends clearly show that the upper flammability limit reduces as the pressure reduces, but the overall change is only 0.079 volume percent. After taking into consideration the entire flight profile and the overall flammability region, it can be said that pressure has a minimal influence on the flammability limits.

Figure 7.7 shows the upper and lower flammability limits calculated with all the dependence correlations at 21% oxygen concentration, while Figure 7.8 shows the flammability limits with all the dependence correlations at 15% oxygen concentration. Hence for a difference of 6% oxygen concentration the upper flammability limit changes by 1.3 volume percent. The values are calculated for the same experimental run as described above. From the two figures we can infer that oxygen concentration has a significant effect on the UFL. As the oxygen concentration in the ullage is decreased the upper flammability limit decreases as well.

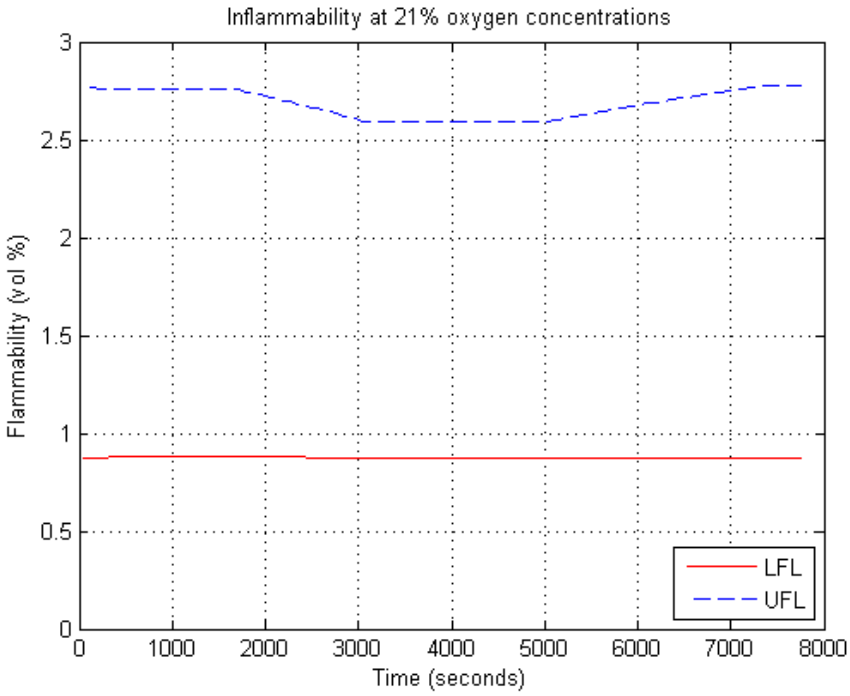


**Figure 7.7 Flammability limits at 21% oxygen concentration for experiment run in the altitude chamber with initial fuel tank temperature of 80°F, cruising altitude achieved of 25,000 feet, and 60% mass loading**

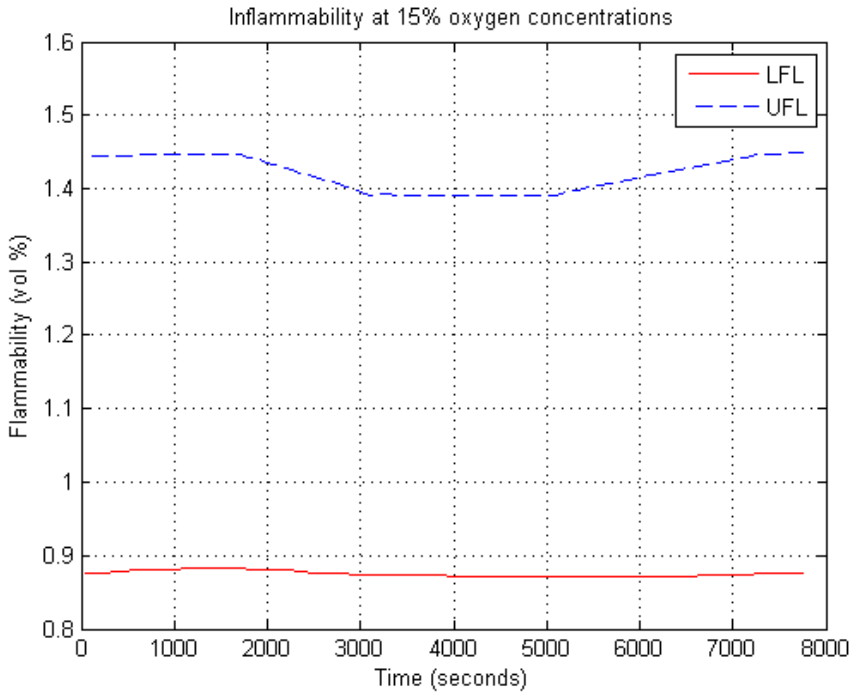


**Figure 7.8 Flammability limits at 15% oxygen concentration for experiment run in the altitude chamber with initial fuel tank temperature of 80°F, cruising altitude achieved of 25,000 feet, and 60% mass loading**

Figure 7.9 shows the upper and lower flammability limits in terms of percent propane which is the units of THC obtained by the experimental data as well as the computational model. The figures show that the experimental THC values are not in the flammable region when only the limiting oxygen concentration is taken into consideration. Whereas, the flammable region generated by calculating the flammability limits shows that the experimental THC values lie in the flammable region for about 18% of the total flight time.

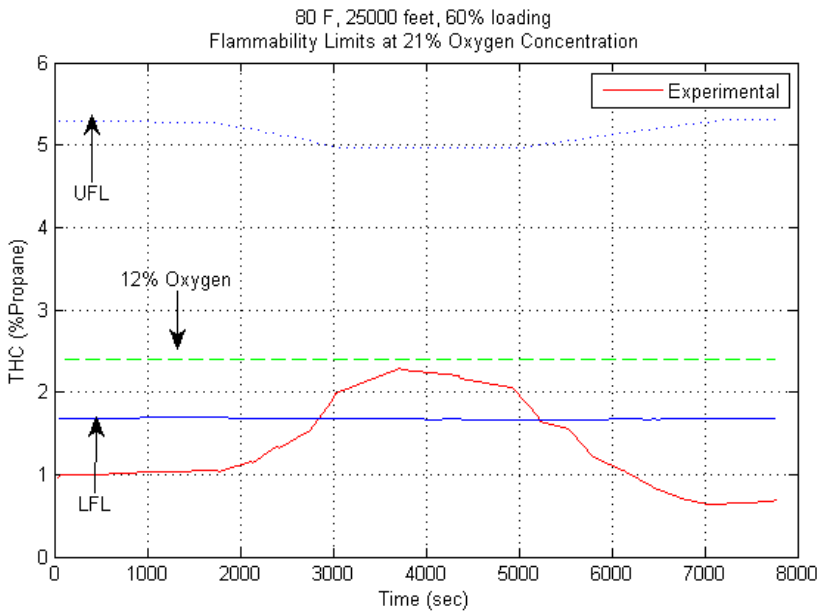


**Figure 7.9 Flammability limits at 21% oxygen concentration for experiment run in the altitude chamber with initial fuel tank temperature of 80°F, cruising altitude achieved of 25,000 feet, and 60% mass loading**

# Chapter 8

# Concluding Remarks

A computational model was built to predict the generation of flammable mixtures in the ullage of wing fuel tanks. The model predicted the flammability of the tank with conditions that simulated an in-flight environment of a wing fuel tank. These conditions are summarized as follows; the wing tank was radiatively heated from the top surface of the tank to simulate heating from the sun and the wing tank was at least 60% full of fuel. This model was designed to help in the development of fuel tank protection methods that will possibly eliminate or reduce the exposure of wing tanks to wing fuel tank fires and explosions. The model was validated through supporting experiments run in the altitude chamber and the wind tunnel facility as well as data obtained from flight tests.

## 8.1 Summary of Results

The computational model that predicts the flammability in a wing fuel tank was successfully built. Experiments were performed in an altitude chamber under varying initial conditions and were put under two different flight profiles and mass loading conditions. The heat transfer correlations used in the computational model that predicts the generation of flammable mixtures in the ullage of a wing tank were to speed up the heat transfer within the ullage to be able to successfully predict the generation of flammable vapors while making changes to an already established model that predicts flammability in CWTs. The results from the experiments were compared to the computational results. They showed good agreement. The results from the computational

model followed the general trend of the experimental results, but produced them at a different flash point value. This was due to the replenishment of species with lower flash point at the surface of the fuel which emulates the flash point of the entire fuel to be lower. The model was compared to other data sets that were available from the experiments run by the FAA in the Air Induction Wind Tunnel facility and from the flight test in the NASA 747 SCA plane. The results from the wind tunnel facility with the aluminum wing were in good agreement with the computational results as well. They followed the general trend of the experiments but at a different flash point. This was due to the replenishment of species with lower flash point at the surface of the fuel which emulates the flash point of the entire fuel to be lower. The results from the wind tunnel facility with the composite wing did not match the computational results due to difference in heat transfer properties of the composite and aluminum wing. The results from the in-flight test didn't agree well with computational model. They seemed to agree with the results for the ground stage and the descent stage of the flight. After changing the input from liquid fuel temperature to the bottom surface temperature, the model seemed to agree well with the experimental results. Thermal stratification of the fuel and cold spots within the fuel tank can be held responsible for the inconsistencies with the model.

A simple model was developed in order to reduce the number of inputs necessary in order to run the model. The inputs necessary would be the ullage temperature, the fuel surface temperature, and the pressure. The model developed calculated a film temperature, which was compared to the ullage temperature in order to see when the calculated film temperature can successfully predict an ullage concentration. The model

worked for unstable mixing configurations throughout the flight profile and stable mixing configuration for the ascending profile. The model did not work for the stable mixing configuration during the descending profile. This correlation was then applied to the data sets for the experiments performed in the altitude chamber and wind tunnel. For the tests conducted in the altitude chamber, the correlation estimated the hydrocarbon concentrations extremely well during ascent and descent. During the on-ground condition the estimation was good, but not as accurate as the ascent or descent conditions. For the tests conducted in the wind tunnel, the computational values follow the general trend of the experimental values, but the computational values estimates the THC approximately 10% lower than the experimental value consistently.

Flammability studies were performed in order to track the effects of temperature, pressure, and oxygen concentration on the upper and lower flammability limits. The temperature and pressure effects are very miniscule on the flammability limits of the vapor in the ullage for the temperature and pressure profiles considered in this work. Whereas the oxygen concentration has a significant effect on the flammability limits of the vapor in the ullage; the flammable region narrows with decrease in oxygen concentration.

## 8.2 Future Work

Further studies are necessary in order to better characterize jet fuel. This could help in building better and more accurate computational models. Improvements can be made to the current computational model by making it sensitive to whether the WT is made of aluminum or composite material. Further detailed experimental data can be

obtained on full scale WTs to better understand the heat transfer that occurs within the complicated internal structure of a WT. Test results from a fully instrumented WT in an in-flight aircraft would help better validate the computational model. Better heat transfer modeling that accounts for the complicated internal flow field, cold spots, hot spots, condensation surfaces, and sloshing of the liquid fuel.

# Appendix A

# Experimental Temperature Data

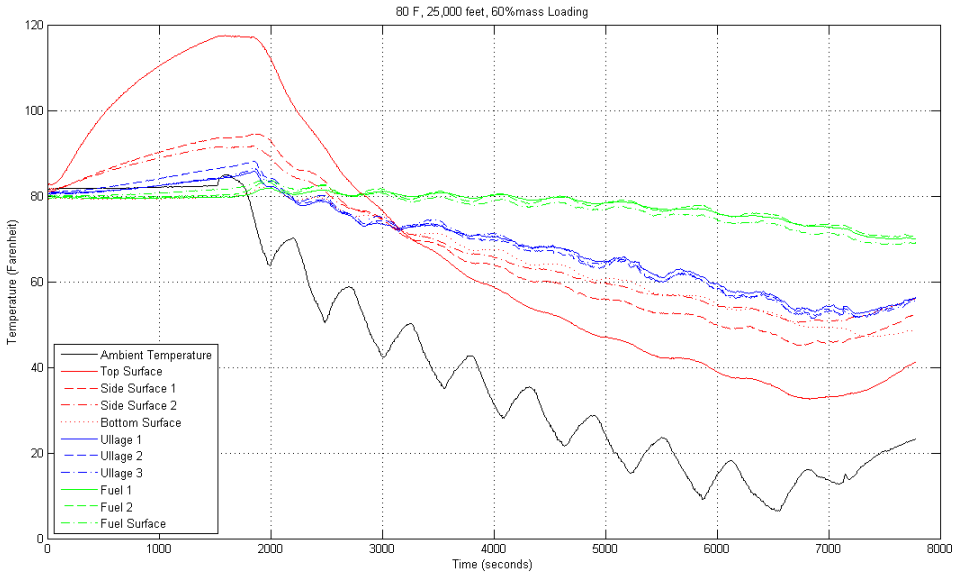


**A.1 Temperature data of experiment run in the altitude chamber with an initial fuel tank temperature was 80°F, cruising altitude achieved was 25,000 feet, 60% mass loading**

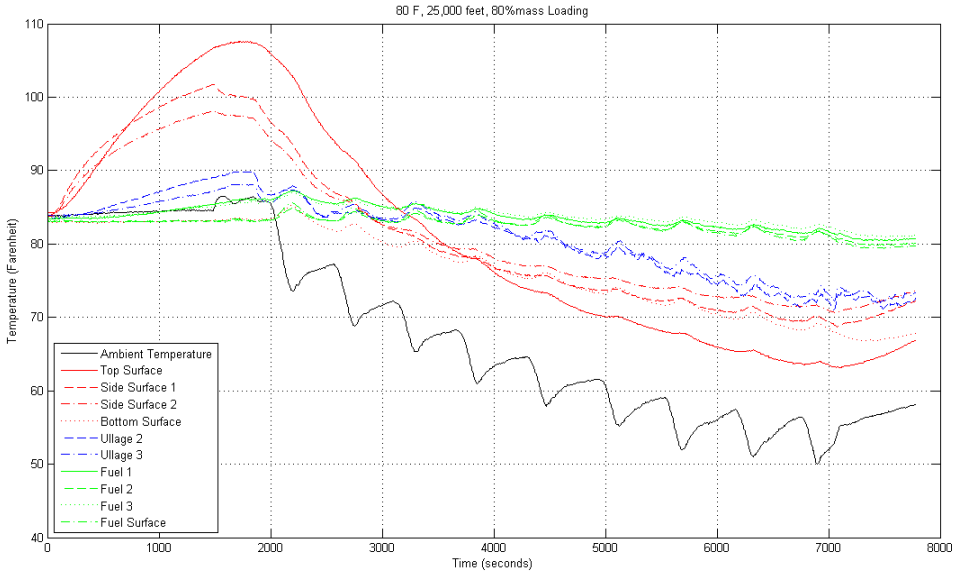


**A.2 Temperature data of experiment run in the altitude chamber with an initial fuel tank temperature was 80°F, cruising altitude achieved was 25,000 feet, 80% mass loading**

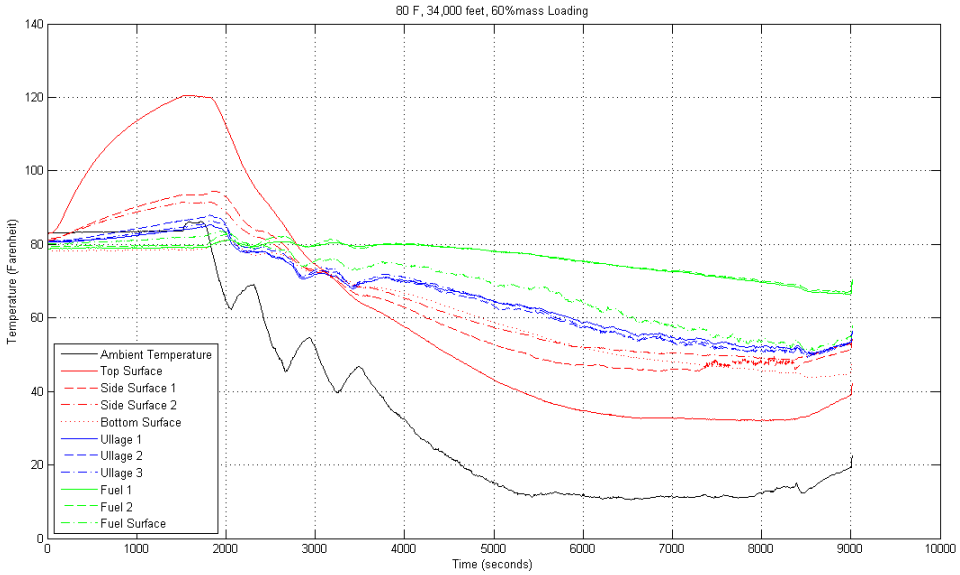


**A.3 Temperature data of experiment run in the altitude chamber with an initial fuel tank temperature was 80°F, cruising altitude achieved was 34,000 feet, 60% mass loading**

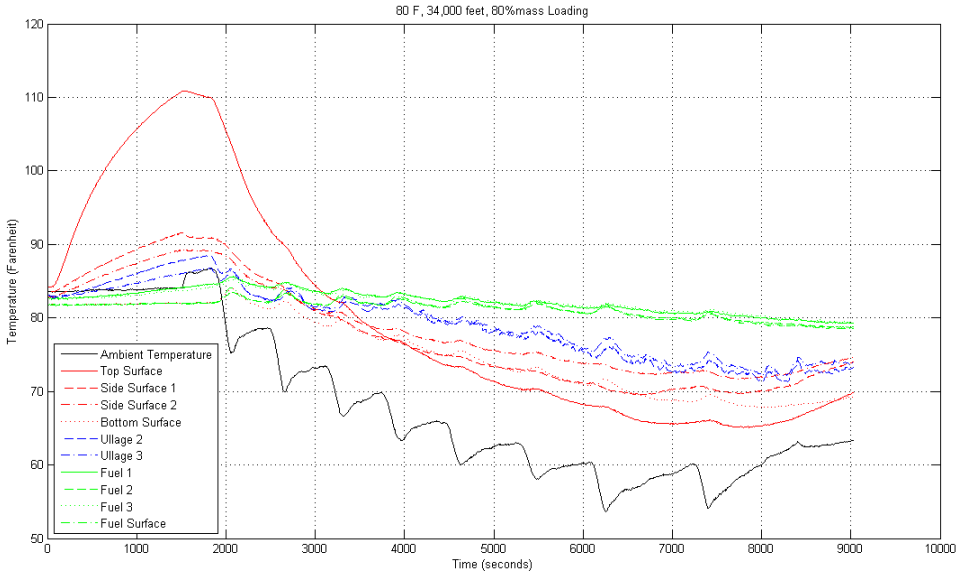


**A.4 Temperature data of experiment run in the altitude chamber with an initial fuel tank temperature was 80°F, cruising altitude achieved was 34,000 feet, 80% mass loading**

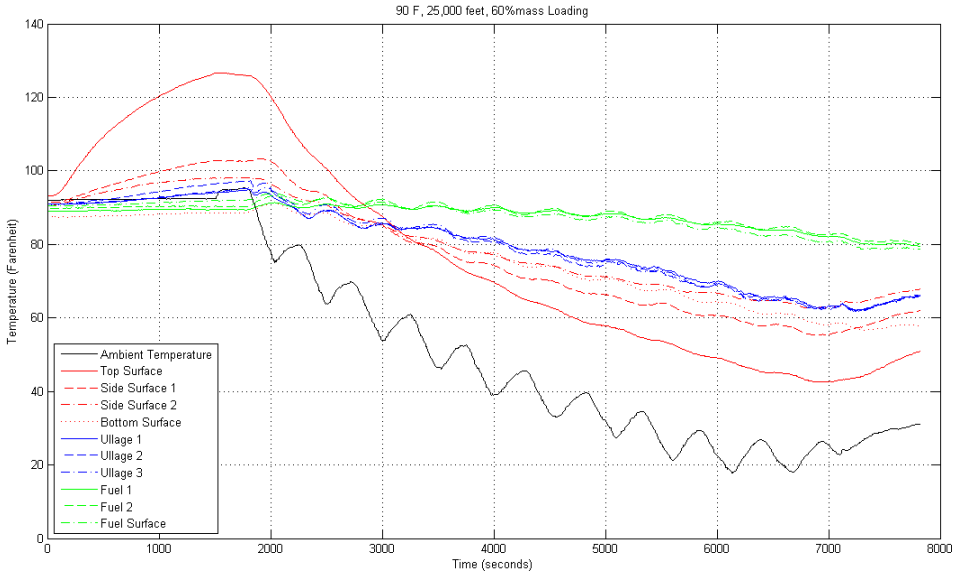


**A.5 Temperature data of experiment run in the altitude chamber with an initial fuel tank temperature was 90°F, cruising altitude achieved was 25,000 feet, 60% mass loading**

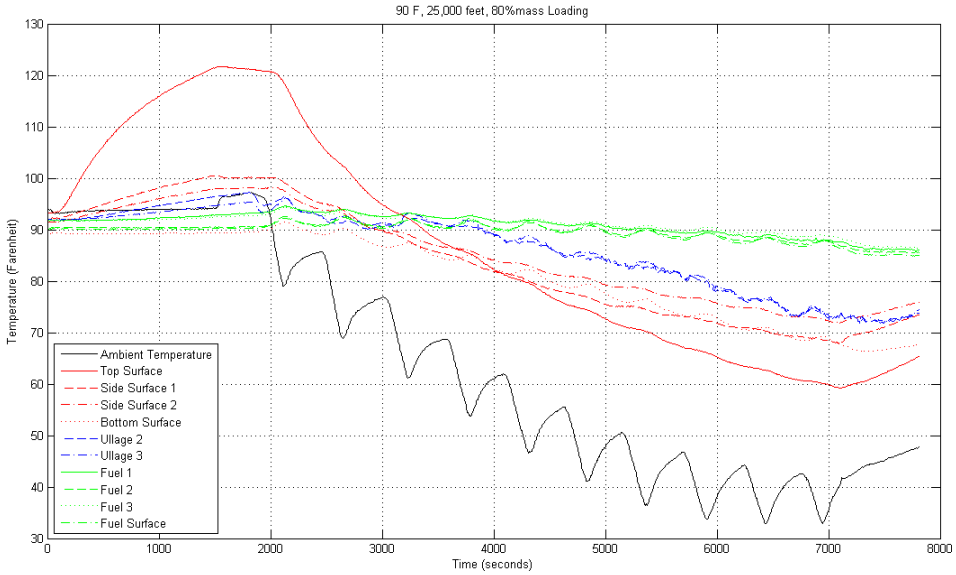


**A.6 Test Temperature data of experiment run in the altitude chamber with an initial fuel tank temperature was 90°F, cruising altitude achieved was 25,000 feet, 80% mass loading**

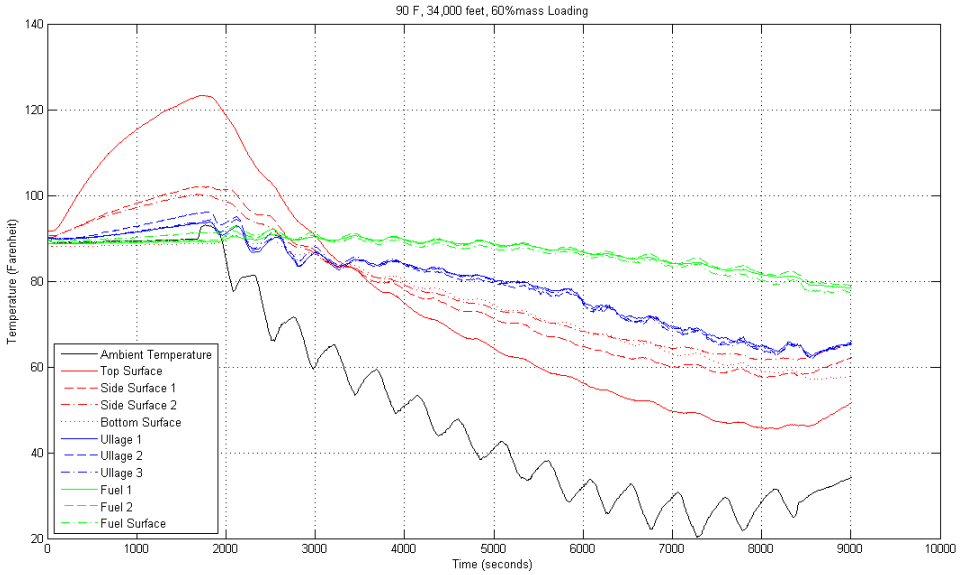


**A.7 Temperature data of experiment run in the altitude chamber with an initial fuel tank temperature was 90°F, cruising altitude achieved was 34,000 feet, 60% mass loading**

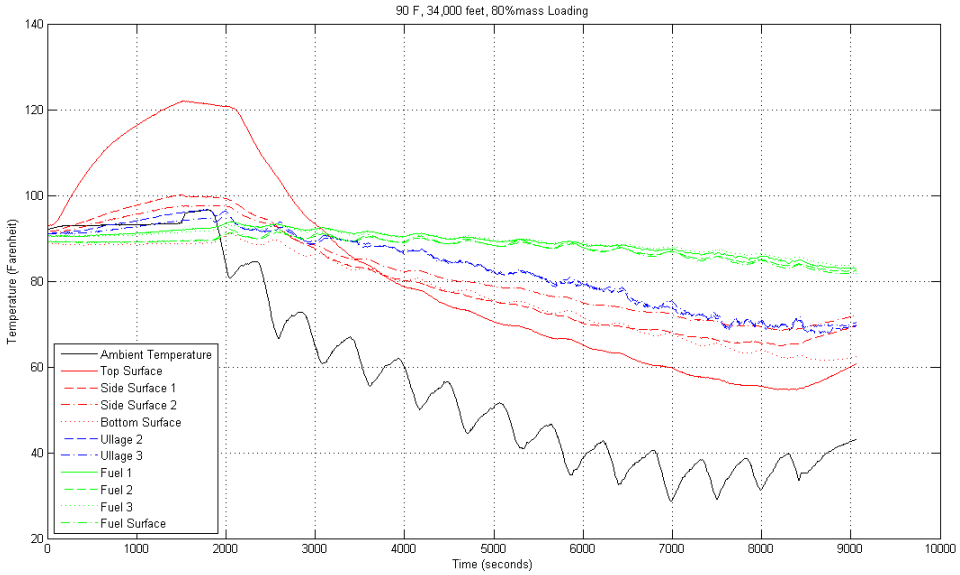


**A.8 Temperature data of experiment run in the altitude chamber with an initial fuel tank temperature was 90°F, cruising altitude achieved was 34,000 feet, 80% mass loading**

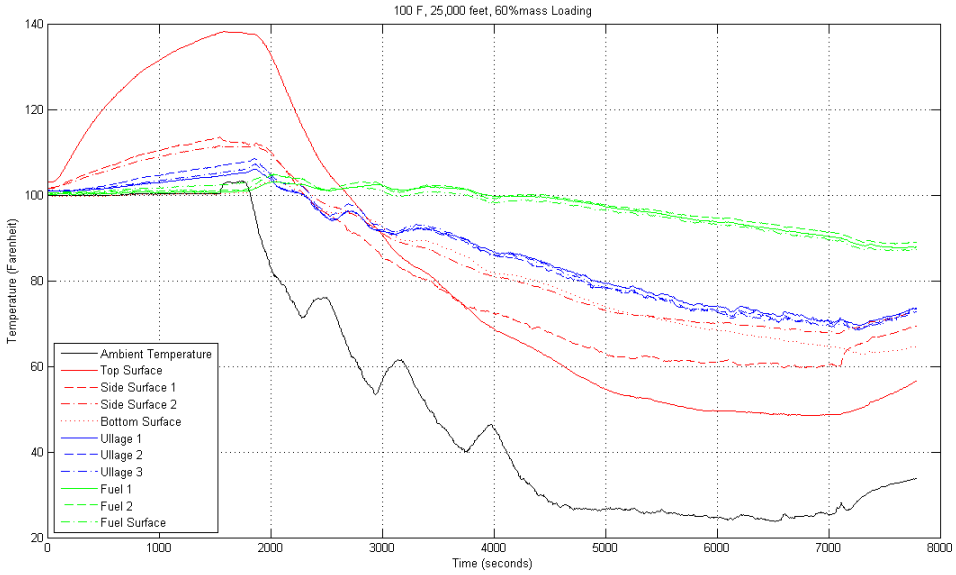


**A.9 Temperature data of experiment run in the altitude chamber with an initial fuel tank temperature was 100°F, cruising altitude achieved was 25,000 feet, 60% mass loading**

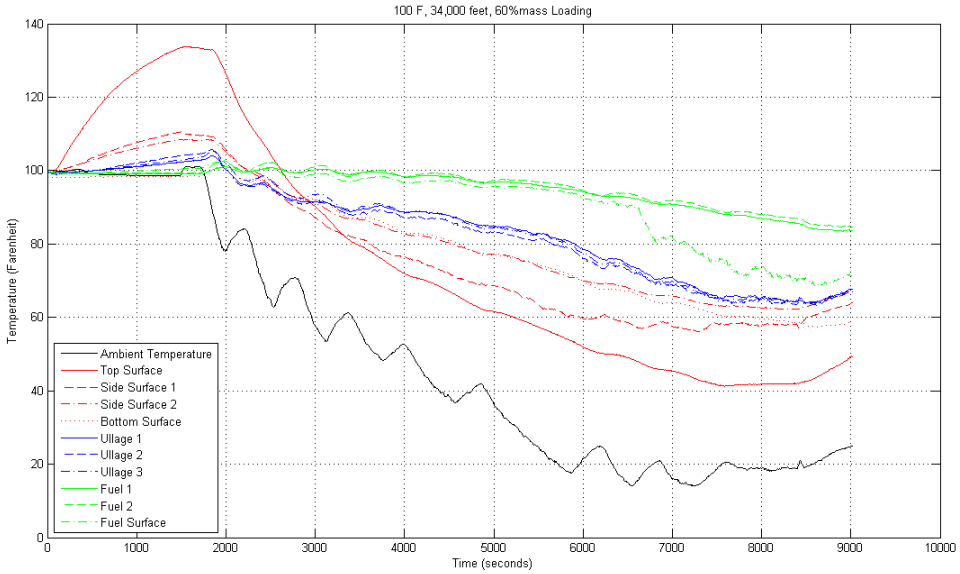


**A.10 Temperature data of experiment run in the altitude chamber with an initial fuel tank temperature was 100°F, cruising altitude achieved was 25,000 feet, 80% mass loading**

# References


[1] "*Reduction of Fuel Tank Flammability in Transport Category Planes; Final Rule*", Federal Register, Vol. 73, No. 140, July 2008.

[2] Chevron Products Company. "*Aviation Fuels Technical Review (FTR-3)*", A Division of Chevron USA. 2000.

[3] Shepherd, J.E., Nuyt, C.D., and Lee, J.J., "*Flash Point and Chemical Composition of Aviation Kerosene (JetA)*", Explosion Dynamics Laboratory Report FM99-4, 1999

[4]Department of Transportation Report, "*Transport Airplane Fuel Tank System Design Review, Flammability Reduction, and Maintenance and Inspection Requirements*", Federal Register Vol. 64, No. 209, October, 1999

[5]Aviation Rulemaking Advisory Committee, "*Fuel Tank Harmonization Working Group, Final Report*", ARAC, June 2001

[6] Summer, S.M., "*Cold Ambient Temperature Effects on Heated Fuel Tank Vapor Concentrations*", FAA Report DOT/FAA/AR-TN99/93 July 2000

[7] Summer, S.M., "*Mass Loading Effects on Fuel Vapor Concentrations in an Aircraft Fuel Tank Ullage*", FAA Report DOT/FAA/AR-TN99/65, September 1999

[8] Summer, S.M., "*Limiting Oxygen Concentration Required to Inert Jet Fuel Vapors Existing at Reduced Fuel Tank Pressures-Final Phase*", FAA Report DOT/FAA/AR-04/8, August 2004

[9] Burns, Michael, et al., *Evaluation of Fuel Tank Flammability and the FAA Inerting System on the NASA 747 SCA*, FAA report DOT/FAA/AR-04/41, December 2004

[10] Polymeropoulos, C., and Ochs, R., Jet A vaporization in a Simulated Aircraft Fuel Tank, *Fourth International Aircraft Fire and Cabin Research Conference*, Lisbon, Portugal, 2004.

[11]Incropera, F.P. and DeWitt, D.P., "*Fundamentals of Heat and Mass Transfer*", 4th ed., Wiley, New York, 1996.

[12]Hollands, K.G.T., Raithby, G.D., and Konicek, L., "*Correlation Equations for Free Convection Heat Transfer in Horizontal Layers of Air and Water*", *International Journal of Heat and Mass Transfer*, 1975, 18:879-884

[13]Poling, B.E., Prausnitz, J.M., and O'Connell, J.P., "*The Properties of Gases and Liquids*", Mc-Graw-Hill, New York, 2000.

[14]Lefebvre, A., *Gas Turbine Combustion*, Hemisphere, Washington, 1983

[15] Handbook of Aviation Fuel Properties, 1988, CRC Rpt. 530, Society of Automotive Engineers, Warrendale

[16]Woodrow, J.E., The Laboratory Characterization of Jet Fuel Vapor and Liquid, *Energy and Fuels*, 2003, 17:216-224

[17]Shepherd, J.E., Nuyt, C.D., and Lee, J.J., Flash Point and Chemical Composition of Aviation Kerosene (Jet-A), *Explosion Dynamics Laboratory Report FM99-4*

[18]Ochs. R., Vaporization of JP-8 Jet Fuel in a Simulated Aircraft Fuel Tank Under Varying Ambient Conditions, Rutgers Thesis, Rutgers University, January 2005

[19] http://www.fire.tc.faa.gov/systems/fueltank/facilities.stm, last visited July 13, 2009

[20] Summer, S.M., "*Composite and Aluminum Wing Tank Flammability Comparison Testing*" International Aircraft Systems Fire Protection Working Group, Köln, Germany, May 2009

[21] Personal Communication, William M. Cavage, William.M.Cavage@faa.gov

[22] Summer, S.M., "*Fuel Tank Flammability Assessment Method User's Manual*", FAA Report DOT/FAA/AR-05/8, May 2008

[23] Bairi, A., *Nusselt-Rayleigh correlations for design of industrial elements: Experimental and numerical investigation of natural convection in tilted square air filled enclosures*, Energy and Conversion Management, 49, 2008, 771-782.

[24]Flammability Reduction Method Workshop presentation

[25] Crowl, D.A., Louvar, J.F., *Chemical Process Safety: Fundamentals with Applications*, 2nd ed., Prentice Hall, New Jersey, 2002

[26] Britton, L.G., "*Using Heat of Oxidation to Evaluate Flammability Hazards*" Process Safety Progress, Vol.

21, Issue No. 1, March 2002

[27] Arnaldos, J., Casal, J., Planas-Cuchi, E., *Prediction of flammability limits at reduced pressures,* Chemical Engineering Science, Vol. 56, June 2001, 3829-3843